NASA CONTRACTOR REPORT

NASA CR-1373

ANALYTICAL AND EXPERIMENTAL STUDIES FOR PREDICTING NOISE ATTENUATION IN ACOUSTICALLY TREATED DUCTS FOR TURBOFAN ENGINES

by Ernest Feder and Lee Wallace Dean III

Prepared by
UNITED AIRCRAFT CORPORATION
East Hartford, Conn.
for Langley Research Center

NATIONAL AERONAUTICS AND SPACE ADMINISTRATION • WASHINGTON, D. C. • SEPTEMBER 1969

ANALYTICAL AND EXPERIMENTAL STUDIES FOR PREDICTING NOISE ATTENUATION IN ACOUSTICALLY TREATED DUCTS FOR TURBOFAN ENGINES

By Ernest Feder and Lee Wallace Dean III

Issued by Originator as Report No. PWA-3486

Prepared under Contract No. NAS 1-7129 by
Pratt & Whitney Aircraft Division
UNITED AIRCRAFT CORPORATION
East Hartford, Conn.

for Langley Research Center

NATIONAL AERONAUTICS AND SPACE ADMINISTRATION

For sale by the Clearinghouse for Federal Scientific and Technical Information
Springfield, Virginia 22151 – CFSTI price $3.00

TABLE OF CONTENTS

TABLE OF CONTENTS (Cont'd)

LIST OF TABLES

LIST OF ILLUSTRATIONS

LIST OF ILLUSTRATIONS (cont'd)

LIST OF ILLUSTRATIONS (cont'd)

LIST OF ILLUSTRATIONS (cont'd)

LIST OF ILLUSTRATIONS (cont'd)

LIST OF ILLUSTRATIONS (cont'd)

LIST OF ILLUSTRATIONS (cont'd)

LIST OF ILLUSTRATIONS (cont'd)

ANALYTICAL AND EXPERIMENTAL STUDIES FOR PREDICTING NOISE ATTENUATION IN ACOUSTICALLY TREATED DUCTS FOR TURBOFAN ENGINES

by Ernest Feder and Lee Wallace Dean III
Pratt & Whitney Aircraft

SUMMARY

Analytical and experimental studies were performed for predicting noise attenuation in acoustically treated ducts for application to turbofan engines. The program included measuring acoustic properties of typical duct lining materials. The results of these tests were used in the analytical prediction section.

A facility was developed for this program for measuring the impedance of acoustic materials in the presence of grazing airflow velocities of from 0 to 700 fps.

Over fifty acoustic specimens were tested. Specimens consisted of perforated plates, resistive materials, and perforated plates with a resistive backing material. The effects on impedance of flow velocities, sound pressure level variations, and boundary layer variations were measured for these specimens.

The rate of change of these acoustic properties was determined for each type of specimen, and it was noted that the resistance of the acoustic specimens increased and the reactance generally decreased with increasing flow velocity and sound pressure level.

The analytical studies obtained solutions for sound wave propagation in terms of modes in a rectangular duct lined on parallel sides with identical acoustic treatments, and the noise attenuation in the duct was determined by means of linear theory from the pressure decay coefficients of the modes. A comparison of analytical and experimental results, while showing good agreement at some frequencies, did not agree in the vicinity of the attenuation peak.

An empirical formula was developed to take into account nonlinear effects that were believed to be occurring at the high sound pressure level, 150 dB, used in the tests. With this formula a significant improvement was obtained in the comparisons between analysis and experiment.

The effect of changing the distance between treatments from 2-1/2 to 20 inches was examined. It was found that for larger treatment separation the maximum attenuation occurs at lower frequencies and for larger values of treatment resistance.

The effect of flow in the duct was examined for flow speeds up to 500 fps. Acoustic attenuation was calculated with the sound wave equation appropriate for zero flow by using the impedance measured while the lining material was subjected to grazing airflows. Good agreement between analytical and experimental results was obtained indicating that the major effect of flow speeds up to 500 fps is to change the boundary impedance.

INTRODUCTION

The predominant source of noise from turbofan engines is generated within the fan section of the engine. Improved fan designs have in some instances been effective in reducing the generated noise. Further significant reductions in the noise emanating from the aircraft can be accomplished by lining the engine inlet and fan discharge ducts with sound absorbent materials.

Considerable testing has been completed to evaluate various acoustic treatments for fan engines. Data from these tests have provided empirical design parameters which can be used to select acoustic lining configurations for engine ducts.

The objective of this program, which was a subcontract under contract NAS-1-7129, was to develop analytical procedures for predicting the noise attenuation in an acoustically lined duct. Methods to predict the attenuation of sound in a straight, rectangular duct at no-flow velocity conditions were evaluated and then extended to include the effects of airflow velocity.

Data on the acoustic characteristics of duct lining materials were required for the analytical program. Since the acoustic properties of materials change when subjected to grazing flow velocities, it was also the objective of this program to develop an impedance-tube-with-flow test facility to measure these changes. Utilizing this test facility, the impedance of acoustic materials subjected to grazing airflows and different boundary layer conditions was determined. Data from these tests were incorporated into the analytical program. Prior to this test program, very little data were available on the acoustic properties of duct lining materials subjected to grazing airflow.

The final objective of this program was to conduct tests to evaluate the effectiveness of the analytical procedures developed. Three configurations were selected for study. Measurements of the acoustic impedance of the liner materials were made in the impedance-tube-with-flow facility and used as input to the analytical program to predict attenuation of sound in a rectangular, lined duct. These configurations were then tested in a dual reverberation chamber test facility to measure the attenuation achieved so that comparisons with predicted values were possible.

TEST PROGRAM

Test Facilities

General

In order to investigate the acoustic properties of duct lining materials under conditions approximating realistic environment of fan engine ducts, a special test facility was required. The impedance-tube-with-flow test facility was developed specifically to meet the objectives of this contract. The test facility provided the capability to subject acoustic specimens to grazing airflow of up to 700 fps. The grazing flow is on the side of the acoustic specimen opposite the incident sound pressure wave propagating in the impedence tube. Provisions were made to mount the specimens at various locations in the test duct so that the effects of boundary layer variations could be studied.

The impedance of the specimens with and without the presence of grazing flow velocities could be measured for frequencies up to 6300 Hz and at sound pressure levels up to 155 dB. For impedance measurements, a standard impedance tube was used. In order to determine the impedance of the specimens in the presence of high grazing flow velocities, improved procedures for measuring the standing wave pattern in the impedance tube had to be developed.

To extend the scope of the test program, the capability to flow air through the specimens was added so that the impedance of the specimens could be measured both with and without the presence of through flows. Hot-wire instrumentation techniques were investigated to determine their applicability to provide a better understanding of the operation of acoustic liners.

Piping and Test Duct

The impedance-tube-with-flow test facility developed specifically for this test program is shown in figures 1 through 5. Figure 1 shows a schematic of the test facility. The airflow, supplied by a Spencer Turbo-Blower, was regulated by varying the blower speed and by a 20 inch butterfly control valve. From the 20 inch valve, the air flowed through 10 inch piping to a diffuser and into a 30

inch diameter plenum chamber. From the plenum, air flowed through a three-dimensional bellmouth into the 5 in. x 5 in. test duct and was discharged to atmosphere through a diffuser at the end of the test duct.

Ports for mounting the test specimens were provided at three longitudinal locations on one of the walls of the 5 in. x 5 in. test duct shown in cross-section in figure 2. These locations were chosen to permit testing at various boundary layer conditions. Through the use of special adapters, the specimens were mounted flush with the duct wall. This wall contained no acoustic treatment and is called the hardwall. The other three walls were acoustically treated to minimize the effects of sound reflecting back into the impedance tube. The acoustic treatment consisted of 1/16 inch thick, 30 percent open-area perforated plate facing material backed by fiberglas cloth and a two inch deep cavity filled with fiberglas.

Impedance Tube

The impedance tubes used for the test programs were, in general, of standard construction and conformed to the requirements specified in reference 1. Two sizes of impedance tubes were used. These were 1-3/8 inch and 1-1/16 inch inside diameter impedance tubes. The 1-3/8 in. tube was used for the hot-wire rig and for some of the preliminary flow facility tests. The 1-1/16 in. tube was employed with the 5 in. x 5 in. test duct and was used for determining all the impedance data presented in this report as it conformed with the requirements for measuring impedance at frequencies between 1250 and 6300 Hz . Incident sound pressure waves for the 1-1/16 inch and the 1-3/8 inch impedance tubes were supplied by an acoustic driver LTV University Model I. D. 75.

Both impedance tubes were modified to incorporate the capability of providing a steady airflow through the specimens. This additional capability permitted measuring impedance due to the normal incident sound pressure waves combined with various levels of steady velocities.

Hot-Wire Rig

In order to measure directly the velocity through perforated plate specimens, a test rig was developed which incorporated hot-wire instrumentation. Photographs and a schematic diagram of the rig are shown in figures 6, 7, and 8. A single-orifice plate was attached to the impedance tube. The orifice diameter was 0.125 inches and the plate thickness was 0.015 inches. The hot-wire probe could be positioned directly in the plane of the orifice or traversed to any desired position by using a fine screw adjustment slide (fig. 7). The sound pressure level of the incident sound wave was measured by an Altec 21 BR 180-7 microphone mounted flush with the orifice plate (fig. 8).

The signals from the hot-wire probe and microphone were displayed on a dual-beam oscilloscope. This arrangement provided a simultaneous visual display of the air velocity through the orifice and the incident sound pressure waves that induced these flows. Impedance values could be determined by measuring the phase relationship and the magnitude of the velocities and sound pressure levels. Thus, effects of superimposing a steady-flow velocity on the velocity due to the incident sound pressure waves could be studied.

Test Facility Characteristics

Airflow Investigations

Velocity and boundary layer profiles at nominal velocities of 550 and 720 fps were measured in the 5 in. x 5 in. test duct at the three port locations. The velocity profiles were measured with a pitot-static tube, and the boundary layer profiles were measured with a Preston tube. Accurate positioning of the Preston tube was accomplished by using a fine screw adjustment slide. The pressure probes and the special adapter plates on which they were mounted are shown in figures 9 and 10. The nominal velocity was measured at the center of the test duct at location-1 (fig. 1). Except where otherwise noted, all air velocities specified were measured at this location. Suitable corrections were made in setting the velocities at location-1 sufficiently above the specified free-stream velocity at the test location to compensate for the normal acceleration of air-flow in the duct.

The airflow test showed that the flows were reasonably uniform and accelerated significantly, as expected, due to the boundary layer build up. The boundary layer thickness increased, also as expected, providing the means for investigating its effects on the impedance of the acoustic specimens. The velocity and boundary layer profiles are shown in figures 11 and 12.

The impedance data from the investigation of the effects of normal boundary layer growth indicated that useful information would be provided by investigating larger boundary layer variations than could be obtained from the normal boundary layer growth along the wall of the test duct. Accordingly, greater variations in the depth and shape of the boundary layers were induced by means of flow spoilers. These spoilers were attached to the hardwall of the test duct at various locations, and boundary layer profiles were measured at the three port locations.

The two flow-spoilers used are shown in figure 13. One of the spoilers consisted of a straight 5/16 x 5/16 inch cross-section bar, and the other consisted of an assembly of five layers of screens of various heights (shown schematically in figure 14). In general, these spoilers increased the boundary layer thickness and distorted the boundary layer profile.

Typical boundary layer and velocity profiles induced by the spoilers are shown in figures 15 through 17.

The aerodynamic "noise" spectra were measured in the 5 in. x 5 in. test duct for flow velocities up to 700 fps. These spectra were sensed by an Altec 21 BR 180-7 vented microphone mounted flush with the wall of the test duct at the three standard port locations. A special adapter, shown in figure 18, was used. "Noise" spectra also were measured with the flow spoilers attached to the test duct.

Typical one-third octave "noise" spectra are shown in figure 19.

Impedance Tube

Background Noise Level - The background noise levels in the impedance tube due to air velocities in the 5 in. x 5 in. test duct were measured at velocities of 100 to 700 fps. A 10-rayl Feltmetal specimen and a 22 percent open-area perforated plate specimen were mounted for these measurements. Table I shows the 1/3-octave band measured background noise levels with the 10-rayl Feltmetal specimen mounted in port B. Values shown were the maximum observed in the impedance tube. The noise levels with the perforated plate were in the same range as those listed for the Feltmetal.

TABLE I

IMPEDANCE TUBE 1/3-OCTAVE BACKGROUND NOISE LEVELS WITH 10-RAYL FELTMETAL

Airflow Velocity	Frequency (Hz)					
	2000	2500	3150	4000	5000	6300
100 ft/sec	78 dB*	80 dB	81 dB	74 dB	74 dB	75 dB
300	88	80	81	79	76	75
500	98	90	91	84	84	85
600	103	95	94	89	89	87
700	108	98	97	94	92	90

* dB re .0002 dyne/cm^2

Probe Tube Response - The values used to correct sound pressure measurements for the microphone probe tube response are shown in table II. These values were determined by measuring the sound pressure level at the face of the hardwall termination of the impedance tube with a probe tube microphone and simultaneously with a microphone flush mounted in the hardwall. The end of the probe tube was positioned immediately adjacent to the hardwall.

TABLE II

MICROPHONE PROBE TUBE CORRECTION VALUES

	Frequency (Hz)					
	2000	2500	3150	4000	5000	6300
Values	8 dB	10 dB	11 dB	14 dB	14 dB	15 dB

Maximum Sound Pressure Levels in the Impedance Tube - The investigation of the effects of sound pressure levels on the acoustic characteristics of the test specimens was limited by the power of the acoustic driver, LTV University Model Number I.D. 75. A typical sound pressure envelope for 0, 300, 500, and 700 fps is shown in figure 20. The curve for each velocity represents the maximum sound pressure level attained in the impedance tube. These data were obtained using a 22 percent open-area perforated plate specimen and are representative for the other specimens tested. It is apparent from the figure that the maximum sound pressure level attainable decreased with frequency and flow velocity. With a single acoustic driver, these sound pressure levels represent the maximum which can be expected.

Radiation Impedance - The radiation impedance of the 1-1/16 inch impedance tube was determined with the impedance tube attached to the 5 in. x 5 in. test duct without a test specimen installed. Tests were performed at ports A and C. Table III shows the average of the results from port A, and table IV shows the average of the results from port C. The values tabulated are the reactive and resistive components of impedance divided by ρc where ρ is the air density and c is the sonic velocity. To determine the impedance of the acoustic specimens, the radiation impedance was subtracted from the measured impedance values.

TABLE III

RADIATION IMPEDANCE AT PORT A

	Frequency Hz					
	2000	2500	3150	4000	5000	6300
Normalized Reactance $X/\rho c$	.41	.60	.61	.70	.76	.59
Normalized Resistance $R/\rho c$	.08	.11	.40	.46	.58	.80

TABLE IV

RADIATION IMPEDANCE AT PORT C

	Frequency Hz					
	2000	2500	3150	4000	5000	6300
Normalized Reactance $X/\rho c$	.34	.54	.45	.57	.66	.41
Normalized Resistance $R/\rho c$	.10	.12	.38	.46	.50	.58

To investigate the validity of using the radiation impedance values to determine the impedance of the acoustic specimens the following procedure was used. The impedance of three specimens mounted in port C of the 5 in. x 5 in. test duct was measured. Then the impedance of these specimens mounted in fixtures which provided a one inch and a half inch backing cavity was again measured. The fixture is shown in figure 21. The specimens were:

- A perforated plate specimen with 15 percent open-area, 0.085 in. hole diameter and 0.015 in. thick (specimen P-17)
- A perforated plate specimen with 30 percent open-area, 0.078 in. hole diameter and 0.015 in. thick (specimen P-18)
- A fibermetal specimen 0.025 in. thick having a D.C. flow resistance of 43 rayls (specimen A-26a)

In order to make a valid comparison of these impedance measurements, suitable corrections were required. For the data obtained with the specimens in the 5 in. x 5 in. test duct with no flow, the radiation impedance listed in table III and IV was subtracted from the measured impedance. For the data obtained with the specimens backed by an air cavity, the calculated capacitive reactance due to the cavity was subtracted from their measured reactance. The capacitive reactance of the backings is

$$X_c = \cot\left(\frac{2\pi L}{\lambda}\right)$$

where X_c = capacitive component of reactance

L = depth of backing cavity

λ = wave length of the incident sound wave

The corrected impedance values for the three test conditions are shown in table V. It is considered that the agreement of these values is acceptable and provides a representative comparison of the results of measuring impedance in the 5 in. x 5 in. test duct at no airflow with conventional methods of testing.

Procedure for Measuring Impedance

A special procedure was developed for measuring the standing wave pattern inside the tube because it was found that conventional methods were inadequate when the specimens were subjected to high grazing air velocities.

To determine the impedance of a specimen, the distance of the first two nodes from the face of the specimen and the difference in sound pressure levels at the nodes and the antinodes of the standing wave pattern caused by the incident sound pressure wave in the impedance tube must be measured. The conventional method of determining these values was to traverse the tube with a microphone probe and monitor the signals with a voltmeter to locate the nodes and difference in sound pressure levels. While this method is acceptable in the absence of grazing flow velocities, random frequency fluctuations in the boundary layer induced by grazing flow velocities caused amplitude modulations of the sound pressure levels in the impedance tube. These fluctuations prevented locating the nodal distances with sufficient accuracy at grazing flow velocities above 300 fps. Because of this limitation, an improved test procedure was required.

TABLE V

COMPARISON OF IMPEDANCE MEASUREMENTS
MADE IN TEST DUCT AND BACKING CAVITIES

Frequency Hz	Reactance-X/ρc			Resistance-R/ρc		
	Test Duct	1 Inch Cavity	1/2 Inch Cavity	Test Duct	1 Inch Cavity	1/2 Inch Cavity
Acoustic Specimen P-17						
Perforated Plate, 15% Open Area, .085" Hole Dia, 015" Thk.						
2000	0.45	0.49	0.49	0.08	0.06	0.03
2500	0.55	0.64	0.62	0.07	0.08	0.05
3150	0.69	0.79	0.75	0.09	0.09	0.06
4000	0.87	1.00	0.93	0.15	0.09	0.09
5000	1.24	1.57	1.12	0.13	0.15	0.11
6300	1.15	*	1.54	0.00	*	0.11
Acoustic Specimen P-18						
Perforated Plate, 30% Open Area, .075" Hole Dia, 015" Thk.						
2000	0.10	0.20	0.23	0.04	0.03	0.10
2500	0.12	0.20	0.23	0.02	0.02	0.05
3150	0.13	0.25	0.27	0.05	0.03	0.03
4000	0.19	0.38	0.31	0.07	0.04	0.03
5000	0.26	0.37	0.36	0.02	0.02	0.03
6300	0.35	*	0.40	0.07	*	0.04
Acoustic Specimen A-26a						
Feltmetal .025" Thk.						
2000	0.27	0.18	0.20	0.96	0.90	1.06
2500	0.23	0.29	0.36	1.06	1.13	1.14
3150	0.29	0.28	0.38	1.11	1.21	1.16
4000	0.36	0.34	0.37	1.13	1.19	1.16
5000	0.38	0.42	0.42	1.45	1.04	1.13
6300	0.49	*	0.50	1.49	*	1.06

* At this frequency and backing depth, antiresonance conditions occur which makes impedance measurements unreliable

The instrumentation schematic for the specially developed procedure is shown in figure 5. With the new procedure, the impedance of the acoustic specimen is determined by recording the standing wave pattern in the impedance tube on a graphic level recorder strip chart. The sound pressure levels are read directly from the ordinate of the strip chart, and the nodal distances are determined on the abscissa as follows:

A cam, geared to the traversing mechanism, actuates a limit switch at even increments of distance from the specimen. Each time the limit switch is actuated, the microphone circuit is interrupted causing a "blip" to appear on the strip chart. Figure 22 shows typical standing wave patterns with the "blips" denoting known increments of distance from probe tip to the acoustic specimen. After determining the distance of the first "blip" from the acoustic specimen, counting the number of "blips" to the nodal points and interpolating between the last "blips" as required, the location of the nodes can be determined accurately.

Boundary layer fluctuations caused by the grazing air flow in the 5 in. x 5 in. test duct were still present and appear as small fluctuations on the strip chart as shown in figure 22. However, a mean-line through these fluctuations provides a quick and effective way of time averaging these fluctuations. Reliable data were thus obtained for grazing velocities up to 700 fps .

The improved method has several additional advantages over the conventional method: it is faster, more accurate, and provides a permanent record of the complete standing wave pattern in the impedance tube.

Impedance Measurements

Preparation of Specimens

Considerable variation in acoustic properties can exist at various locations on the same sheet of many types of acoustic facing materials. Since several types of tests were performed on each specimen, a special procedure was followed to eliminate possible problems due to sample variations and to minimize handling errors. This procedure consisted of bonding each acoustic specimen permanently to its own adapter plate and marking each adapter plate so as to identify the specimen. Figure 23 shows three acoustic specimens mounted in their respective adapter plates. Special fixtures were used which permitted the same specimen and its adapter plate to be mounted in the 5 in. x 5 in. test duct, the D.C. flow resistance measurement rig, and acoustic resistance measurement facilities.

Classification of Specimens

In order to classify the acoustic characteristics of the specimens tested, standard D.C. flow resistance measurements were made. Figures 24 through 29 show the test data. The D.C. flow resistance used to describe the acoustic specimens is the resistance at a velocity of 10 cm/sec. These values are presented in table VI, which describes the acoustic specimens tested.

In addition, the acoustic resistance of the test specimens was measured using the adapter with a one inch air-gap shown schematically in figure 21. The resistance was measured at a frequency of 2800 Hz. At this backing depth and frequency, the reactive part of the impedance is generally near zero. For specimens A-15 and A-16 the reactance was in the order of one ρc which may account for the lack of agreement of the acoustic reactance with the D.C. flow resistance.

Grazing Flow Velocity Tests

In order to determine the effect of grazing airflow on acoustic materials, a series of tests was performed in the 5 in. x 5 in. test duct acoustic facility. The impedance of 54 specimens was measured in port A of the test duct at grazing airflow velocities of 0, 300, and 500 fps. The test materials consisted of 27 perforated plate specimens, 23 resistive specimens, and four specimens consisting of a combination of perforated plate and screen. A description of these 54 acoustic specimens is given in table VI. From these specimens, three typical specimens were selected for additional testing in port A. These typical samples were tested at three sound pressure levels at grazing airflow velocities of 0, 300, 500, and 700 fps. The following specimens were selected for this series of tests:

- P-22 - A perforated plate with 22 percent open area
- A-14 - A polyimide specimen
- A-26 - A fibermetal specimen.

TABLE VI

DESCRIPTION OF ACOUSTIC SPECIMENS TESTED

Perforated Plate Specimens					
Specimen No.	Percent Open Area	Hole Diameter, Inches	Thickness Inches	D. C. Flow Resistance Rayl*	Acoustic Resistance Rayl
P-28	0.35	.0625**	.050	Over 200	Over 200
P-23	1.45	.125**	.050	48	Over 200
P-29	5.5	.250**	.050	7	Over 200
P-50	2.5	.046	.041	30	60
P-51	4.5	.062	.041	9	17
P-52	7	.078	.041	4	12
P-16	9	.085	.015	3	2
P-6	11.5	.050	.015	-	6
P-7	14	.093	.015	-	5
P-17	15	.085	.015	-	4
P-3	22	.093	.040	-	2
P-5	22	.023	.016	-	2
P-22	22	.093	.015	-	1
P-10	23	.050	.016	-	2
P-8	26	.100	.060	-	2
P-9	26	.093	.040	-	2
P-11	27	.102	.015	-	1
P-20	28	.085	.039	-	0
P-12	30	.055	.015	-	2
P-13	30	.125	.065	-	2
P-15	30	.125	.015	-	1
P-18	30	.078	.015	-	2
P-14	32	.101	.040	-	2
P-21	37	.082	.040	-	0
P-4	38	.085	.040	-	2
P-19	39	.099	.015	-	1
P-1	40	.085	.039	-	1
Combination - Perforated Plate & Screen***					
P-25	9	.085	.015	40	79
P-27	22	.093	.040	20	24
P-26	30	.078	.015	11	29
P-24	40	.085	.039	9	19

TABLE VI (Cont'd)

DESCRIPTION OF ACOUSTIC SPECIMENS TESTED

Resistive Specimens

Specimen No.	Type	Thickness	D.C. Flow Resistance Rayls	Acoustic Resistance Rayls
A-14	Polyimide	.068	4	8
A-8	****Screen	.037	10	17
A-10	Feltmetal	.040	12	17
A-17	Rigimesh	.025	17	19
A-30	Feltmetal	.043	17	21
A-15	Polyimide	.045	15	54
A-24	Brunsmet	.027	26	26
A-23	Brunsmet	.022	29	34
A-25	Brunsmet	.025	30	39
A-11	Feltmetal	.043	38	59
A-16	Polyimide	.047	40	93
A-26	Brunsmet	.025	43	48
A-19	Rigimesh	.037	50	57
A-22	Rigimesh	.045	58	65
A-12	Feltmetal	.025	60	79
A-27	Brunsmet	.020	68	69
A-13	Feltmetal	.050	70	92
A-20	Rigimesh	.040	74	70
A-18	Rigimesh	.033	80	76
A-21	Rigimesh	.045	88	86
A-28	Feltmetal	.048	150	110
A-29	Feltmetal	.047	160	172
A-9	Clevite	.066	over 200	

* Extrapolated to 10 cm/sec flow velocity in the flow resistance tube

** Single hole in center

*** Perforated plate and screen are mounted in series in adapter holder. The perforated plate is subjected to the grazing air flow.
For screen specifications see specimen A-8

**** Aluminum wire cloth .037" thick
20 x 200 mesh, twilled (Dutch weave)
.013" dia. wire for 20 mesh
.010" dia. wire for 200 mesh

Because the condition of the boundary layer is of major interest, a series of tests was performed to determine the effect of the boundary layer profile on impedance characteristics. The three typical specimens (i.e., P-22, A-14, and A-26) were tested in port C which is 40 inches upstream of port A and their impedance measured at the nominal velocities of 0, 300, 500, and 700 fps. To obtain greater variations in the depth and shape of the boundary layer, tests were also performed using the two flow-spoilers (fig. 13 and 14). With the spoilers installed, impedance measurements were taken as follows:

- Measurements at port A with 5/16 x 5/16 spoiler located at port B which is 20 inches upstream of port A
- Measurements at port C with the 5/16 x 5/16 spoiler located 3 inches upstream of port C

Representative plots of the grazing airflow tests are presented in figures 30 through 36. These data are discussed in the analytical portion of the test program section of the report.

Through-Flow Velocity Tests

The effect on impedance of a steady airflow through acoustic materials was investigated. In this series of tests the capability of flowing air at a steady velocity through the modified impedance tube was utilized (fig. 37.) The test procedure consisted of inducing a steady airflow in the impedance tube without generating incident sound pressure waves. Next, sound pressure waves were generated by the acoustic driver while the pressure differential across the specimen that produced the steady airflow was held constant, and the acoustic impedance due to the sound pressure waves with superimposed velocity was measured. The sound pressure level of the incident sound waves was increased at various increments and the impedance at each level was measured. When the maximum sound pressure level was reached, the steady flow velocity was increased and the procedure repeated.

The tests were performed for a range of velocities of about 10 to 1000 cm/sec in the tube, and the frequency range of the incident sound waves was from 1250 to 4000 Hz. The following specimens, described in table VI, were tested:

- P-17 - Perforated plate with 15 percent open area
- P-18 - Perforated plate with 30 percent open area
- A-10 - Fibermetal specimen
- A-26a - Fibermetal specimen

Figures 38 through 42 show the effect on acoustic impedance of superimposing a steady airflow on the incident sound pressure waves. The data obtained from these tests are discussed in the analytical portion of the test program section.

Hot-Wire Tests

Tests were conducted in the hot-wire test rig (fig. 8) to investigate the applicability of hot-wire instrumentation to the acoustic characteristics of perforated plate linings. A single-orifice plate was used for these tests. Hot-wire instrumentation was employed to measure directly the velocity of the air flowing through the orifice, and a microphone was used to measure the incident sound waves that induced the velocity. The signals from the two instruments were displayed simultaneously on a dual beam oscilloscope. Through the use of this arrangement, the following were studied:

- The effects of increasing the sound pressure levels on the magnitude of the air velocity through the orifice and the phase relationship of the pressure wave to velocity
- The effects of superimposing steady airflow on an oscillating flow induced by incident sound pressure waves and the phase relationship of the pressure wave to velocity
- The asymmetry of the airflow due to the incident sound pressure waves outside of the orifice.

Oscilloscope traces, representative of the velocities and sound pressures measured, are presented in figures 43, 44, and 45. These findings are discussed in the analytical portion of the test program section.

Analysis of Test Results

General

As described in the previous portion of the report, the impedance characteristics of acoustic materials were measured with the specimens subjected to grazing flow velocities, different boundary layer conditions, sound pressure levels, and through-flow velocities. The data obtained were analyzed and several observations of considerable importance apply equally to these test conditions.

The overall characteristic trends of all of the acoustic specimens tested were similar. If the effect of a particular test condition was to increase the acoustic resistance of one material, all of the materials were similarly affected. There were no test conditions, for example, where the resistance of perforated plates increased while the resistance of one of the fibermetals decreased. While the magnitude of the effect of these test conditions was different for each specimen tested, definite patterns were observed which could be characterized by the acoustic specimen type.

A definite relationship seems to exist between the various test conditions and the effects of these test conditions on the acousticial characteristics of the specimens. The mechanism relating these effects is believed to be associated with the air velocity induced through the acoustic specimen. Grazing airflows induce boundary layer fluctuations at the duct walls which cause fluctuating airflows through the porous acoustic materials. It is believed that the significant frequencies of the boundary layer fluctuations are low compared to the acoustic frequencies and their effects are similar to those of a steady velocity. It was, therefore, pertinent to investigate the effect of different boundary layer conditions produced by the same free-stream velocity. Relationships between grazing flow and through flow were studied. As described later, an equivalence between these flows has been established.

D. C. Flow Resistance

The D. C. flow resistance of the 54 acoustic specimens listed in table VI was measured. Figures 24 through 29 present the test data. The nominal D. C. flow resistance was defined as the resistance at a flow velocity of 10 cm/sec. These values are listed in table VI and serve to acoustically identify the specimens. D. C. flow values for the perforated plates with the higher percent of open areas are not listed. For these specimens the D. C. flow resistance was below two rayls. In this region extrapolation of the existing data to a flow velocity of 10 cm/sec is difficult, and it was felt that the exact values in the zero to two-rayl region are of little significance.

Of considerable interest are the slopes of the D. C. flow curves. It is evident that each type of acoustic material has its own distinct characteristic in the velocity range of primary interest, i.e., in the 10 to 1000 cm/sec range. The slopes give a qualitative indication of the degree to which the acoustic properties of each type of acoustic material will change because of environmental conditions. Figure 46 shows a composite of slopes with each line representing an average for each type of acoustic material tested. The differences in the various fibermetals and the various polyimide specimens should be taken to be representative of the specific specimens tested. Variations of fiber size, thickness, and manufacturing

process could change these results significantly. An indication of some of these construction details is given by figure 47 which shows enlarged views of typical specimens.

Effects of Grazing Flow

The analyses of the data from the grazing flow tests show that increasing grazing flow velocities had the effect of increasing resistance and, in general, decreasing reactance. However, each of the types of acoustic materials tested exhibited a distinct behavior pattern.

Acoustic Resistance

Perforated Plates - Of the several types of acoustic materials tested, the data for the perforated plates showed the clearest trends when grazing-flow velocities were increased. The most important parameter of this type of material appeared to be percent open-area. Other factors, such as hole size and plate thickness, did not appear to be very significant for the range tested.

Figure 30 shows the effect on resistance of increasing grazing flow velocities from 0 to 700 fps for perforated plate specimen P-22. The sound pressure level at the impedance-tube antinodes for this data was about 140 dB. The trends shown in the figure were typical of perforated plates with only the magnitude of the resistance change varying with percent open-area.

The change in acoustic resistance as a function of percent open-area of perforated plates is presented in Figure 48 for nominal velocities of 300 and 500 fps. The points on the curves show the average increase in resistance over the tested frequency range. The change of resistance increased as percent open-area decreased and appears to be asymptotic with the zero percent open-area axis.

Single-hole plate (specimens P-28, P-23, and P-29) data were not included in these curves. The test data for these specimens were erratic. The reason for the data being erratic is not fully understood, but is is believed that for these specimens the standard subtraction of radiation impedance may not be valid.

Resistive Specimens - The effect of grazing flow velocities on the acoustic resistance of resistive specimens was similar to that of the perforated plates. While these materials do not have as convenient a parameter as percent open-area to use for comparison, they do exhibit definite behavior patterns which appear to be governed by the manufacturing process. Enlarged views of several of these resistive specimens are shown in figure 47.

Figure 30 shows the typical effects on resistance of grazing flow at nominal velocities of 0 to 700 fps on a Polyimide (A-14) and a fibermetal (A-26) specimen, and figures 49 and 50 show the characteristic pattern for Brunsmet, Rigimesh, and Feltmetal specimens. The change of resistance due to grazing flow at nominal velocities of 300 and 500 fps is different for each of these materials. It is evident, for example, that the Brunsmet specimens were less affected by flow velocities than an equivalent specimen of Feltmetal.

It is very interesting to note that a similar trend and ranking was present in the D.C. flow data and is shown in figure 46. This again shows the similarity of behavior patterns noted for the various types of tests.

Acoustic Reactance

In general, the data trends for reactance were not as clear as those for resistance. Typical reactance data are shown in figure 35. It can be seen that the reactance generally decreased with increasing grazing flow velocity.

The relationship of reactance to frequency can be approximated by the linear equation $X = Kf$, where K is a constant for the acoustic specimen and f is frequency. Analysis of reactance data from the perforated plates showed that, unlike data for resistance, the relationship of K to percent open-area did not fall into clearly defined patterns. Further investigation will be required to determine the cause.

As expected, the reactance data for resistive specimens showed greater scatter than for perforated plates. This was due to the generally higher impedance values of resistive materials which makes the data more sensitive to measurement errors and possibly to greater variations in the manufacturing process which make comparisons between specimens difficult.

Effects of Boundary Layer Variations

In order to evaluate the applicability of the data obtained from the 5 in. x 5 in. test duct to that of a fan-jet engine duct, the effects of boundary layer variations were investigated. The effect of the velocity of the grazing airflow on the acoustic properties of the specimens tested was discussed in the previous portion of this section. It should be noted that the velocity specified was the free-stream velocity in the section of the test duct where the specimen was located. It is evident that a more precise description of the flow that grazes the specimen is required. The velocity immediately adjacent to the specimen (i.e, in the boundary layer) is a very important parameter and requires evaluation. If boundary layer variations are a major factor affecting the acoustic properties of duct lining materials, application of the data obtained from a test duct to a fan-engine duct would be difficult. The test results indicated that for a given free-stream velocity small variations in the shape of the boundary layer profile did not cause large changes in the impedance of the acoustic specimens.

To investigate the effects of normal growth of the boundary layer in the 5 in. x 5 in. test duct, the three typical specimens A-14, A-26, and P-22 were tested in ports A and C. Port C is 40 inches upstream from port A. The boundary layer velocities shown in figure 12 were replotted for easier comparison and are shown in figure 51. These figures show that boundary layer growth was in general as expected. Analysis of the impedance data showed no significant trends to correspond with the change in boundary layer.

To further investigate boundary layer effects, the two flow-spoilers (fig. 13) were used to develop more extreme changes in the boundary layer. In general, the effect of these spoilers was to increase boundary layer thickness and distort the boundary layer velocity profile. To determine the effect of a small boundary layer distortion, the 5/16 x 5/16 flow spoiler was attached at the port B location and acoustic specimens were tested at port A. The change of boundary layer due to the flow spoiler is shown in figure 15. This boundary layer change produced insignificant changes in the impedance of the acoustic specimens.

In order to investigate larger boundary layer changes the 5/16 x 5/16 flow spoiler was places three inches upstream of port C and acoustic specimen P-22 was tested at port C. Figure 36 shows the effect of the spoiler on the impedance of the specimen at a velocity of 500 fps. Figures 16, 17, and 19 show respectively the effects of the boundary layer, velocity profile, and "noise" spectra for this test condition. It is evident that this particular flow configuration resulted in a decrease of acoustic resistance. This probably was due to a sheltering effect which substantially decreased the flow velocity across the specimen rather than the change in velocity profile.

Considerably more testing will be required to fully evaluate boundary layer effects.

The "noise" spectra data (fig. 19) may prove a valuable tool for analyzing and comparing boundary layers. Because these spectra are related to the pressure field at the wall of the duct, analysis of the spectra could facilitate calculation of the flow through acoustic specimens. The "noise" spectra could therefore be used to predict the acoustic properties of a liner for the total environmental conditions of velocity, boundary layer, and sound pressure level.

The important parameters in the "noise" spectra are the major peaks of sound pressure levels and their frequencies. These parameters provide a basis for comparing the various test conditions. The important parameters are listed in table VII for velocities of 300, 500, and 700 fps for flows both with and without spoilers.

TABLE VII

NOISE SPECTRA IN THE 5" × 5" TEST DUCT INCLUDING EFFECTS OF FLOW SPOILERS

NOISE SPECTRA LOCATION Port	VELOCITY Ft/Sec	SPOILER Type	SPOILER Location Port	FIRST PEAK SPL dB	FIRST PEAK Freq. Hz	SECOND PEAK SPL dB	SECOND PEAK Freq. Hz
A	300	None		128	70		
A	500	None		132	65		
A	700	None		137	45		
B	300	None		128	60		
B	500	None		128	55		
B	700	None		132	40		
C	300	None		125	110		
C	500	None		125	48		
C	700	None		132	33		
B	300	5/16 × 5/16	B	130.5	75		
B	500	5/16 × 5/16	B	132.5	70		
B	700	5/16 × 5/16	B	135.5	50		
B	300	5/16 × 5/16	C-3"*	130.5	80		
B	500	5/16 × 5/16	C-3"	133.5	70		
B	700	5/16 × 5/16	C-3"	136.5	40		
B	300	5/16 × 5/16	C-3"	128	60	124.5	150
B	500	5/16 × 5/16	C-3"	129.5	60	126.5	140
B	700	5/16 × 5/16	C-3"	134	40	125.5	115
C	300	5/16 × 5/16	C-3"	128.5	130	133	800
C	500	5/16 × 5/16	C-3"	129.5	55	139	1500
C	700	5/16 × 5/16	C-3"	135	40	135	2600
A	300	Screen	B	130.5	80	124.5	500
A	500	Screen	B	133	70	130.5	750
A	700	Screen	B	135.5	50	132.5	1400
A	300	Screen	C-3"	129.5	90		

TABLE VII (Cont'd)
NOISE SPECTRA IN TEST DUCT INCLUDING
EFFECTS OF FLOW SPOILERS

NOISE SPECTRA LOCATION Port	VELOCITY Ft/Sec	SPOILER		FIRST PEAK		SECOND PEAK	
		Type	Location Port	SPL dB	Freq. Hz	SPL dB	Freq. Hz
A	500	Screen	C-3"	133.5	70		
A	700	Screen	C-3"	139	45	134.5	120
B	300	Screen	C-3"	128	65	126.5	175
B	500	Screen	C-3"	130.5	60	130	950
B	700	Screen	C-3"	135.5	40	133	1600
C	300	Screen	C-3"	121	55	124	110
C	500	Screen	C-3"	126.5	45	125.5	500
C	700	Screen	C-3"	134.5	35	118	2600

* Flow spoiler located 3" upstream from port C

Effect of Velocity Through Acoustic Specimens

It was apparent that the effect on the acoustic characteristics of the specimens due to grazing flow were similar to the effect due to airflows through the specimens. Grazing flows and through flows produced an increase in the resistance and a decrease in the reactance of the specimens. The reason for this similarity is believed to be due to boundary layer fluctuations, induced by the grazing flow velocities, causing airflows through the specimens. The frequency of these fluctuations is believed to be low enough so that the resulting through flows affect the acoustic characteristics of the specimens in a manner similar to steady through flows.

A study was made to determine the ratio of through flow velocities to grazing flow velocities which produced the same change of resistance of the perforated plate specimens. Figure 48 shows the effect of grazing flow velocities on the acoustic resistance of perforated plates. These results were obtained by measuring the impedance of the specimens due to the normal incident sound pressure waves from the impedance tube acoustic driver in the presence of grazing flow velocity. To obtain the magnitude of through-flow velocity which caused an equivalent resistance increase, D.C. flow resistance test results were used. Figure 52, which is a cross plot of the D.C. flow resistance data for perforated plate, shows the increase of resistance due to increasing steady through flows.

The following example illustrates how the ratio of through flow to grazing flow which produced the same resistance change was obtained. Figure 48 shows that at a velocity of 300 fps grazing flow, a 10 percent open-area perforated plate had a change of resistance of 0.5 $R/\rho c$ or 21 rayls. Figure 52 shows that for this perforated plate at 21 rayls, the velocity in the D.C. flow tube was about 100 cm/sec. The nominal velocity through the perforations, therefore, was about 1000 cm/sec, neglecting the discharge coefficient of the holes.

Equivalent values for 300 and 500 fps grazing flow velocity are listed in table VIII. These clearly show a consistent relationship. For these tests, 300 and 500 fps grazing flow velocities were respectively equivalent to nominal velocities of about 1100 cm/sec and 3000 cm/sec through the holes of the perforated plates or respective ratios of grazing to through velocities of approximately eight and five to one.

To further study the effects of velocity through the acoustic specimens, the impedance tube (modified as shown in figure 37) was used. The impedance of acoustic specimens P-17, P-18, A-10, and A-26a was measured in the presence of through velocities. The results of these measurements are shown in figures 38 to 42 . Several items of interest should be noted. As generally was the case during the test program, the qualitative effects were the same for all the specimens tested. Airflow through the specimens increased acoustic resistance and generally decreased acoustic reactance. As with grazing flow velocities, the trends of the reactance were not as clear as for the resistance changes.

At low velocities of through flow, increasing sound pressure levels significantly increased the acoustic resistance. As the through velocity increased, the effect of increasing sound pressure levels decreased. At high through-flow velocities, increasing sound pressure levels in the attainable range produced no significant effect.

D.C. flow resistance measurements also were taken to determine the combined effect of sound pressure levels and through flow. Figure 53 shows typical data taken with D.C. flow instrumentation. The bottom curve is representative of a conventional D.C. flow test. Sound pressure levels below about 130 dB had no significant effect on the D.C. flow readings. Higher sound pressure levels increased the differential pressure across the specimens resulting in an apparent higher D.C. flow resistance. At high through-flow velocities for the range of sound pressure levels tested, the effect of sound pressure level on the apparent D.C. flow resistance was not significant.

TABLE VIII

EQUIVALENCE OF AIR VELOCITY THROUGH PERFORATED PLATE WITH GRAZING FLOW VELOCITY PRODUCING EQUAL RESISTANCE

Open Area (Percent)	Acoustic* Resistance Due to Vel. ($R/\rho c$)	Equivalent** Vel. in D.C. Flow Tube (Cm/sec)	Vel. Through Holes (Cm/sec)	Velocity Ratio ***
Grazing Flow Velocity 300 fps				
10	0.50	120	1200	7.6
15	0.35	180	1200	7.6
20	0.25	220	1100	8.3
25	0.15	250	1000	9.1
30	0.10	330	1100	8.3
35	0.08	380	1100	8.3
Grazing Flow Velocity 500 fps				
10	1.05	300	3000	5.1
15	0.70	420	2800	5.4
20	0.50	600	3000	5.1
25	0.35	800	3200	4.8
30	0.25	800	2700	5.6
35	0.20	900	2600	5.8

* From figure 48
** From figure 52
*** Ratio of grazing velocity to through velocity

Effect of Sound Pressure Level

Increasing sound pressure levels in standard no-flow impedance tests increases the resistance of acoustic specimens. The effects on impedance of sound pressure levels at grazing flow velocities representative of fan-jet ducts is of prime importance and therefore was investigated.

Acoustic specimens P-22, A-10, and A-26 were chosen for this investigation. The sound pressure levels that were investigated ranged from the linear region of the specimens to the maximum obtainable. In the linear region, resistance is not a function of the velocity through the specimens. Therefore, the acoustic resistance is not affected by sound pressure level variations.

Typical sound pressure level envelopes are shown in figure 20. The curves represent the maximum sound pressure level obtainable in the impedance tube. It can be seen that the maximum sound pressure level dropped off considerably as the frequency and flow velocity increased.

Figures 31 through 33 show the effect of increasing the sound pressure levels on acoustic resistance at various flow velocities for frequencies of 2000 and 2500 Hz. Since high sound pressure levels at higher frequencies could not be maintained, data for those frequencies were not plotted. However, it is expected that the trends for higher frequencies would be similar to those shown. It can be clearly seen that resistance of the specimens increased as the sound pressure level increased. The increase appears to be most pronounced at low test-duct velocities.

Hot-Wire Investigation

A hot-wire test rig was developed to investigate the applicability of hot-wire instrumentation to duct lining test programs. A single-orifice plate was installed in the impedance tube (fig. 8) and various parameters were studied.

The effect of increasing sound pressure levels is shown in figure 43. This figure depicts simultaneous oscillograph traces of the sound pressure levels and velocity. By noting the magnitude and phase relationship of the velocity in the plane of the orifice and sound pressure levels, the impedance for these conditions can be calculated.

The effect of superimposing steady flow velocities through the orifice with the incident sound pressure waves is shown in figure 44. At no flow, it can be noted that the frequency of the velocity fluctuations appear to be twice that of the pressure waves inducing them. This is due to the inherent inability of the hot wire to differentiate between direction of air velocity. Effects of increasing steady flows through the orifice are shown. The bottom right hand oscilloscope picture shows the condition where the steady flow velocity was greater than the

velocity due to the incident sound pressure waves. The frequency of velocity fluctuation now appears to equal the pressure waves since there no longer are reversals in the direction of flow.

The effect of traversing the hot-wire probe out of the plane of the orifice is shown in figure 45. The upper left hand oscilloscope picture is the same as for figure 44 and shows the relationship of pressure to velocity. The other traces show this relationship with the probe out of the plane of the orifice. The lower right hand picture again shows the frequency of the velocity equal to the incident pressure. This was due to the asymmetry of the flow through the orifice. The hot-wire probe sensed only the velocity flowing out of the impedance tube which was a jet of air. The reverse flow into the orifice was drawn from all directions and was not sensed by the hot-wire probe at that distance from the orifice.

It appears from this investigation that hot-wire instrumentation could be a very useful tool in future test programs evaluating duct lining materials.

ANALYTICAL PROGRAM

General

The purpose of the analytical program was to provide a method for predicting acoustic attenuation in a treated, rectangular duct. Two parallel sides of the duct were assumed to be lined with identical sound-absorbing treatments, and two sides were assumed to be unlined. The method predicts attenuation for the condition of flow through the duct at a high sound pressure level.

Solutions to the wave equations are obtained for the first five modes in the duct. The attenuation is then expressed in terms of the pressure decay coefficients for these five modes. Acoustic attenuation is defined as minus ten times the common logarithm of the ratio of the power flowing through the treated duct to the power flowing through the same duct without treated walls (hardwalls).

The formula for attenuation based on linear acoustic theory was modified to account for nonlinear effects believed to accompany the high sound pressure level. This modification introduced into the calculations an empirical parameter that is independent of the type of lining material used but is a function of its length. Attenuation characteristics were studied for different duct sizes using this modified formula.

The influence on attenuation of airflow in the duct was examined for flow velocities up to 500 fps. Over this range of velocities, attenuation was calculated using solutions to the wave equation for zero flow velocity along with properties of the boundary measured in the presence of flow.

Experimental data for comparison with analytical results were obtained from a test facility consisting of two reverberation chambers connected by a duct. Sound energy generated in one chamber flows through the duct, which may be either treated or untreated, to the other chamber. The treatment attenuation can be ascertained by comparing the difference in sound pressure levels in the two chambers for a treated and an untreated duct.

The impedance of three lining materials was measured in an impedance tube for both flow and no-flow conditions. These measured impedances were used to predict attenuation, and the predictions were compared with experimental results obtained from the reverberation chamber test facility.

Sound Propagation in a Rectangular Duct Without Flow

The sound field in a duct can be considered to consist of a series of modes, each mode being a solution to the wave equation and each having its own amplitude and propagation properties. The acoustic attenuation in the duct is related to the rate at which these various modes decay as they propagate along the duct, and these decay rates can be found by solving the wave equation in the duct. In this portion of the report the equations that relate the acoustic mode decay coefficients to the impedance of the duct wall lining are developed.

A cross section of the rectangular duct considered for this analysis is shown in figure 54. The sides of the duct parallel to the x axis are lined with a sound absorbing material and are a distance D apart. The sides parallel to the y axis are hardwalls (unlined). Solutions to the equation for sound waves traveling in a positive z direction - i.e., normal to the xy plane - and which are appropriate to the choice of boundary conditions are (from ref. 2):

for modes symmetric about the center plane ($y = 0$)

$$p = P_o \cosh(2\pi g y/D) \exp ik(\tau z - ct) \qquad (1)$$

for asymmetric modes

$$p = P_o \sinh(2\pi g y/D) \exp ik(\tau z - ct) \qquad (2)$$

where p is the sound pressure and k is defined as $2\pi/\lambda$, τ is defined as $\sqrt{1 + (g\lambda/D)^2}$, c is the speed of sound, and $i = \sqrt{-1}$.

The boundary conditions are expressed by the equation

$$\left[\frac{\rho \frac{\partial p}{\partial t}}{\frac{\partial p}{\partial y}}\right]_{y = \pm D/2} = \pm \rho c Z \qquad (3)$$

For the complex wave-parameter g, the equations are:

for the symmetric mode - by substituting eq. (1) into (3)

$$g \tanh(\pi g) = iD/Z\lambda \qquad (4)$$

for the asymmetric mode - by substituting eq. (2) into (3)

$$g \coth(\pi g) = iD/Z\lambda \qquad (5)$$

For the five equations:

P_o = sound pressure amplitude

t = time
ρ = density of air
Z = normalized impedance of wall treatment
λ = wave length

The solutions to equations (4) and (5) can be arranged in an order corresponding to an increasing number of nodes in the y direction. The pressure patterns for the first five modes are shown in figure 54.

The transcendental equations for the complex wave parameters are solved by a computer program, described in detail in a later section. The solutions for a particular duct can be plotted as a series of points in the complex g-plane - samples for equation (4) are given in figures 55 and 56.

The axes for figures 55 and 56 are the real and imaginary parts of $g = g_1 + ig_2$ and $he^{i\phi} = D/Z\lambda$. For eq. (4), there are a series of branch points determined by the equation

$$\frac{d}{dg}(g \tanh \pi g) = 0$$

or $\sinh(2\pi g) + 2\pi g = 0$

The lines ϕ = constant, that pass through these points, divide the plane into regions containing one and only one solution.

The complete solution includes modes that have a pressure variation along the x direction. The error incurred in neglecting these modes is discussed later in the report.

The decay coefficient (α) for each mode is the imaginary part of $k\tau$.

$$\alpha = \text{Im}\,(k\tau) = \text{Im}\,\frac{2\pi}{\lambda}\left[1 + (g\lambda/D)^2\right]^{1/2}$$

$$\alpha = \text{Im}\,\frac{2\pi}{\lambda}\left[1 + (g_1\lambda/D)^2 - (g_2\lambda/D)^2 + 2i(g_1 g_2 \lambda^2/D^2)\right]^{1/2} \qquad (6)$$

If $g_1\lambda/D$ and $g_2\lambda/D$ are small, α may be approximated by

$$\alpha = (2\pi/\lambda)\,(g_1 g_2)\,(\lambda/D)^2$$

Within this restriction the locus of points of equal decay coefficients is a line $g_1 g_2$ = constant.

The duct lining material can be described at each frequency as hard or soft according to whether the impedance is greater than or less than the impedance of air and as mass reacting or stiffness reacting according to the sign of the reactive part of the impedance. The g-plane can be divided into corresponding regions: M_s standing for mass controlled soft, S_h for stiffness controlled hard, etc. Qualitatively speaking, it can be seen that larger mode decay coefficients correspond to a stiffness controlled boundary. In the case of a boundary displaying resonances, the maximum attenuation will occur at a frequency below resonance.

The type of boundary considered in this report consists of honeycomb of depth d, covered by a porous or perforated material. If the honeycomb cell width is small compared to a wavelength of sound, the boundary can be considered to be point reacting and the impedance consists of a resistance (R) and a mass reactance (X) of the porous (or perforated) material in series with the reactance of a cell of depth d.

The equation

$$Z = R - iX + i\cot(2\pi d/\lambda) \qquad (7)$$

is taken to represent the boundary, with R and X taken from impedance tube measurements.

Energy Flow

The experimental results discussed later in this report were taken in an existing facility (shown in fig. 57) used for measuring acoustic attenuation in a duct. This facility consists of two reverberation chambers connected by a duct. Sound energy is generated in the source chamber and is transmitted through the duct to the receiving chamber. Insertion loss is the difference in sound pressure level between the two chambers, and attenuation is defined as the increase in insertion loss between source and receiver chambers in the treated duct case over that observed in the hardwall case.

In this section attenuation, as defined above, is related to the pressure decay coefficients for the various modes previously described. The assumption, discussed in the appendix, is made that there is negligible net energy flow through the duct due to mode coupling.

In a reverberation chamber the sound field is made up of many waves traveling in all directions with equal probability. Under these conditions, the sound field can be specified by its energy density (E) and the energy density is proportional to the square of the measured sound pressure (p).

Power enters the receiving chamber (chamber-2) by various acoustic modes. The contribution of each mode is the power entering at that mode from the source chamber (chamber-1) multiplied by a mode transmission factor (A_m) which accounts for the power absorbed by the duct lining. The total power flow out of chamber-2 is the sum of the power absorbed by the walls of chamber-2, lost through the air-discharge passage, and transported back to chamber-1. As the energy entering the leaving are equal, the energy balance equation for chamber-2 is

$$E_1 \Sigma (a_{1m} A_m) = E_2 \Sigma (a_{2m}) + E_2 a_2 \tag{8}$$

a_{1m} and a_{2m} are coefficients such that a_{1m} multiplied by the energy density E_1 and a_{2m} multiplied by the energy density E_2 give the power into the duct in mode m. The sums are taken over the range of acoustic modes. (a_{1m} and a_{2m} are assumed to be the same for the hardwall and lined ducts.) The quantity $E_2 a_2$ is the power lost to the walls and air exit passage of chamber-2; so that a_2 is the fraction of E_2 lost per second. The effect of changing the values of a_{1m} and a_{2m} on attenuation is examined in the next section.

If p_1 and p_2 are the sound pressure levels measured respectively in chambers 1 and 2, the energy-density ratio is

$$\left(\frac{p_2}{p_1}\right)^2 = \frac{E_2}{E_1} = \frac{\Sigma (a_{1m} A_m)}{\Sigma (a_{2m}) + a_2} \tag{9}$$

For the case where the duct linings are hard, A_m will equal one or approximately zero. If, for the hardwall case, we substitute B_m for A_m (equaling either one or approximately zero) then the energy-density ratio becomes

$$\frac{E_2}{E_1} = \frac{\Sigma(a_{1m}B_m)}{\Sigma(a_{2m}) + a_2} = C \tag{10}$$

This is the hardwall insertion loss. In the experiments considered, the value of C is at least -10 dB at all frequencies, and a_{1m} and a_{2m} are substantially equal because of the symmetry of the two reverberation chambers. In the experimental set up, the loss of power from chamber-2 is large enough so that the loss of power to chamber-1 through the duct can be neglected. Consequently, C can be approximated by

$$C = \frac{\Sigma(a_{1m}B_m)}{a_2} \tag{11}$$

If the transmission factors for the lined duct are designated A_m, the insertion loss for the lined duct is therefore

$$\frac{E_2}{E_1} = \frac{\Sigma(a_{1m}A_m)}{a_2} = C\left[\frac{\Sigma(a_{1m}A_m)}{\Sigma(a_{1m}B_m)}\right] \tag{12}$$

It is necessary to calculate the a_{1m}, A_m, and B_m for all of the modes in the duct that transport a significant fraction of energy.

Finally, the attenuation is minus ten times the common logarithm of the ratio of the lined-duct insertion loss to that for the hardwall duct, or

$$\text{Attenuation} = -10 \log \frac{\Sigma a_{1m}A_m}{\Sigma a_{1m}B_m} \tag{13}$$

The B_m terms are equal to either one or zero according to whether or not a mode propagates in the hardwall case, and A_m is calculated from the equation

$$A_m = \exp(-2\alpha_m L) \tag{14}$$

where α_m is the pressure-decay coefficient for mth mode and L is the length of treatment in the duct.

It was assumed for the calculations that the input energy was equally divided among the propagating modes, so that all the values of a_{1m} were taken as one. This assumption is discussed subsequently. Calculations were terminated with the mode m = 4 since no significant energy is transported in higher modes for the geometry under consideration.

Equation (4) or (5) and (6), (13), and (14) are combined to calculate attenuation in terms of wavelength, duct width, and boundary impedance.

Excitation of Modes by a Diffused Sound Field

The amplitude of each mode in the duct can be calculated by assuming that the mode is excited by noncoherent plane-waves arriving at the duct entrance from all angles. Plane waves arriving at normal incidence excite the plane wave mode in the duct; plane waves arriving at other angles excite higher modes. A detailed calculation was carried out by computer, and the results showed that propagating modes have approximately equal amplitudes and nonpropagating modes are only weakly excited.

The power into the duct in each mode, $A_{1m}E_1$, is the product of the amplitude squared and the group velocity of the mode. As mode number increases the group velocity decreases very slowly until cutoff is approached, at which point it drops rapidly to zero. The net result is that the major part of the acoustic power into the duct is carried by the first few propagating modes, i.e., the modes with nearly equal amplitudes and group velocity.

Based on the assumptions that the power into the duct is carried by one of the following:

- The mode of least attenuation only
- Modes of equal amplitude
- Modes of equal power,

the predicted attenuation for a set of duct parameters is shown in figure 58. The mode of least attenuation is usually the principal (plane wave) mode; occasionally it will be the second even mode. The equal energy assumption assigns the largest amount of energy to the higher order (and more highly attenuated) modes; it gives, therefore, the highest attenuation.

To calculate the attenuation for the mode of least attenuation, only one mode is involved at a time, and a_{1m} is set equal to one for this mode. To calculate the attenuation assuming equal power in each mode, all a_{1m} values are set equal to one. For the equal amplitude mode calculation, the values of a_{1m} used are shown in table IX.

TABLE IX

EQUAL MODE AMPLITUDE a_{1m} FACTORS

Frequency Hz	1300	1600	2000	2500	3150	4000	5000	6300
m = 0	1.0	1.0	1.0	1.0	1.0	1.0	1.0	1.0
1		.54	.74	.85	.90	.94	.96	.97
2					.52	.74	.84	.90
3							.58	.76
4								.50

D = five inches

It can be seen from figure 58 that the predicted attenuation does not depend strongly on whether the modes are assigned equal energy or equal amplitudes at the duct entrance. The equal energy assumption is more convenient mathmatically, since all a_{1m}'s equal one for propagating modes, and it is used in all subsequent calculations.

Errors Due to Neglect of Cross-Modes

The prediction program takes into account only those modes that have a uniform sound pressure along a line in the duct cross-section parallel to the acoustic treatment (the x axis in fig. 54). The error associated with this approximation can be calculated, and the results for a few points are given in table X. The values listed under the heading "All Modes" are the actual number of modes, including those having pressure variation in the x direction in fig. 54, that propagate in the five by twenty inch hardwall duct, and the attenuations listed were calculated taking into account all of the modes. The values listed under "Prediction Program" are for the case where the sound pressure is constant in the x direction. As can be seen, the errors are not large. They are not large because the additional modes are similar in terms of decay coefficient to those included in the prediction program.

TABLE X

ERRORS ASSOCIATED WITH THE FIVE MODE ASSUMPTION

Frequency	Prediction Program		All Modes	
	Number of Modes	Attenuation	Number of Modes	Attenuation
1300 Hz.	1	17.6 dB.	4	19.2 dB.
1600	2	33.8	7	35.7
3150	3	20	20	20.8
4000	3	12	32	12.7

Attenuation including cross modes for the case d=1, R=1, X=0

Comparison Between Analysis and Experiment

Acoustic attenuation predictions were calculated for a duct whose treated sides were separated by a distance of five inches. The treatments considered were fibermetal with a normalized resistance ranging from 0.25 to 2 placed over honeycomb of depths from 0.25 to 1 inch. These were compared with existing experimental results for the same duct configuration.

Two of these comparisons are shown in figures 59 and 60. Good agreement between predicted and measured attenuation is obtained at low and high frequencies, but the agreement is poor in the vicinity of the attenuation maximum. These comparisons were typical of the several cases investigated.

In the above calculations, based on ref. 2, it was assumed that the acoustic modes all have equal energy at the duct entrance. Changing to the assumption that the modes have equal amplitudes did little to improve the results. In addition, the experiment was checked thoroughly to see whether the measured attenuation was limited by noise or by the presence of flanking sound paths, and the result was negative.

This serious and consistent disagreement between predicted and measured attenuation in the vicinity of the attenuation maximum was thought to be attributable to nonlinear behavior. It therefore was considered essential, before proceeding with an examination of the effect of flow, to improve the no-flow results in a manner described in the next section.

Effects of High Levels of Sound Pressures

As is shown in the previous section, the model for attenuation based on the linear sound equations leads to predicted attenuations over an important part of the frequency range for certain materials that far exceed measured values. Good agreement was obtained, however, away from the region where peak attenuation occurs. Since the model is based on an assumption of linearity and since the sound pressure in the duct is relatively high, about 150 dB in the source chamber, it is possible that the linear model fails because of the existence of nonlinear conditions throughout the entire volume of the duct as well as at the duct walls.

The simplifying feature of linearity is that the energy produced in a given frequency band always remains in that band. However, when nonlinearity occurs, energy can be exchanged between frequency bands by the processes of modulation and distortion. In the case of wide-band noise in a duct, the energy exchange between frequency bands may cause the spectrum to change as the noise propagates down the duct, even when attenuation is not present. The spectrum can eventually reach some steady-state shape when the energy into and out of each frequency band per second balances. When nonlinearity is present, waves of two frequencies combine to generate sum and difference frequencies, and energy may be transferred to lower (difference) frequencies as well as to higher ones. If absorption is present in the duct, the eventual shape of the energy spectrum depends on a balance between the energy fed into each frequency band per second because of modulation and distortion and the sum of that removed by modulation, distortion, and absorption.

To facilitate analysis of the nonlinear effects, it was assumed that the net energy per second flowing into each frequency band per unit duct length is proportional to the difference between the average energy in the overall spectrum (E_o) and the energy in that band. This quantity will vanish when the energy in each band is equal to the overall average. The change in energy per duct length becomes:

$$dE/dx = -k_m E(x) + b[E_o - E(x)] \qquad (15)$$

The term $-k_m E$ is the energy removed by absorption. The term $k_m = 2\alpha_m$ is the energy decay coefficient in the absence of modulation, and b is a parameter selected to fit experimental results. Integrating the expression, the transmission factor becomes

$$A_m = \frac{(k_m e^{-(k_m + b)x} + b)}{(k_m + b)} \qquad (16)$$

The attenuation is calculated using eq. (16) rather than eq. (14) for the lined duct transmission factors.

Although the above is not a well founded physical model, it is thought to be a more useful scheme for predicting attenuation in the vicinity of the attenuation maximum than that given by the linear analysis. Further work is required to achieve a satisfactory understanding of the effects of nonlinearity on attenuation.

Acoustic attenuation predictions were calculated using the modified equation for the lined duct transmission factors (eq. (16) for a duct with treated sides seperated by a distance of five inches. The treatments considered were fibermetal with a normalized resistance of 0.25 to 2 placed over honeycomb of depth 0.25 to 1 inch. In each case the value of b used was 0.0055. The results for five of these cases along with the predictions based on linear acoustic theory (eq. (14) are shown in figures 61 through 65. It can be seen from these figures that using a single value of b, chosen to give the best fit for one of the curves, considerably improves the agreement between predictions and measurements for a variety of cases.

If the assumptions of nonlinearity are correct, it should follow that as the sound pressure level is reduced from the 150 dB used in the tests, the measured attenuation should approach that predicted by linear acoustic theory. This would amount to an increase in measured attenuation in the vicinity of the attenuation maximum with a decrease in sound pressure level. Attenuation values were measured at three sound pressure levels with fibermetal which has properties that vary only slightly with sound pressure level. The values of resistance and honeycomb depth for the lining material were chosen so that attenuation would be at a maximum for these parameters, preventing large changes in attenuation from being attributed to a small change in their values. The results for these values of sound pressure level in the source chamber are shown in figure 66. As can be seen from the figure, the attenuation did increase in the vicinity of the attenuation maximum as the sound pressure level was decreased.

The value of b in eq. (16) that gives the best agreement for different lining materials was found to change with treatment length, L. An empirical relationship was found to be $b = 2.8/L^2$, and this equation is used in the calculations of attenuation for the treatment lengths discussed in the next section. In addition, the value of b should decrease as the sound pressure level decreases so the equation (16) reverts to the equation derived from linear theory at low sound pressure levels. Due to the interdependence of b on sound pressure level and duct length, a general formulation of this factor was not possible within the scope of the tests conducted during this contract.

Lined Duct Attenuation Characteristics

The equations modified for nonlinear effects were used to compute attenuation for a variety of duct configurations. Ducts with treated sides separated by from 2-1/2 to 40 inches and with treatment lengths of from 5 to 45 inches were considered. The results were examined to determine the resistance of the facing

material and the depth of the honeycomb for which maximum attenuation occurred. The frequency at which maximum attenuation occurred was also noted.

With boundary properties held constant, the maximum attenuation as a function of frequency was chosen for a series of duct widths, D, and treatment lengths, L. These values along with available experimental points were plotted as a function of L/D. The curves, shown in figure 67, indicate that attenuation approximately doubles when the treatment length is doubled for values of L/D of about five. Beyond this point the increase in attenuation with treatment length is less rapid.

The depth of the honeycomb backing and the resistance of the covering material for which maximum attenuation occurs were plotted for four duct widths. The resulting curves, shown in figures 68 and 69, illustrate that maximum attenuation for the larger duct sizes is attained with the larger values of backing depth and resistance. The frequency at which maximum attenuation occurs is plotted as a function of duct width in figure 70. This figure indicates that for the larger duct widths maximum attenuation occurs at lower frequencies than it does for the smaller widths.

Effects of Flow on Sound Attenuation

The wave equation for axial flow (normal to the xy plane, fig. 54) in the duct is

$$\left[\frac{1}{c}\frac{\partial}{\partial t} + M\frac{\partial}{\partial z}\right]^2 p = \nabla^2 p \qquad (17)$$

where M is the ratio of axial-flow velocity to the velocity of sound (c).

Solutions to eq. (17) exist which are of the same form as eqs. (1) and (2). By placing these solutions into eq. (17), the dispersion relationship is expressed by

$$\tau^2 - (g\lambda/D)^2 = (1 - M\tau)^2 \qquad (18)$$

where τ, when multiplied by k, is the propagation factor for the z direction.

The relationship between sound pressure and sound particle velocity is expressed by the equation

$$\rho\left(\frac{\partial}{\partial t} + cM\right) u_i = -\frac{\partial p}{\partial x_i} \tag{19}$$

where ρ is the density of air and the subscript i refers to the coordinates x, y, or z.

The equation relating the ratio of sound pressure to velocity and impedance at the boundary then is

$$g \tanh(\pi g) = \frac{iD}{Z\lambda}(1 - M\tau) \tag{20}$$

and

$$g \coth(\pi g) = \frac{iD}{Z\lambda}(1 - M\tau) \tag{21}$$

Equations (20) and (21) replace eqs. (4) and (5).

Equation (18) can be solved for the axial propagation factor, and

$$\tau = \frac{-M + \sqrt{1 + (g\lambda/D)^2 (1 - M^2)}}{(1 - M^2)} \tag{22}$$

According to eqs. (20) and (21), the effect of flow can be considered to be equivalent to a change in wavelength. These equations can be rewritten in the form

$$g \tanh(\pi g) = \frac{iD}{Z\lambda'} \tag{23}$$

and

$$g \coth(\pi g) = \frac{iD}{Z\lambda'} \tag{24}$$

where

$$\lambda' = \frac{\lambda}{1 - M\tau} \tag{25}$$

It can be seen that a positive value of M, corresponding to a flow in the direction of the sound propagation, increases the apparent wavelength, λ' . One can expect that the frequency of maximum attentuation, as derived from the equations, remains constant with apparent wavelength and, therefore, shifts to shorter wavelengths, λ , with positive values of M. The frequency of maximum attentuation should shift to a higher frequency for those cases where the sound waves propagate with the flow and to a lower frequency for those cases where they propagate against the flow.

Attempts to obtain a convergent machine-computation procedure for determining the roots of equations (20), (21), and (22) were not successful. It was decided, therefore, to use the equations for sound propagation without flow. It was assumed that this equation could be employed if the acoustic impedance used for the boundary was experimentally determined in the presence of flow and the flow velocity is less than Mach 0.5. The acoustic impedance with grazing airflow was determined for a number of specimens including fibermetal and perforated plate, and the results were used to compute the acoustic attenuation. The impedance with grazing airflows was determined in the manner described in the test program part of this report.

Comparison Between Analysis and Experiment With Flow For Three Liners

Using the no-flow equations along with the properties of duct lining materials measured in an impedance tube with flow, acoustic attenuation was calculated and the results compared with test measurements. Attenuation measurements were taken in a 5 in. x 20 in. duct. The distance between treatments was five inches, and the treatment length was 22-1/2 inches. Three flow velocities were used: 0, 300, and 500 fps.

The predicted and experimental values of attenuation may be compared in figures 71 through 79 for the following three lining materials:

- 9 percent open-area perforated plate over 3/4 inch honeycomb
- 15 percent open-area perforated plate over 3/4 inch honeycomb
- 40-rayl fibermetal over one inch honeycomb.

The figures for the 9 percent and the 15 percent open-area perforated plates show poor agreement between predictions and measurements of zero flow. With airflow, however, the impedance of perforated plates is strongly dependent on flow, and the predicted and measured attenuations are in better agreement. The materially improved attenuation characteristics of perforated plate facing in the presence of grazing airflows should be noted.

The results for fibermetal with a normalized resistance of one over one inch honeycomb (figs. 77, 78, and 79) show good agreement between measurement and prediction. There is a shift in the frequency of maximum attenuation to higher values with flow that appears in the predictions as well as in the measurements.

Computer Program

The analytical study of sound attenuation required the solution of the transcendental equations (4) and (5) and the computation of the normalized boundary admittance of the lined portion of the duct. A computer program was developed to determine these factors from the physical parameters of the duct. This computer program also calculates the normalized reactance of the facing material, the mode transmission factors, the mode decay coefficients, and the regeneration coefficient. (The experimentally determined parameter, b, of equation (15). These results are combined to yield the complete attenuation value in decibels.

The computer program contains a main program with four subroutines. A brief program flow chart is presented in figures 80 and 81. The symbols utilized conform with the usage employed throughout the report.

From the flow charts (figs. 80 and 81), it can be seen that the bulk of the computations is performed in the subroutine "Search". The main program is used to input the variables required for the attenuation calculation and to compute the normalized boundary admittance.

For the subroutine "Search", the first problem was that of finding an adequate first approximation for g which is required to solve transcendental equations (4) and (5) using the Newton-Raphson technique. The modes are defined as being first-even, second-even, third-even, first-odd, or second-odd according to the location of solutions in the complex g-plane, and a method was required, therefore, which would not only produce the five required solutions but would also identify the solutions with their mode numbers. The technique which proved to be best for the largest number of cases is indicated in figure 81. In this method, the initial values of g_1 and g_2 for each mode was selected from experience and form the starting points for the calculations. The real and imaginary parts are then incremented to produce four new trials. The best of the five values replaces the central value and the process is repeated until the central

value is no longer improved. This value becomes the starting point in the Newton-Raphson technique. The remainder of subroutine "Search" computes the mode decay coefficients and attenuation.

CONCLUSIONS

Program Results

Impedance Measurements

- The effects on impedance of increasing grazing airflow velocities, increasing sound pressure levels, and increasing steady flow through the specimen were similar for all the acoustic specimens tested. This effect was that the resistance increased and the reactance generally decreased.

- The rate at which the impedance properties changed was different for each specimen. These rates fell into definite and recognizable patterns for each type of material.

- It is believed that boundary layer fluctuations due to grazing flow velocities cause low-frequency airflows through the specimens. Thus ratios of grazing-flow-velocities to through-flow-velocities producing the same change in the resistance of the specimens can be established. For the test conditions of this facility, the respective ratios for 300 and 500 fps were approximately eight and five to one.

- Comparison of the acoustic characteristics of specimens subjected to different boundary layer profiles and having the same free-stream velocity showed that small changes of boundary layer had no major effect on the impedance of the specimens.

- Hot-wire instrumentation can be a valuable aid in investigating the acoustic characteristics of perforated plates.

Analytical Studies

- From the analysis, it was concluded that the linear sound wave equations do not lead to correct predictions of acoustic attenuation in a lined duct when the sound pressure level is high. An overall level of 150 dB was used in these tests. It is possible to empirically modify the linear theory so as to improve agreement between predicted and measured values. The modification introduces one parameter that is determined experimentally and depends on treatment length and sound pressure level but not on the type of material used.

- The effect of flow in the duct on acoustic attenuation can be approximated with the wave equation that does not account for flow if the impedance of the lining materials was measured in an impedance tube with flow and the flow velocity is below Mach 0.5. At high flow velocities, the wave equations for a moving medium, derived in the section titled "Effects of Flow on Sound Attenuation" must be used.

Recommendations for Future Duct Lining Programs

Impedance Measurements

Future investigations of the characteristics of duct lining materials should place emphasis in relating the environmental conditions of the test facility to those of a fan duct. Impedance data of acoustic specimens should be obtained for boundary layer fluctuations, flow velocities, and sound pressure levels which have been demonstrated to be realistic fan engine conditions.

Representative acoustic specimens should be selected for the following tests:

- The investigation of the effect of boundary layer variation on the impedance of specimens subjected to grazing flow velocities should be continued. As part of this program, the boundary layer "noise" as sensed by a microphone flush mounted in the wall of the test duct should be investigated. Similar boundary layer "noise" measurements should be made at various locations in fan-engine ducts to establish a comparision with the rig test condition.

- The investigation of the effects of a steady, air velocity through the specimens on the acoustic impedance should be continued. Since it is believed that boundary layer fluctuations produced by grazing air flows cause airflow through acoustic specimens, the relationship of the grazing and through-flow velocities should be investigated further. Hot-wire instrumentation should be utilized for this investigation.

- An investigation of the effect of increasing the sound pressure levels on the acoustic impedance should be continued. Means for generating greater sound pressure levels should be developed.

- The effects on acoustical properties of grazing airflow, through airflow, boundary layer variations, and sound pressure levels should be related to the acoustic properties described by the D.C. flow resistance curves. It should be an aim to develop the capability to relate the environmental conditions in a turbofan duct to the D.C. flow

resistance curves for an acoustic lining material so that these curves could be used to estimate the acoustic properties of the material for that condition.

- The effect on impedance of superimposing two incident sound pressure waves of significantly different frequencies should be investigated. This would be the first step in determining whether standard impedance tube data on the properties of materials subjected to discrete frequencies is applicable to the broad band noise spectra in turbofan engines.

Analytical Section

Additional analytical studies are recommended for the following three areas:

- Effects of large values of sound pressure levels
- Effects of altering the structure of honeycomb materials
- Effects of duct geometry.

The effect of large values of sound pressure level on attenuation should be studied further. While part of the change in attenuation associated with high levels of sound pressure can be attributed to a change in properties of the boundary material, some of the change must also be ascribed to the onset of nonlinearity in the volume of the duct. This area will require additional work if the problem is to be sufficiently understood.

Experience has shown that the introduction of drainage holes in honeycomb materials sometimes reduces attenuation. Replacing honeycomb material with a set of channels has had the same effect. A study into the basic causes could provide important information. To properly understand and to utilize this effect,the equation for sound waves in the honeycomb cell will have to be solved and the cell waves matched with those in the duct. Since resonances can occur in the cells, it can be expected that attenuation will be enhanced with a proper choice of cell size.

The effects of the various duct geometries on attenuation should also be examined. This study should include annular ducts and offset ducts.

REFERENCES

1. Standard Method for Impedance and Absorbtion of Acoustical Materials by the Tube Method, ASTM Designation C 384-58, 1958

2. Morse, P.M., Vibration and Sound, 2nd Edition, McGraw-Hill, 1948

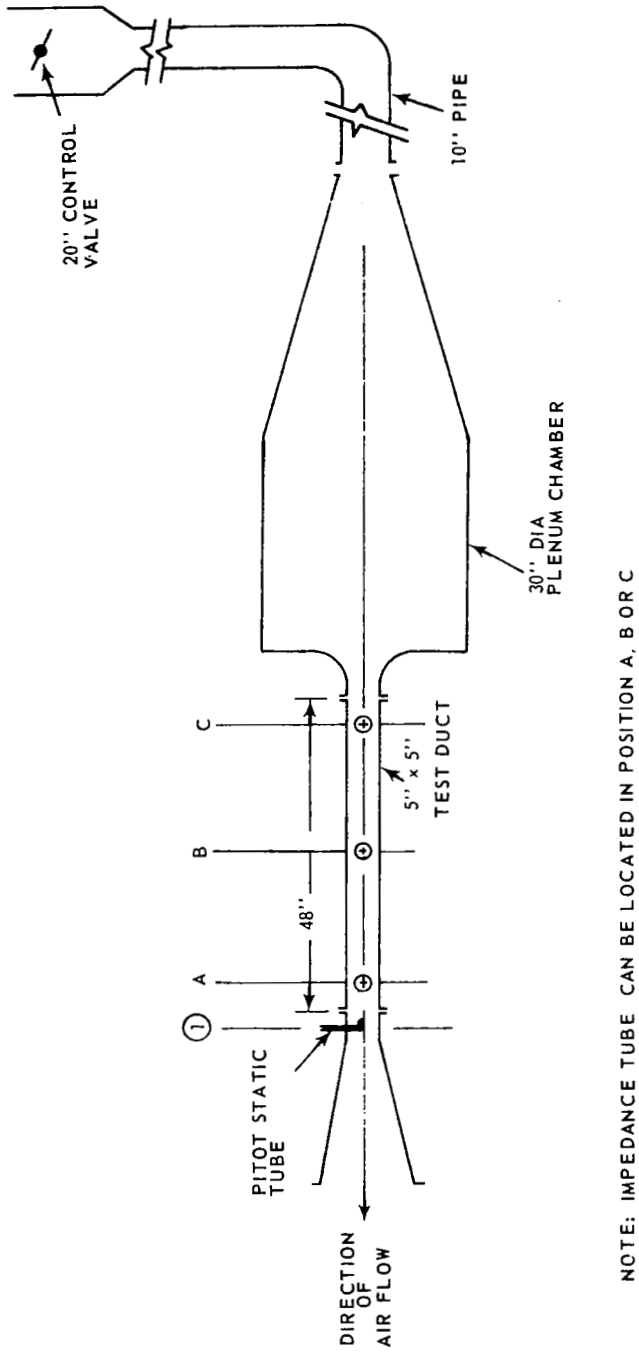

Figure 1 Impedance-Tube-With-Flow Test Facility Piping Layout

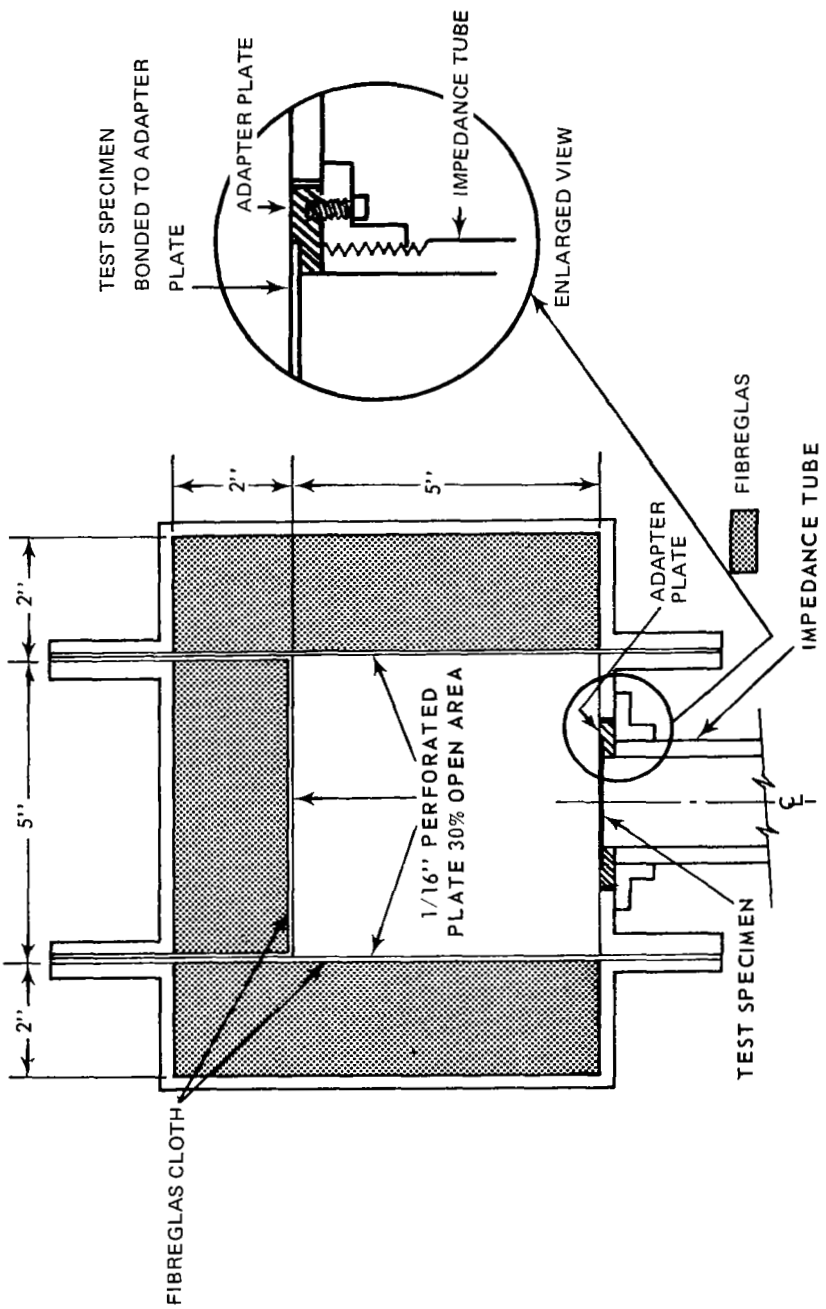

Figure 2 Cross-Section of 5 in x 5 in. Test Duct

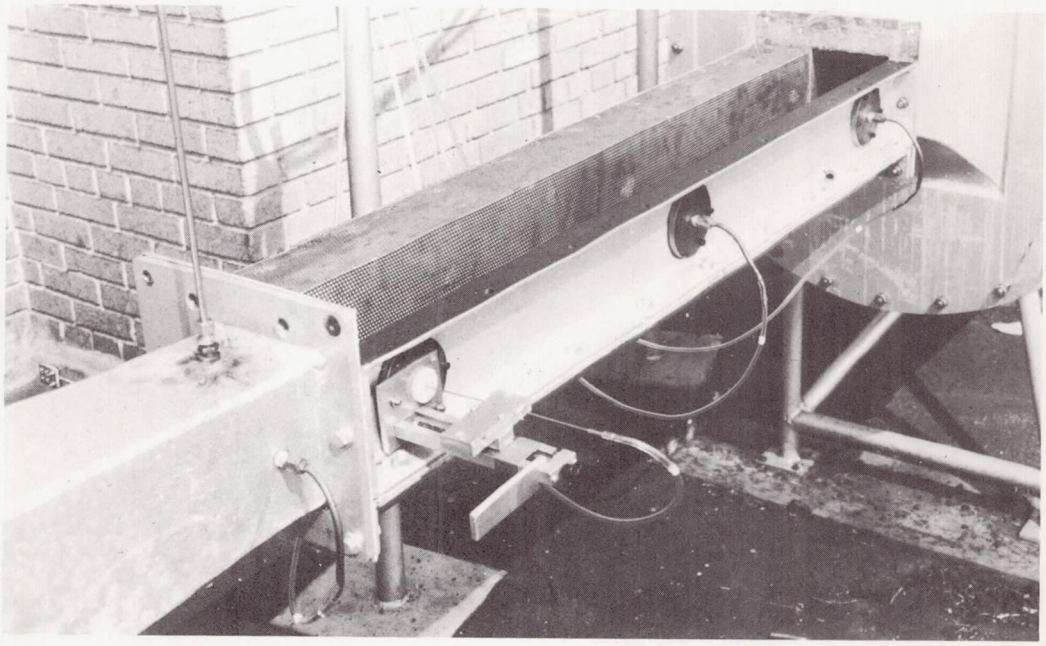

Figure 3 Impedance-Tube- With-Flow Test Facility

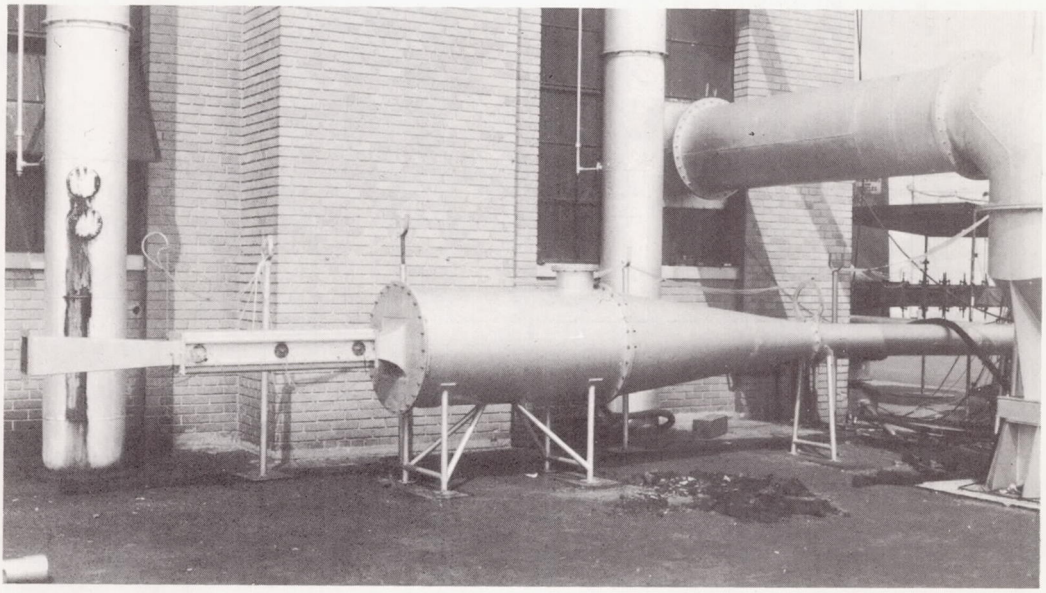

Figure 4 Impedance-Tube-With-Flow Test Facility Showing Piping and Test Duct

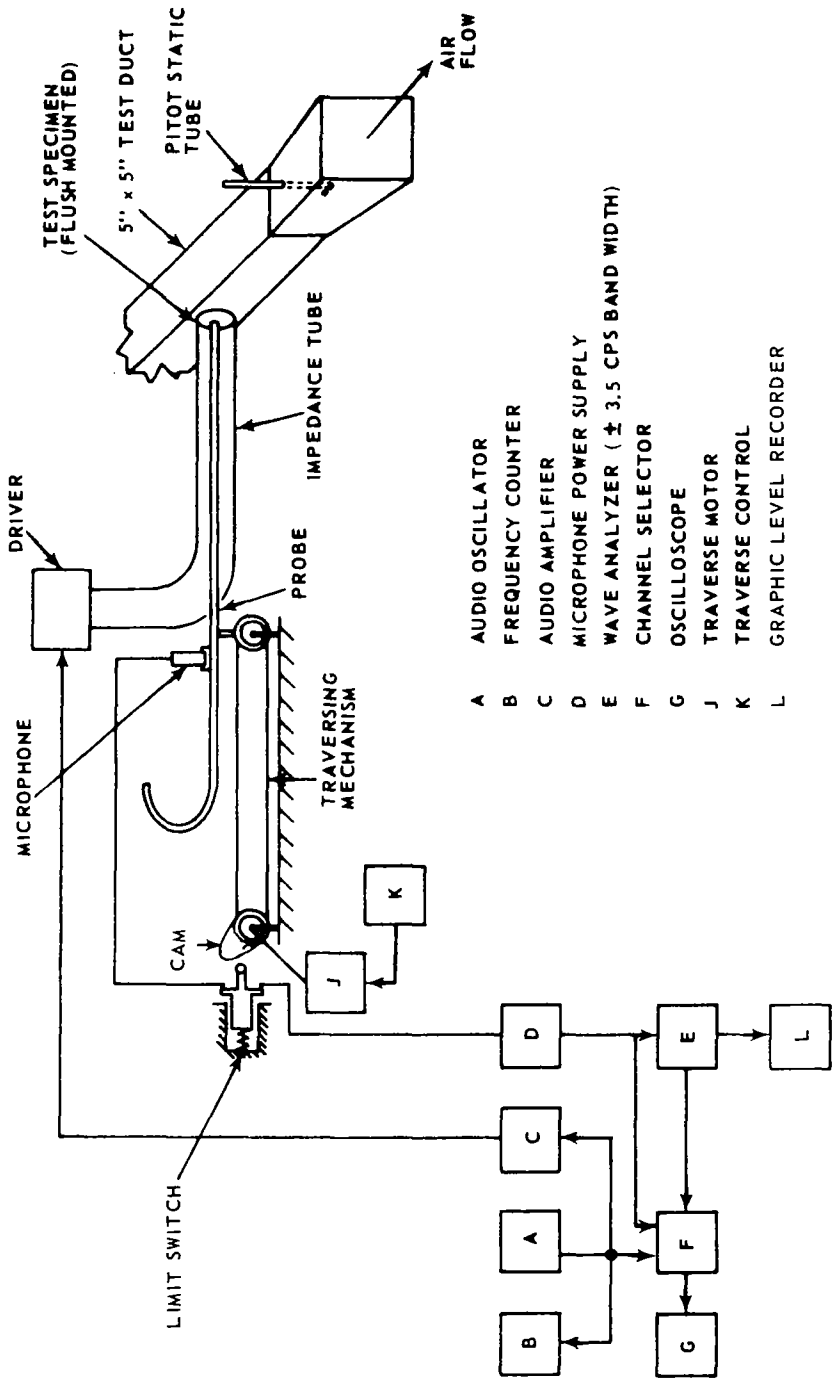

Figure 5 Impedance Tube Test Rig Electrical Schematic

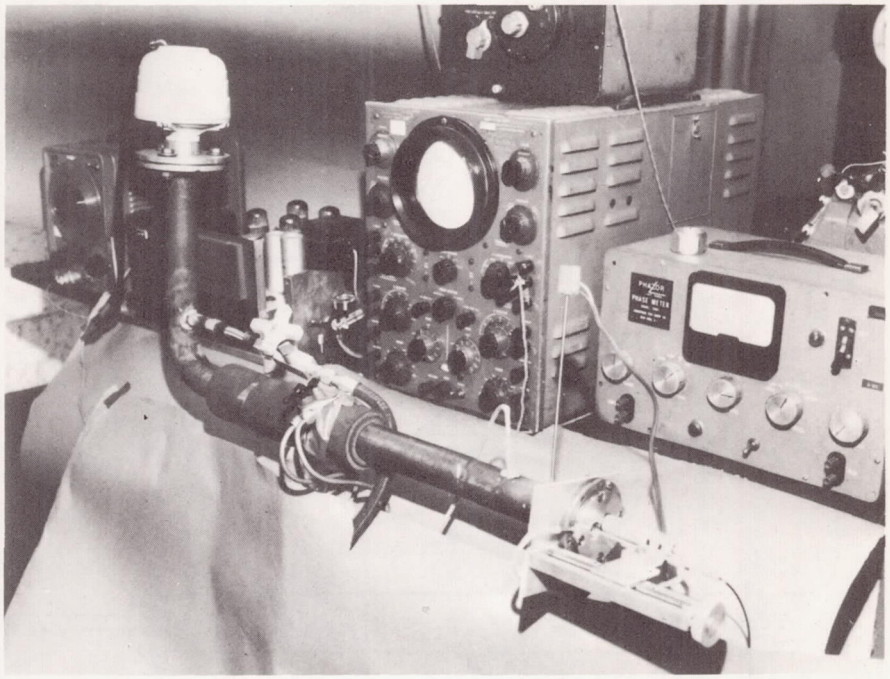

Figure 6 Impedance Tube With Hot-Wire Instrumentation

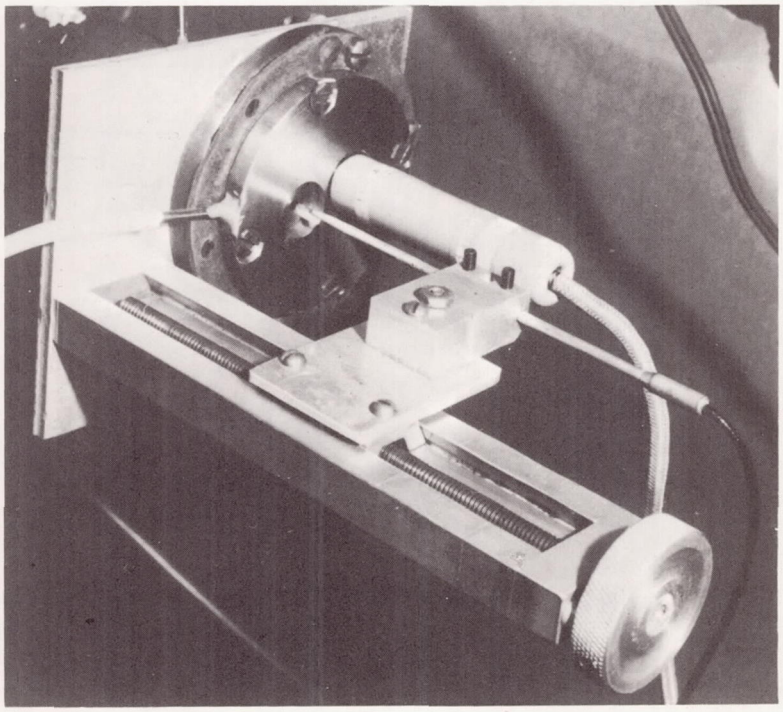

Figure 7 Hot-Wire Probe and Traversing Mechanism

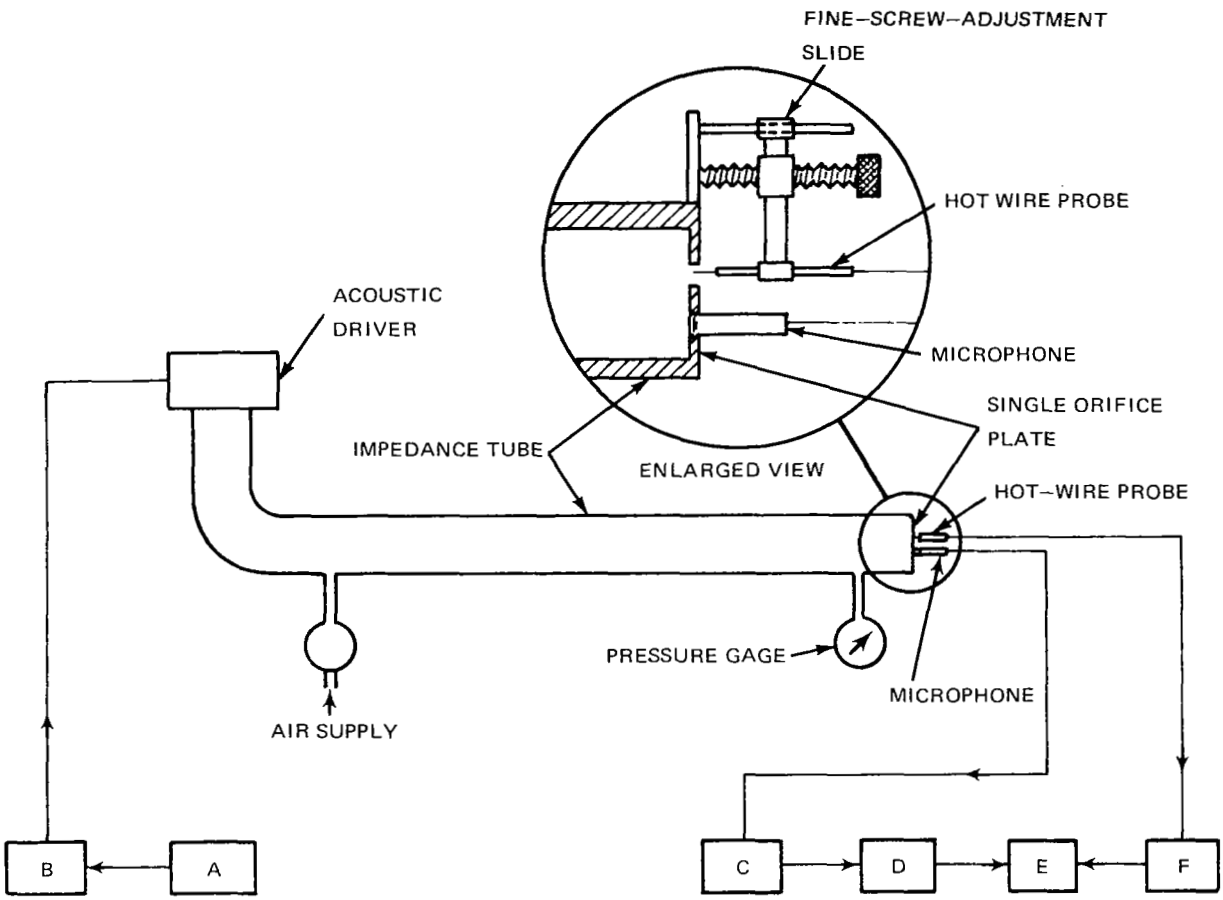

A AUDIO OSCILLATOR
B AUDIO AMPLIFIER
C MICROPHONE POWER SUPPLY
D WAVE ANALYZER (±3.5 CPS BAND WIDTH)
E DUAL BEAM OSCILLOSCOPE
F HOT–WIRE ANNEMOMETER

Figure 8 Impedance Tube With Hot-Wire Instrumentation Electric Schematic

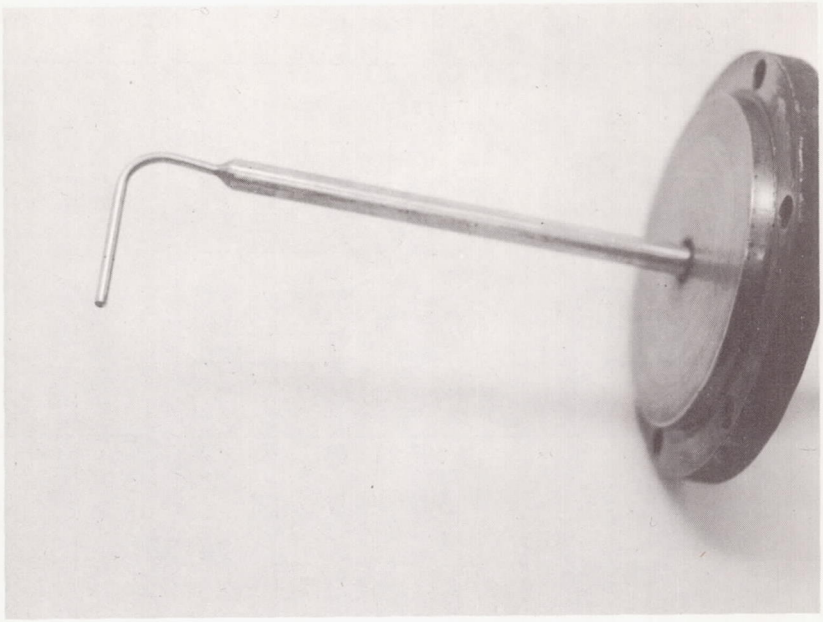

Figure 9 Pitot Static Tube With Adapter Plate

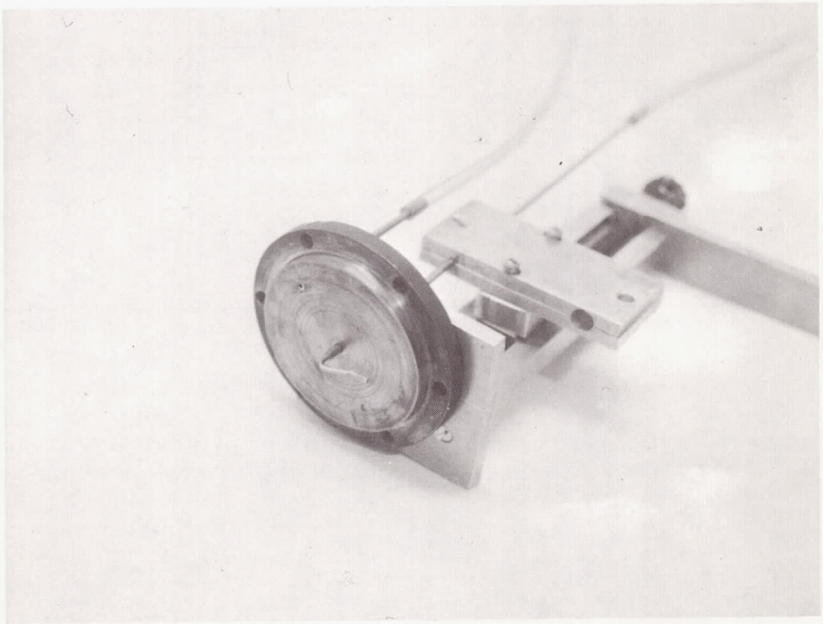

Figure 10 Preston Tube With Adapter Plate

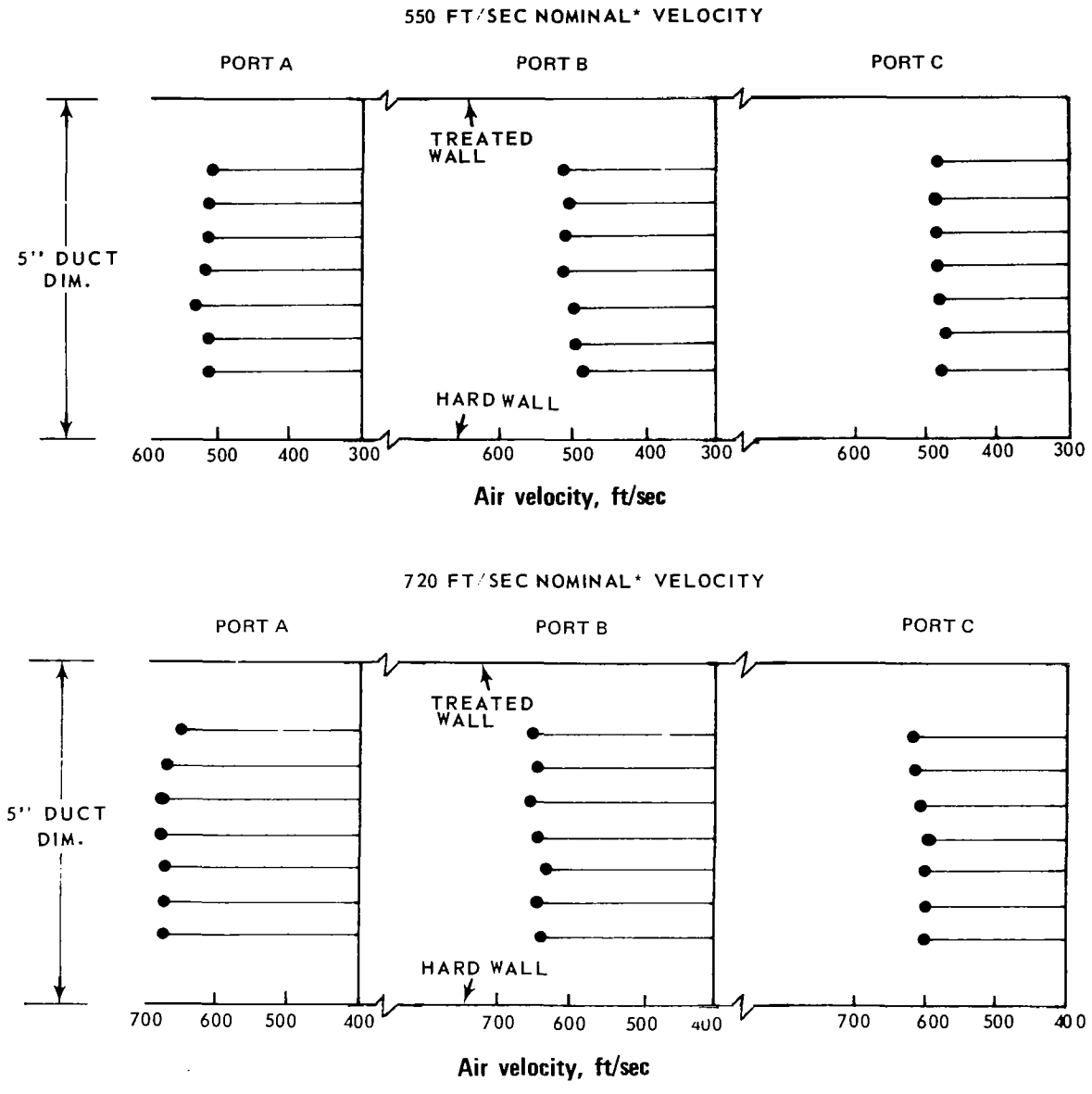

*NOMINAL VELOCITY MEASURED AT CENTER OF 5" x 5" DUCT IN POSITION 1 LOCATION OF POSITION 1, A, B, AND C SHOWN IN FIGURE 1.

Figure 11 Velocity Profile in 5 in. x 5 in. Test Duct

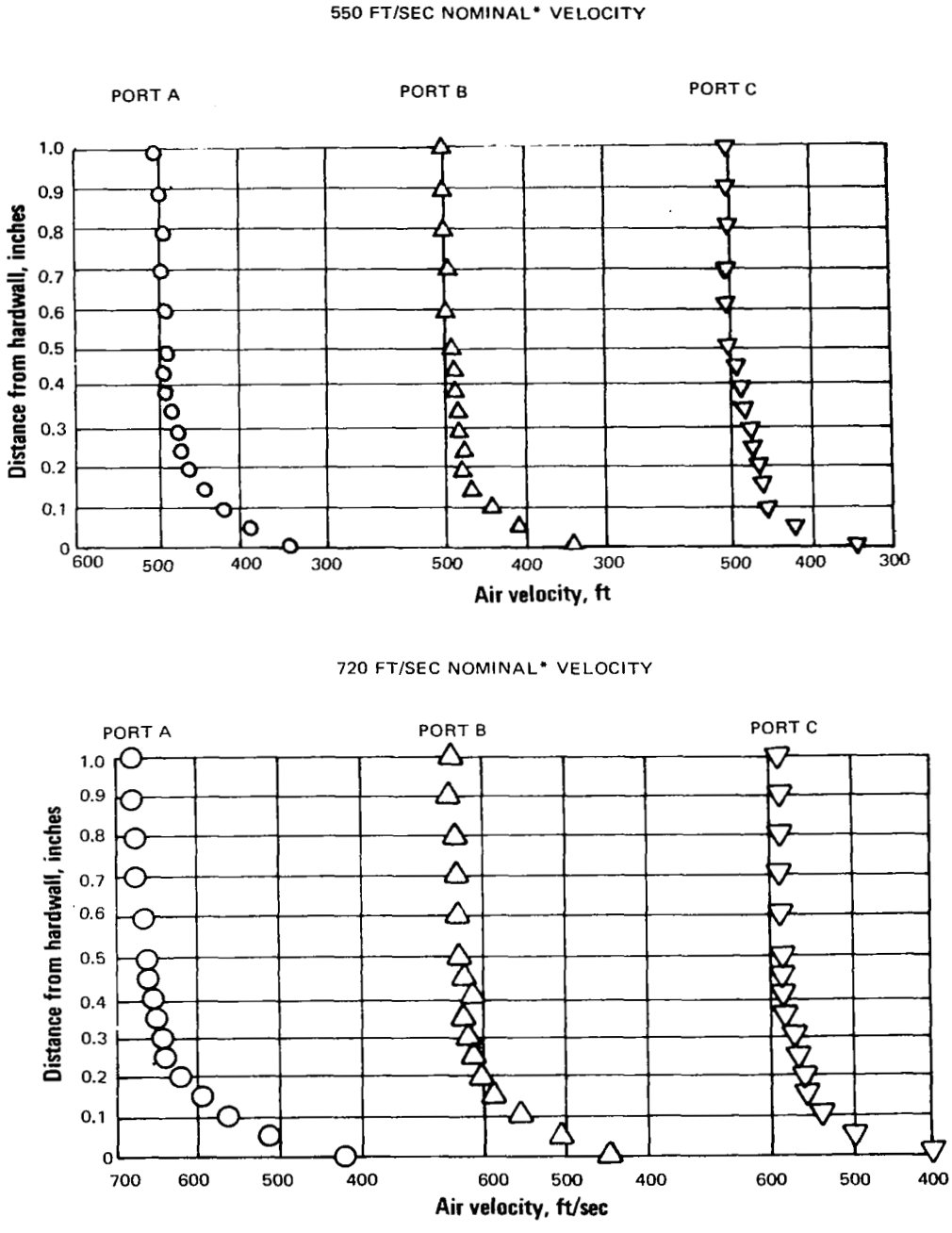

*NOMINAL VELOCITY MEASURED AT CENTER OF 5" x 5" DUCT IN POSITION 1
LOCATION OF POSITION 1, A, B, AND C SHOWN IN FIGURE 1.

Figure 12 Boundary Layer Profile in 5 in. x 5 in. Test Duct

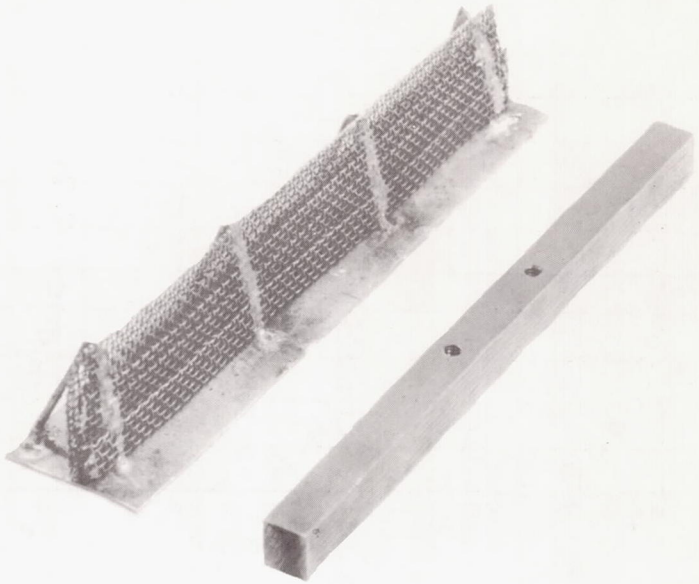

Figure 13 Variable Resistance and 5/16 x 5/16 Flow Spoilers

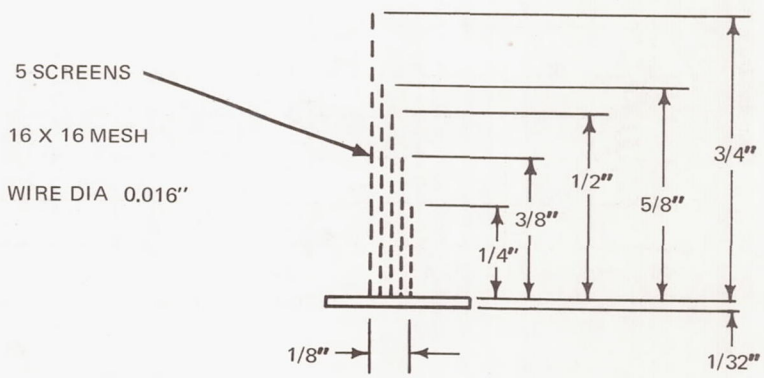

Figure 14 Variable Resistance Flow Spoiler

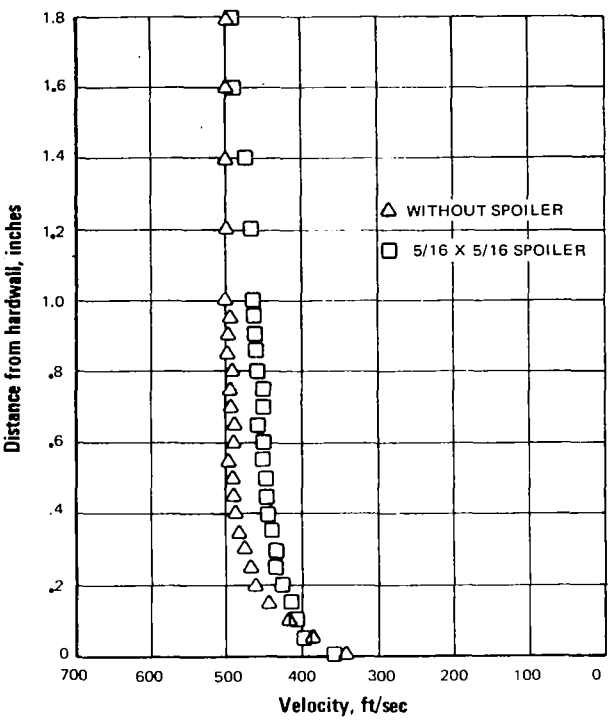

Figure 15 Boundary Layer Profile in Port A at 500 fps - Profiles are With and Without 5/16 x 5/16 Flow Spoiler in Port B

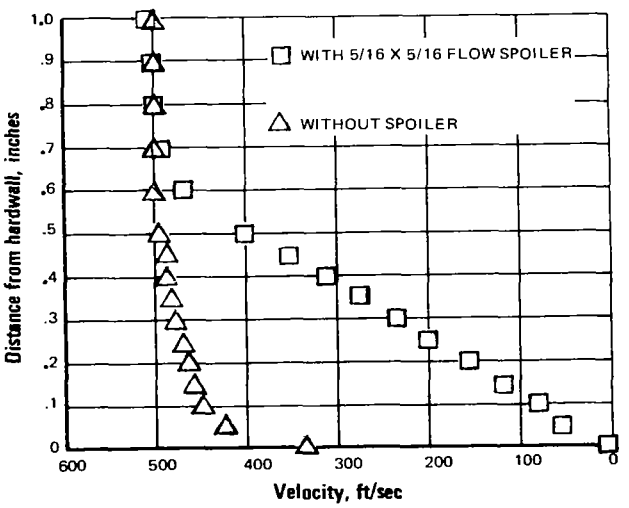

Figure 16 Boundary Layer Profile in Port C at 500 fps - Profiles are With and Without 5/16 x 5/16 Flow Spoiler Located Three Inches Upstream of Port C

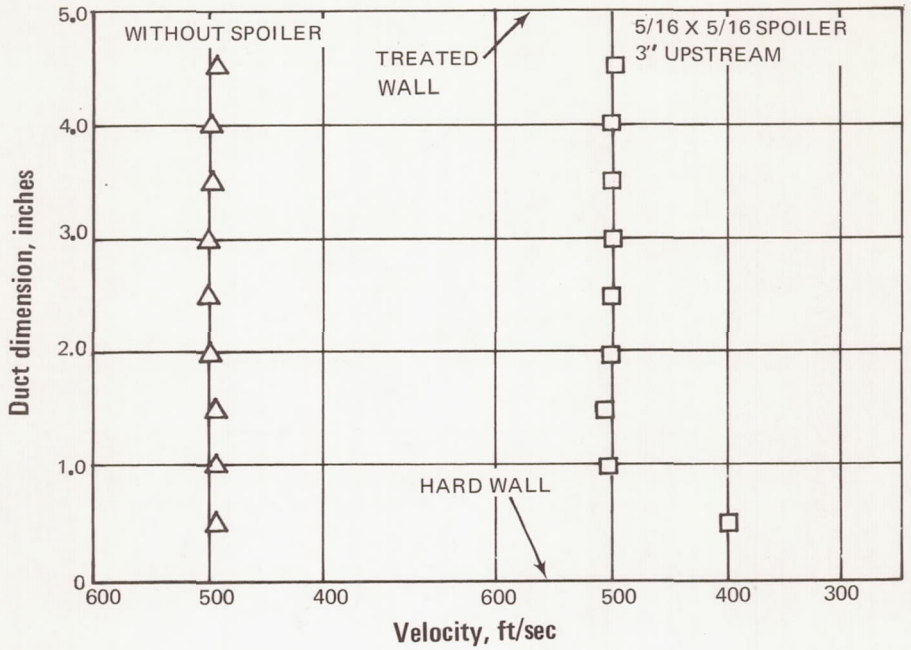

Figure 17 Velocity Profile in Port A at 500 fps - Profiles are With and Without 5/16 x 5/16 Flow Spoiler Located Three Inches Upstream of Port C

Figure 18 Microphone Used for Boundary Layer Fluctuation Measurements

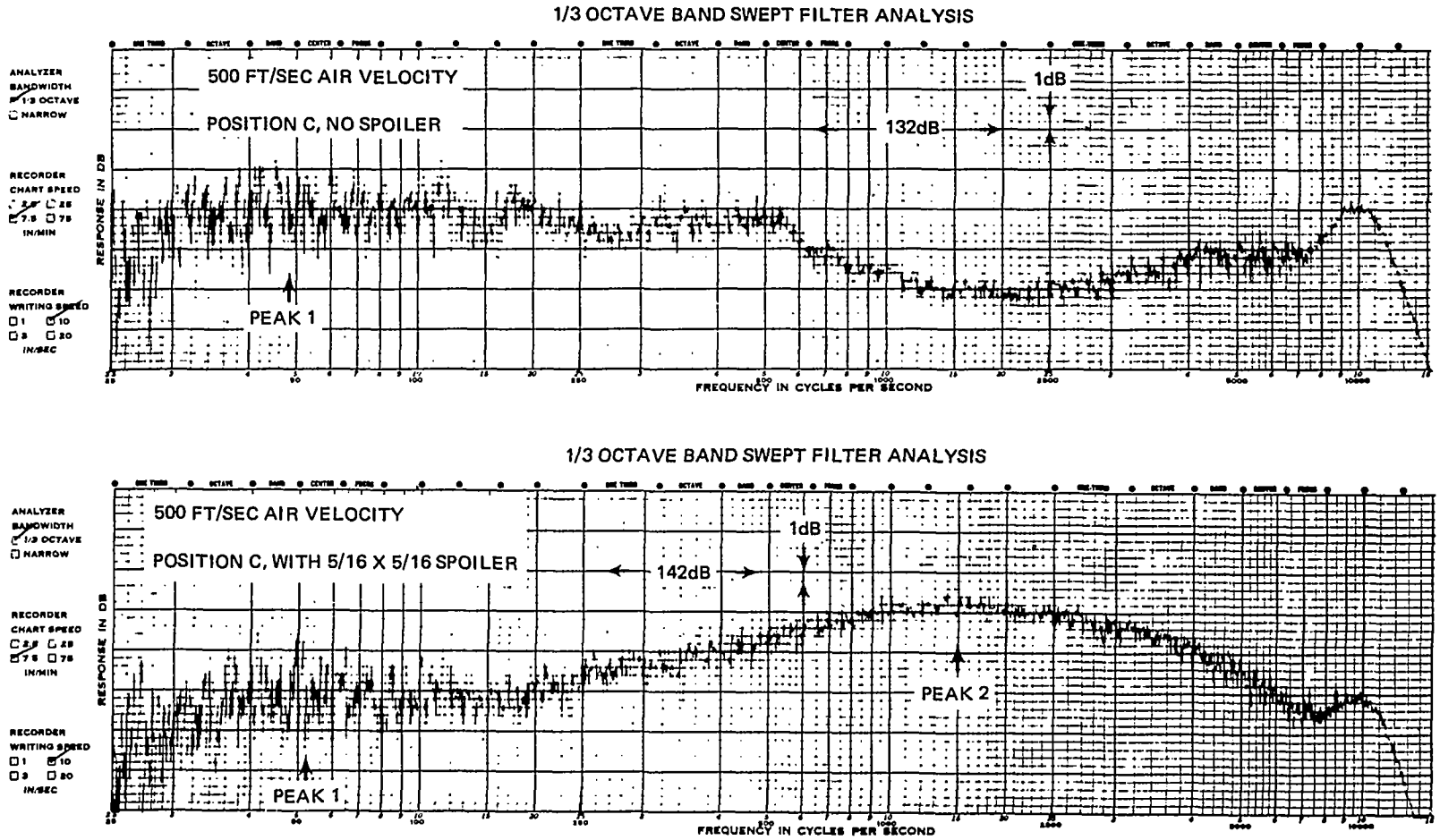

Figure 19 Noise Spectra at Port C at 500 fps With and Without Spoiler
Spectra Measured With ALTEC 21BR 180 - 7 Microphone

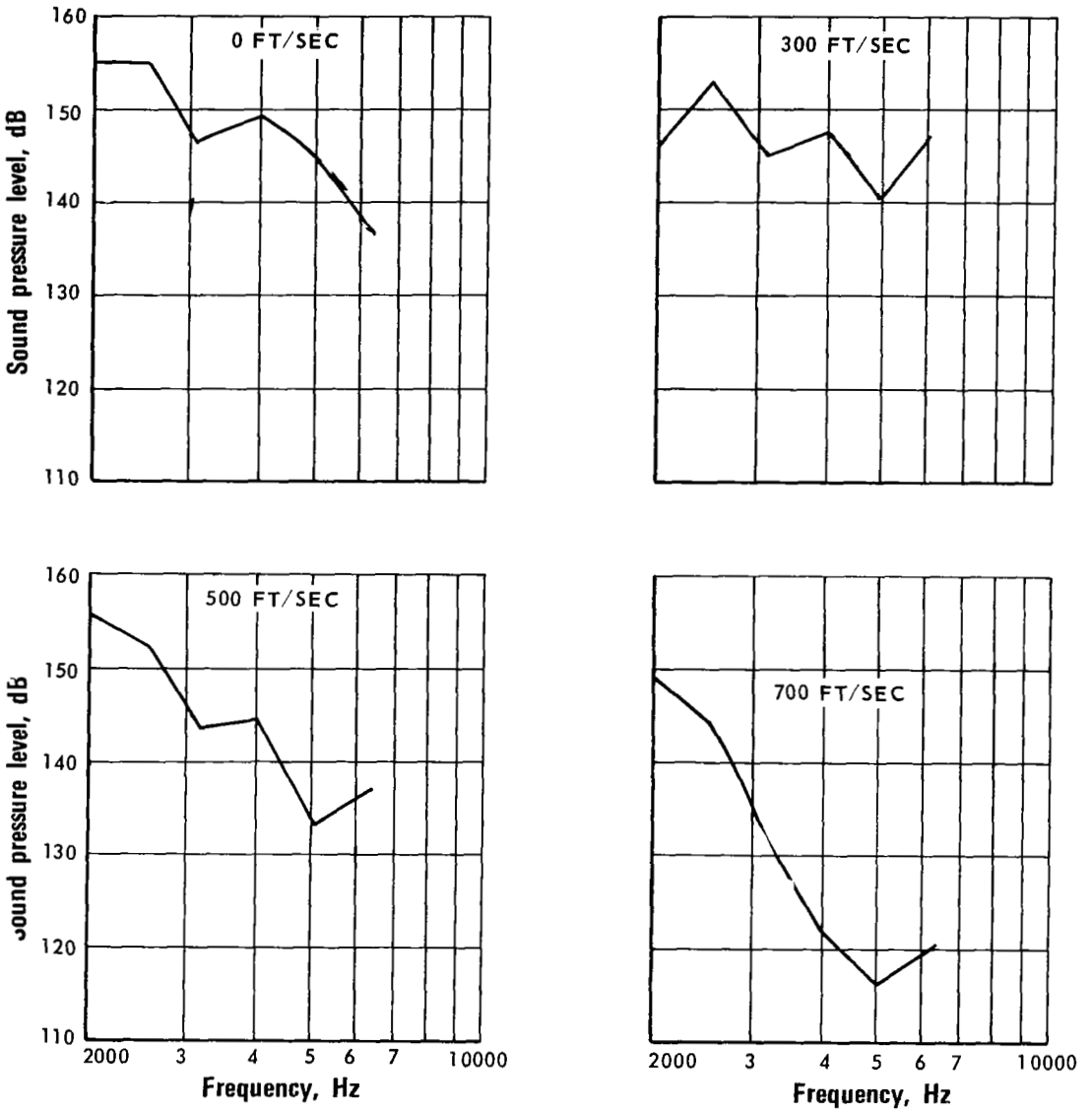

Figure 20 Sound Pressure Level Envelope for 0, 300, 500, and 700 fps Flow Velocity for a 22 Percent Open-Area, 0.098 in. Hole Dia., 0.015 in. Thick Perforated Plate (Specimen P-22)

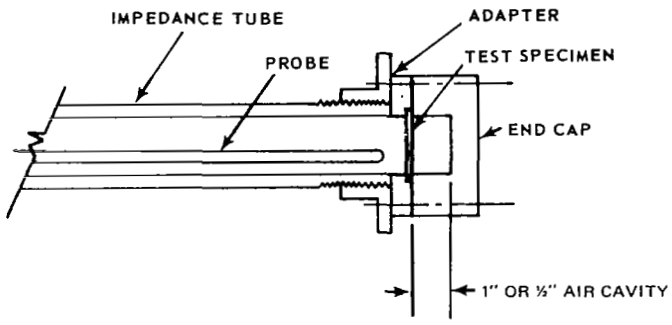

Figure 21 Test Fixture With Air Cavity

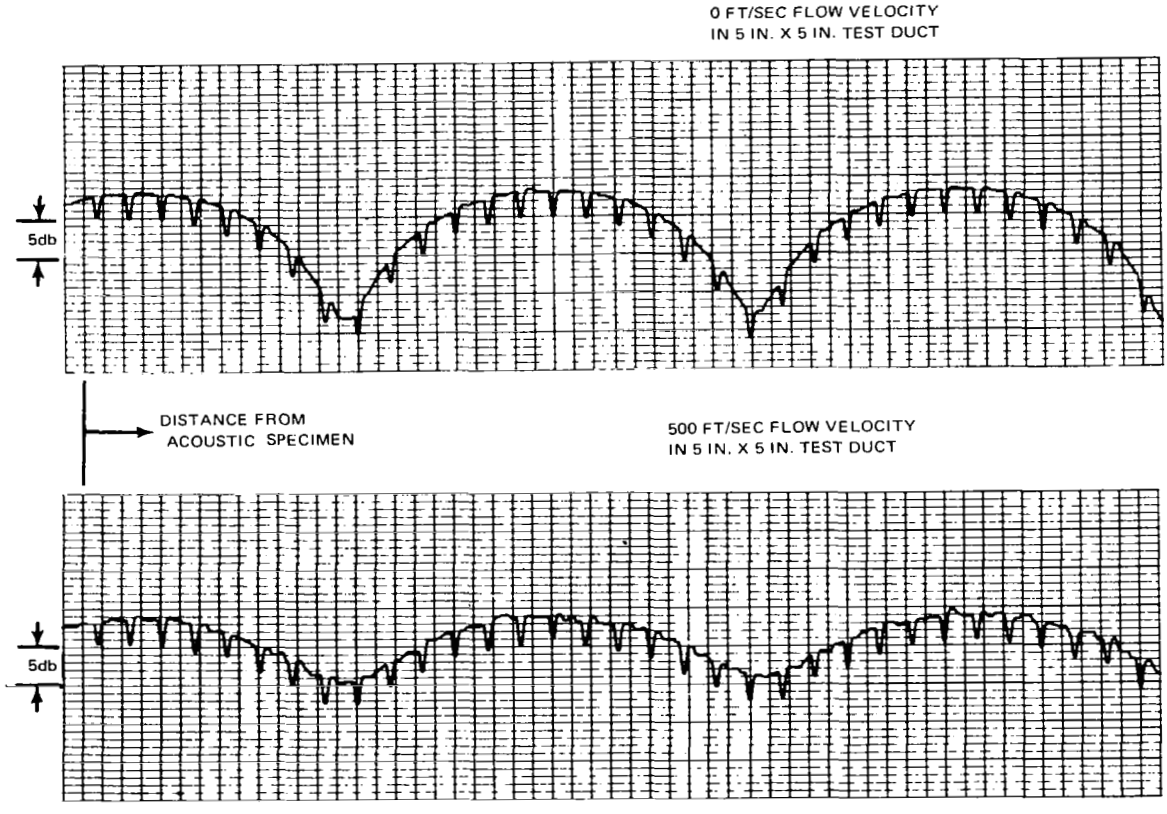

Figure 22 Typical Traces of Standing Wave Patterns in Impedance Tube

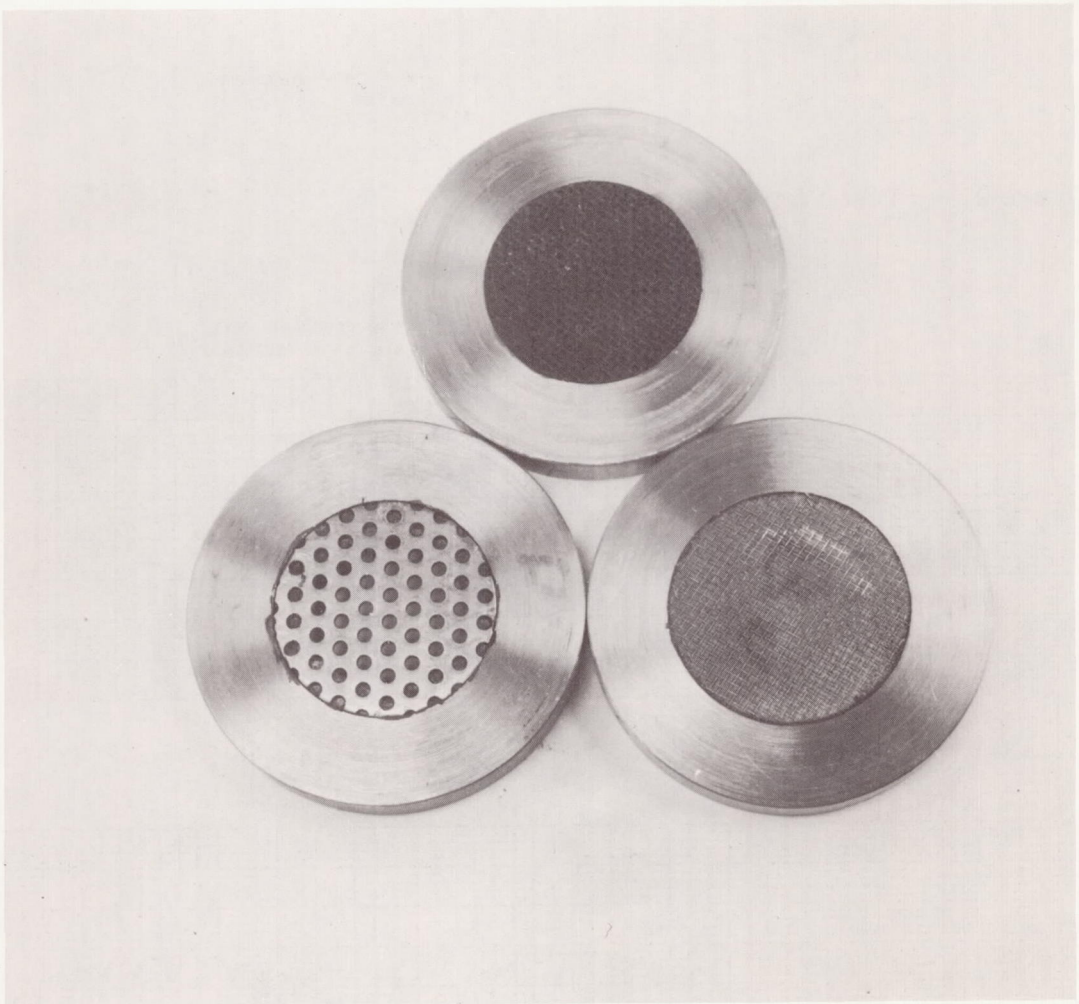

Figure 23 Acoustic Specimens Bonded to Adapter Plates for Testing

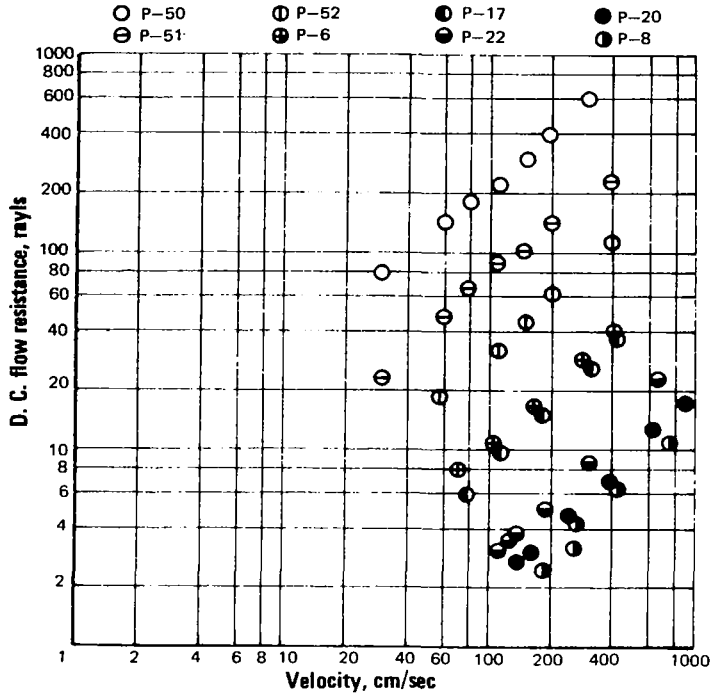

Figure 24 D.C. Flow Resistance, Perforated Plates

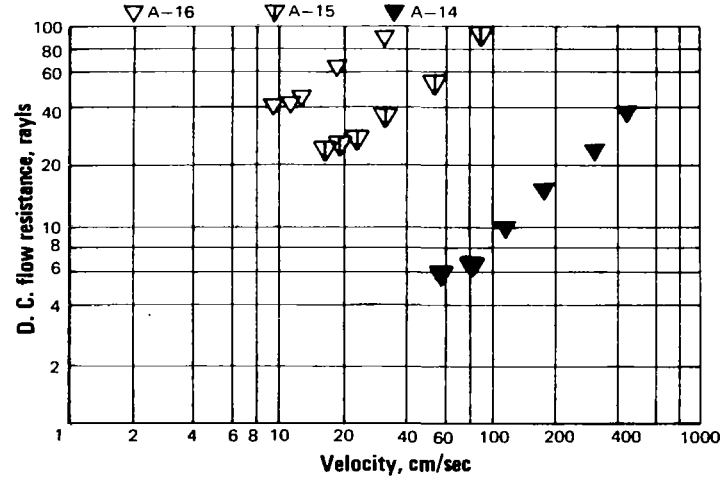

Figure 25 D.C. Flow Resistance, Polyimide Laminated Glass Cloth

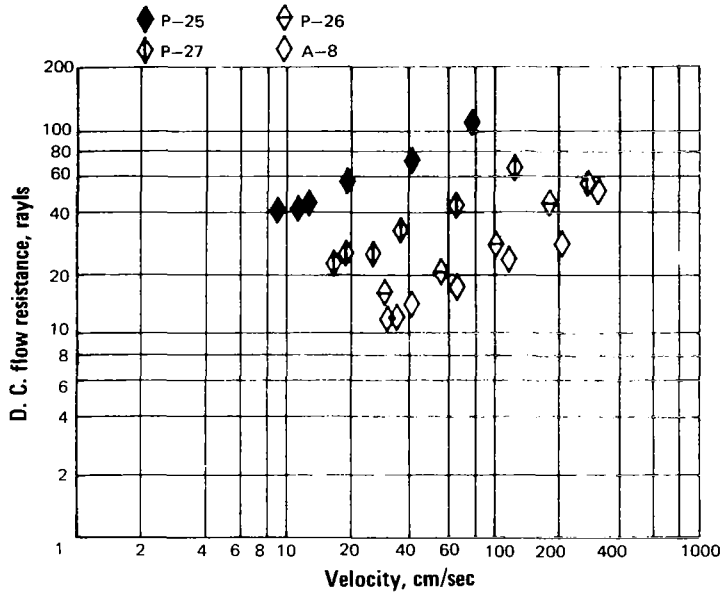

Figure 26 D. C. Flow Resistance, Screen and Perforated Plates With Screen

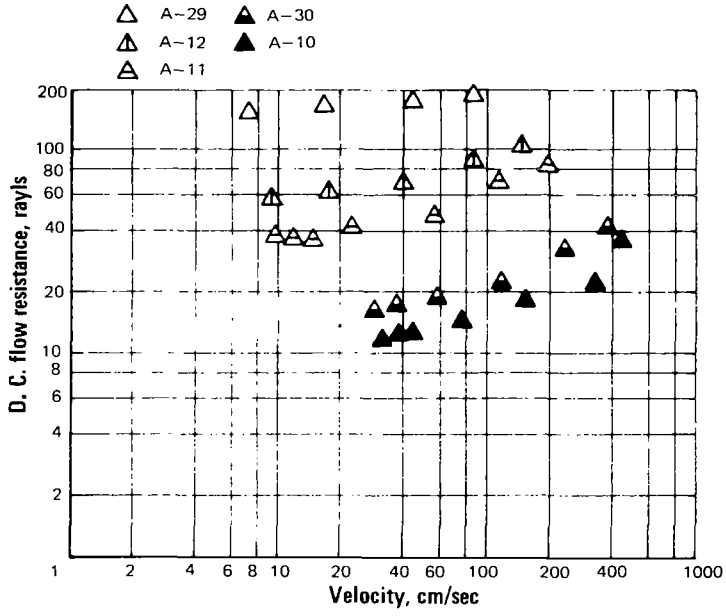

Figure 27 D. C. Flow Resistance, Feltmetal

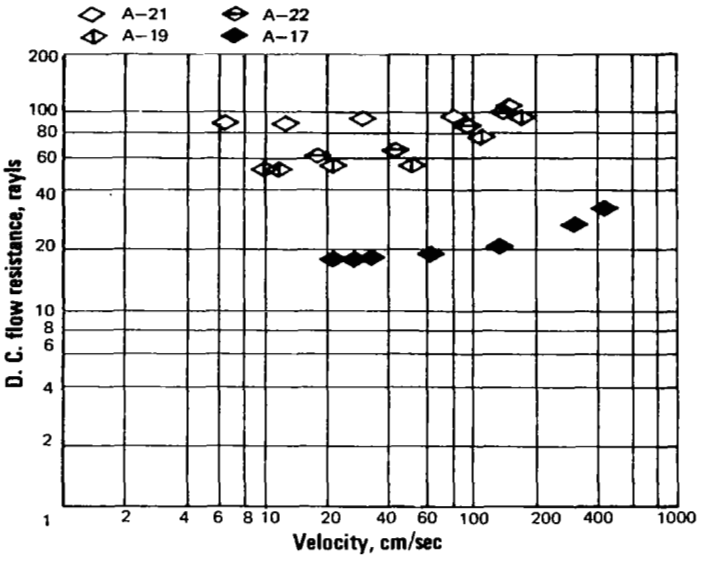

Figure 28 D.C. Flow Resistance, Rigimesh

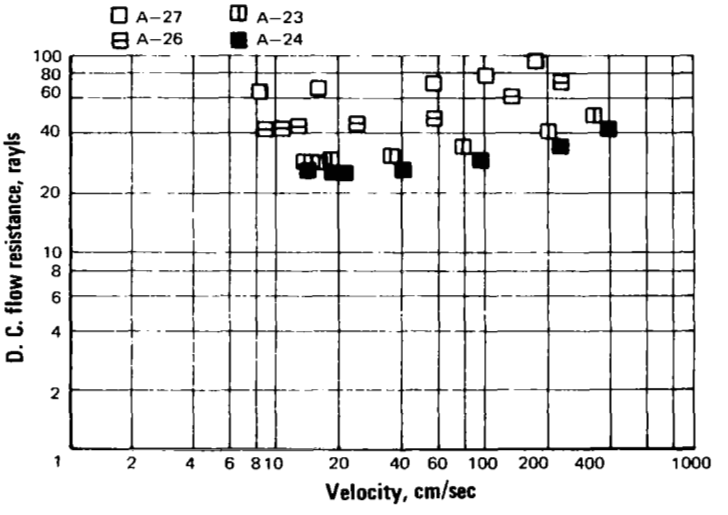

Figure 29 D.C. Flow Resistance, Brunsmet

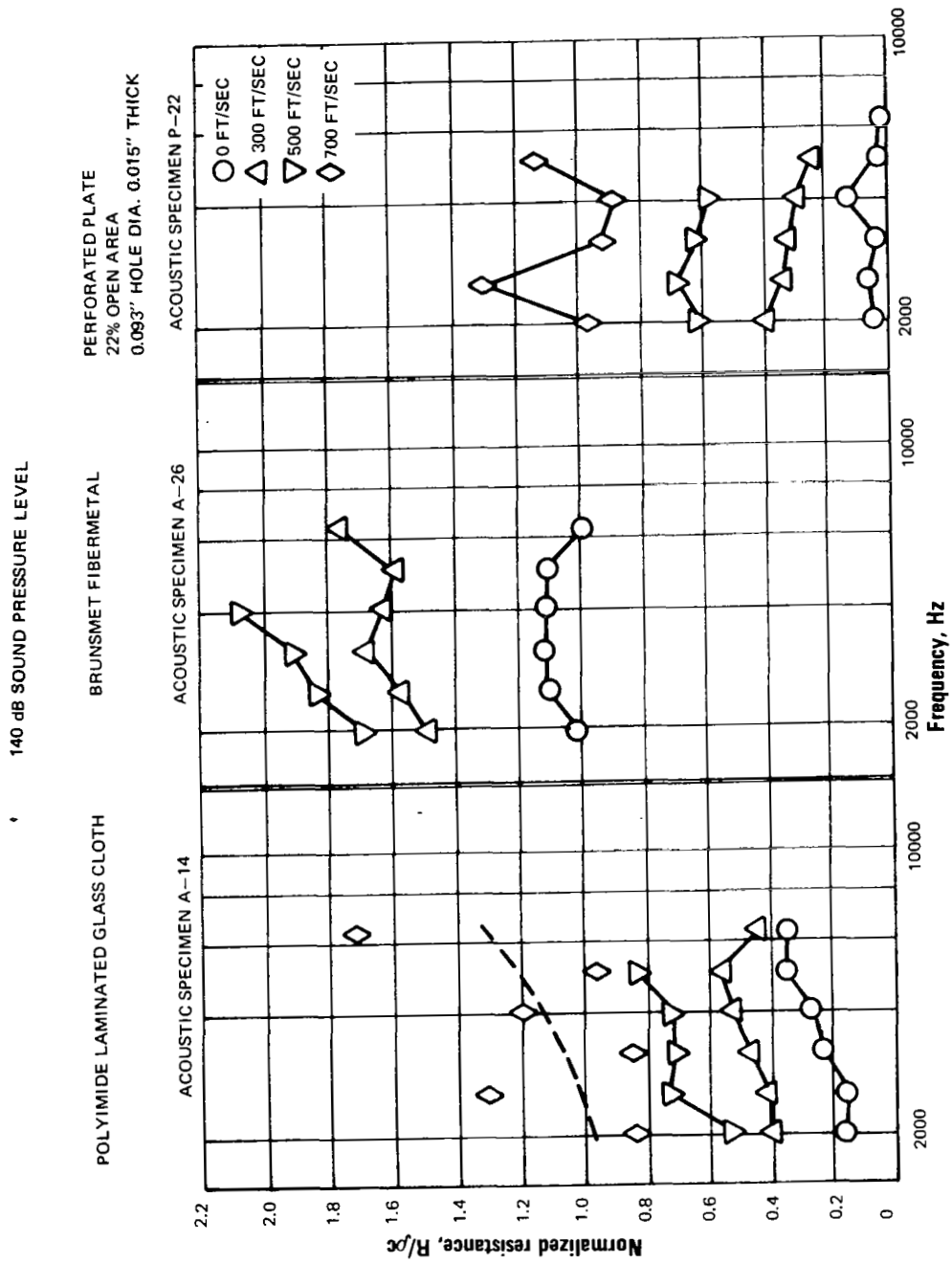

Figure 30 Effect on Acoustic Resistance of Grazing Flow Velocity at Port A for Three Specimens (A-14, A-26, and P-22)

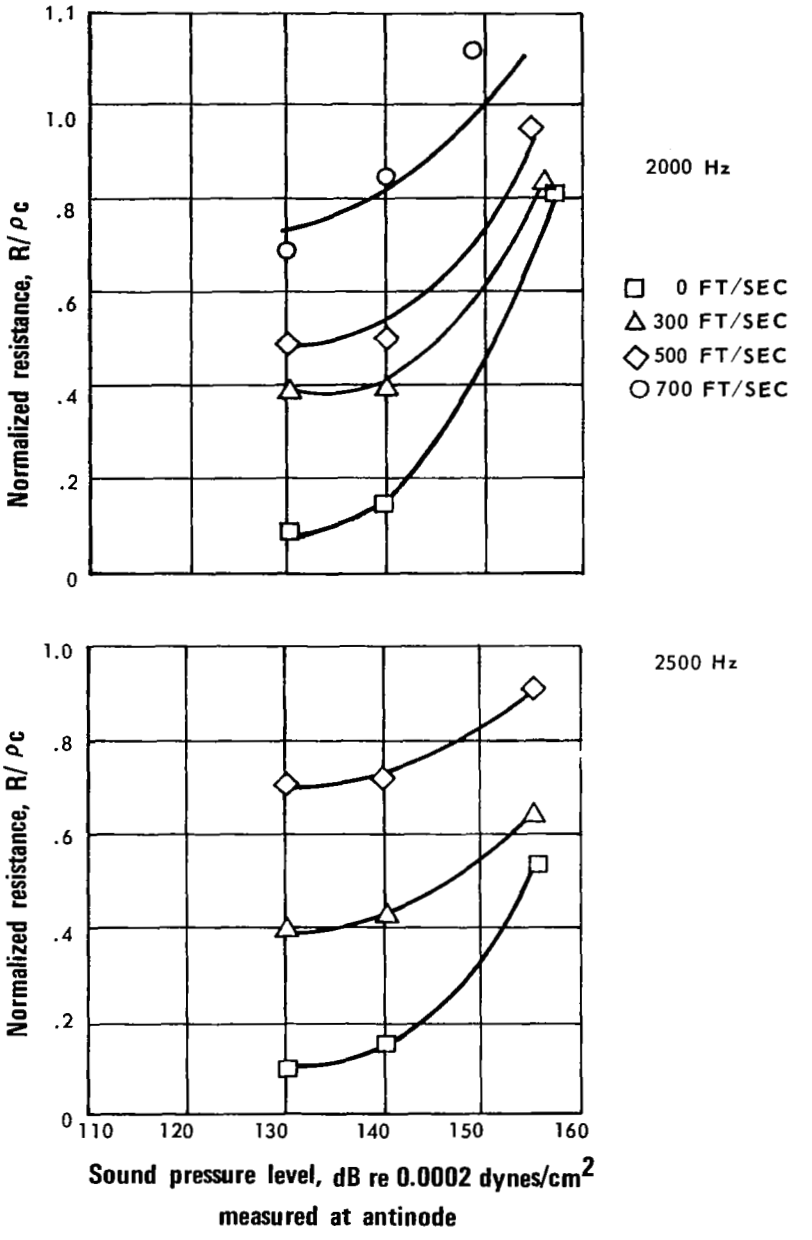

Figure 31 Effect on Acoustic Resistance of Sound Pressure Level at 2000 Hz and 2500 Hz for Polyimide Laminated Glass Cloth (Specimen A-14)

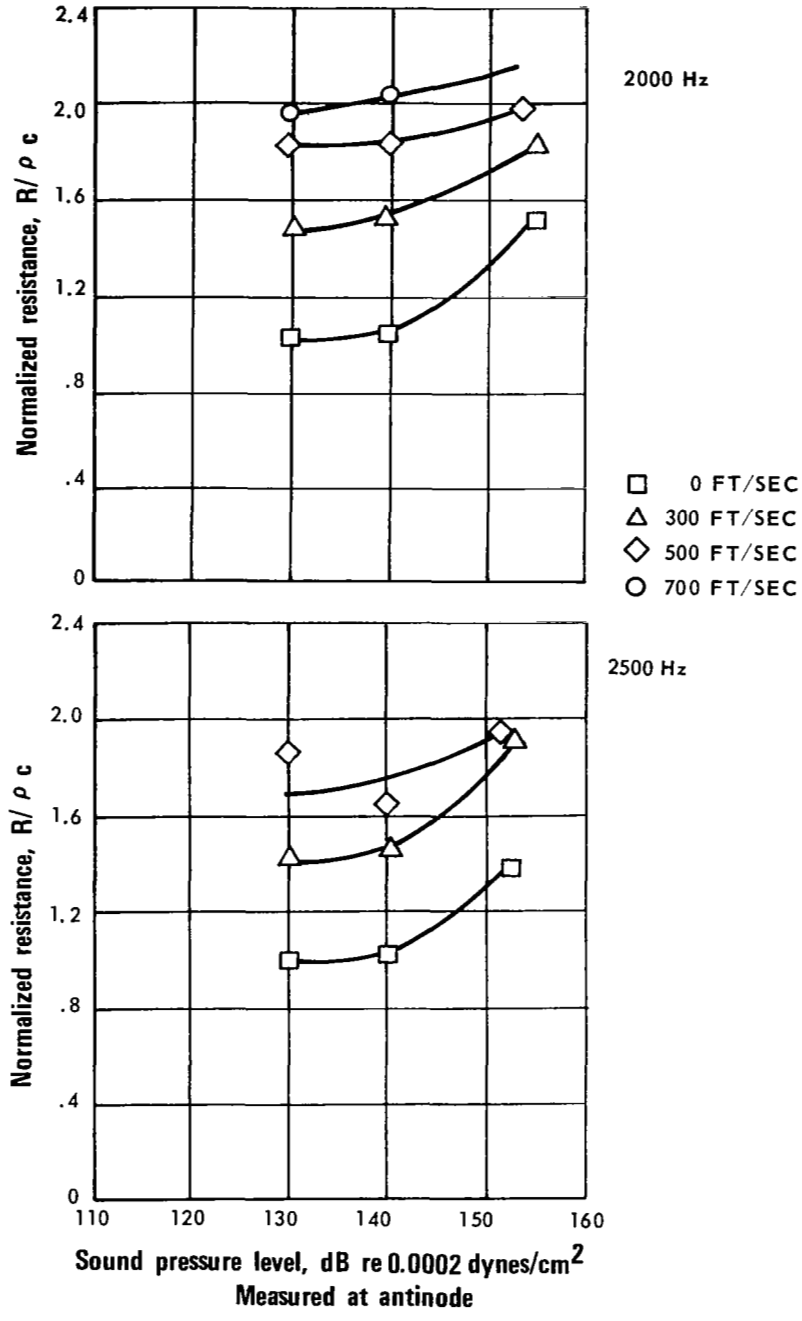

Figure 32 Effect on Acoustic Resistance of Sound Pressure Level at 2000 Hz and 2500 Hz for Fibermetal (Specimen A-26)

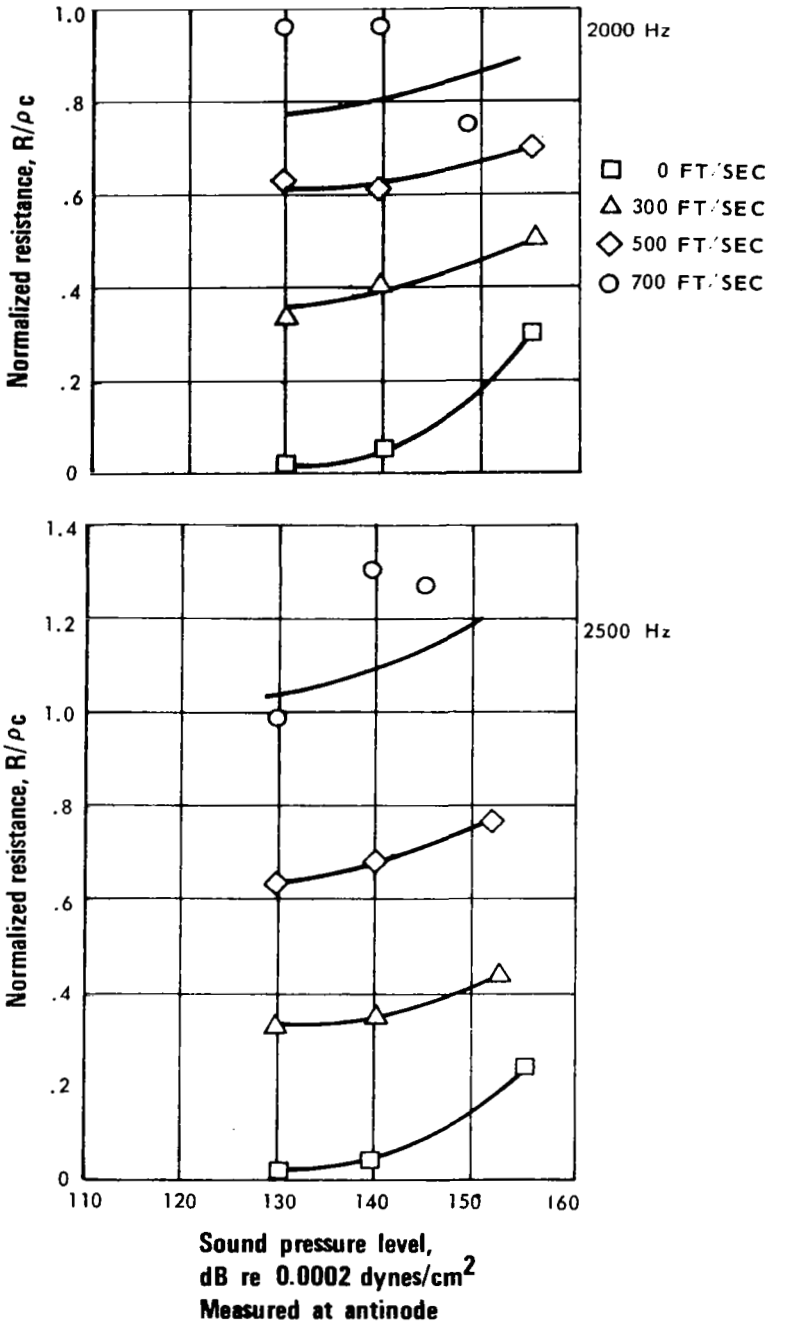

Figure 33 Effect on Acoustic Resistance of Sound Pressure Level at 2000 Hz and 2500 Hz for a 22 Percent Open-Area, 0.093 in. Hole Dia., 0.015 in. Thick Perforated Plate (Specimen P-22)

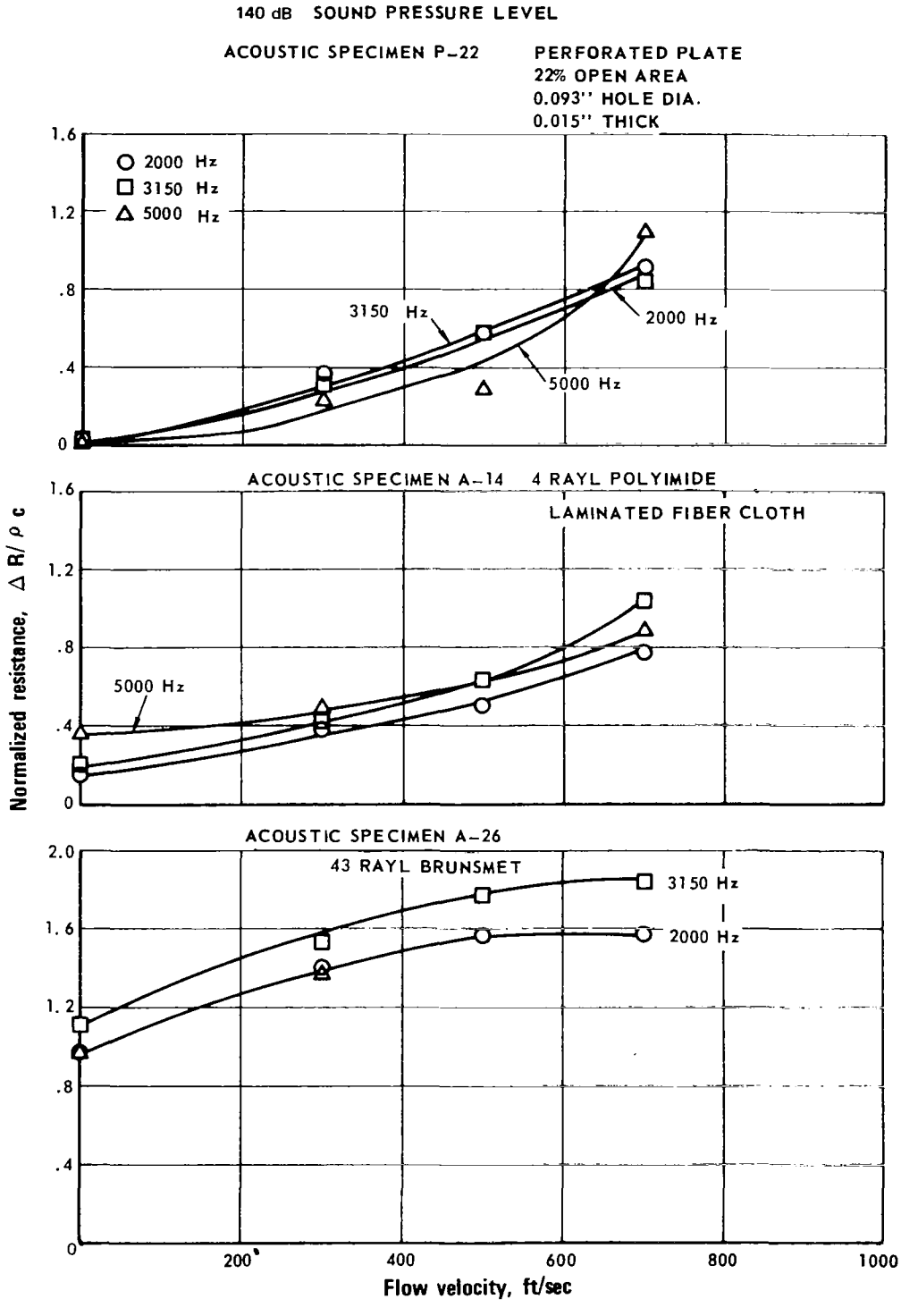

Figure 34 Effect on Acoustic Resistance of Grazing Flow

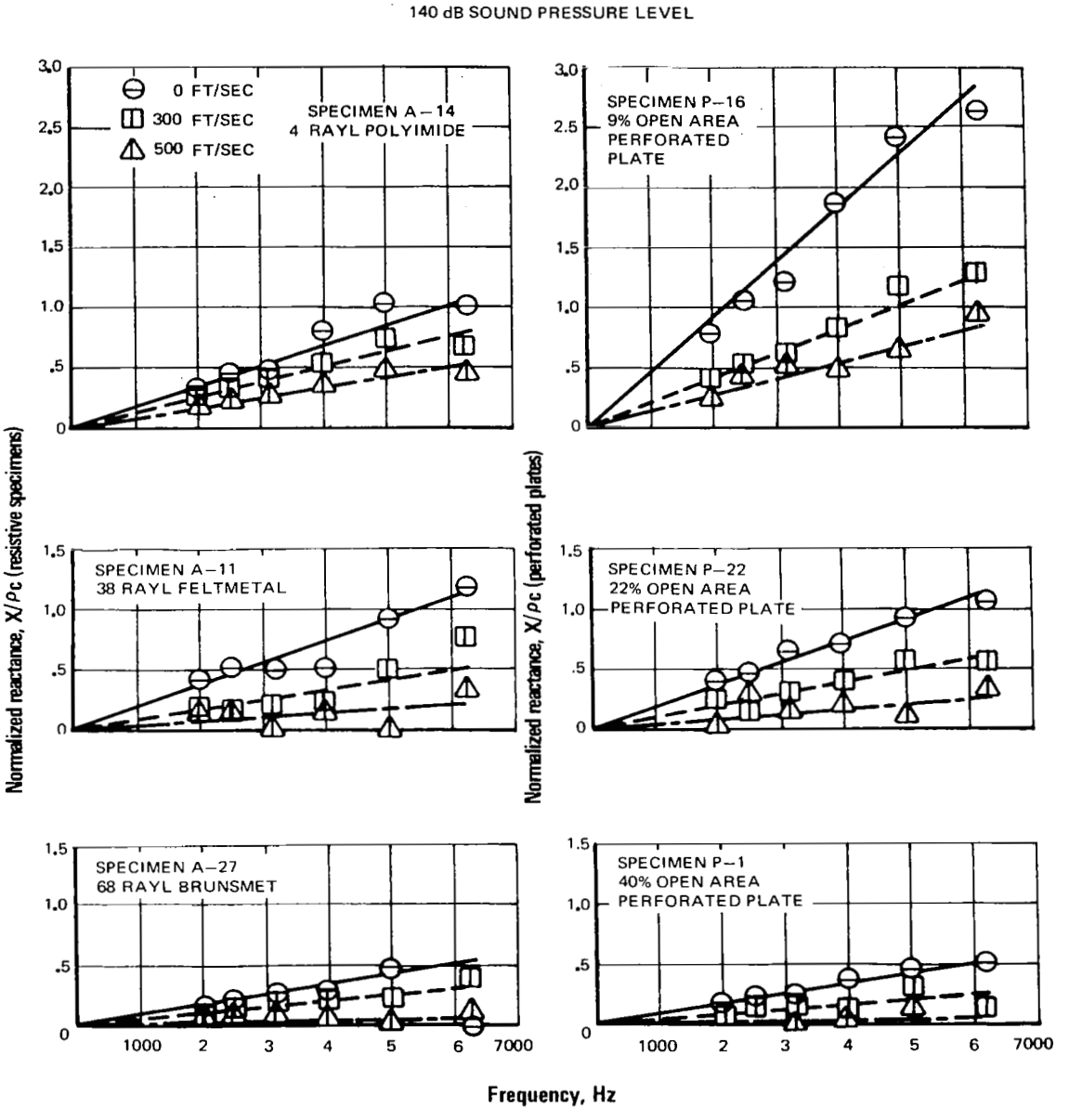

Figure 35 Effect on Reactance of Grazing Flow at Port A

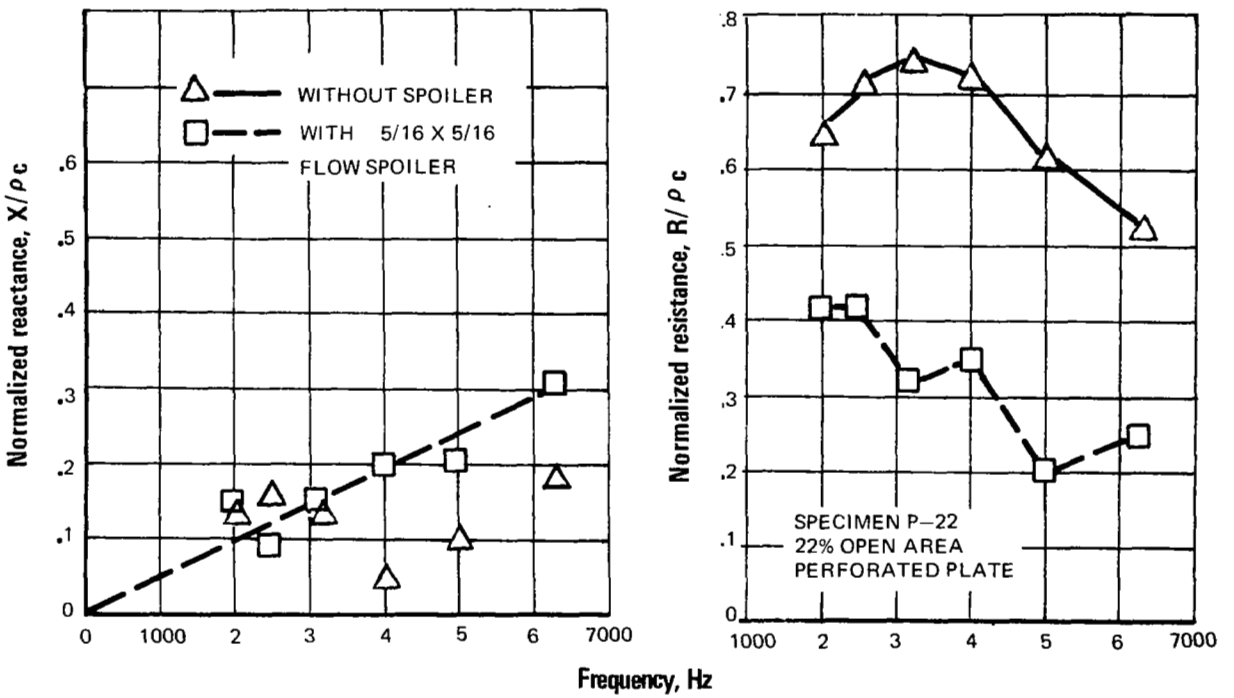

Figure 36 Effect on Impedance of 5/16 x 5/16 Flow Spoiler With Specimen Located in Port C, Spoiler Located Three Inches Upstream of Port C, Nominal Flow Velocity 500 fps

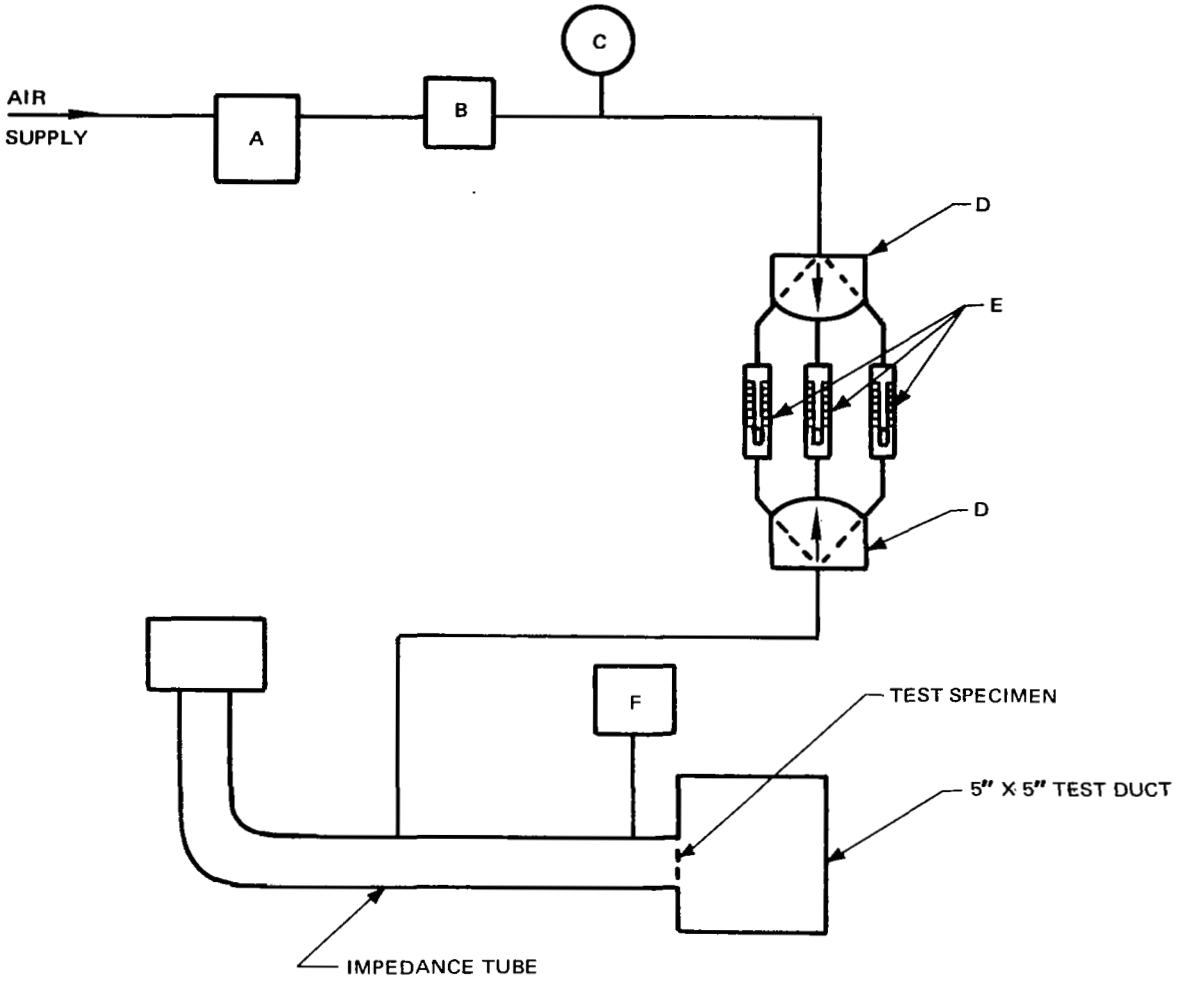

A FILTER

B PRESSURE REGULATING VALVE

C PRESSURE GAGE

D FLOW METER SELECTOR VALVE

E FLOW METERS

F BACK PRESSURE MANOMETER

Figure 37 Impedance Tube Flow Through Specimen Schematic

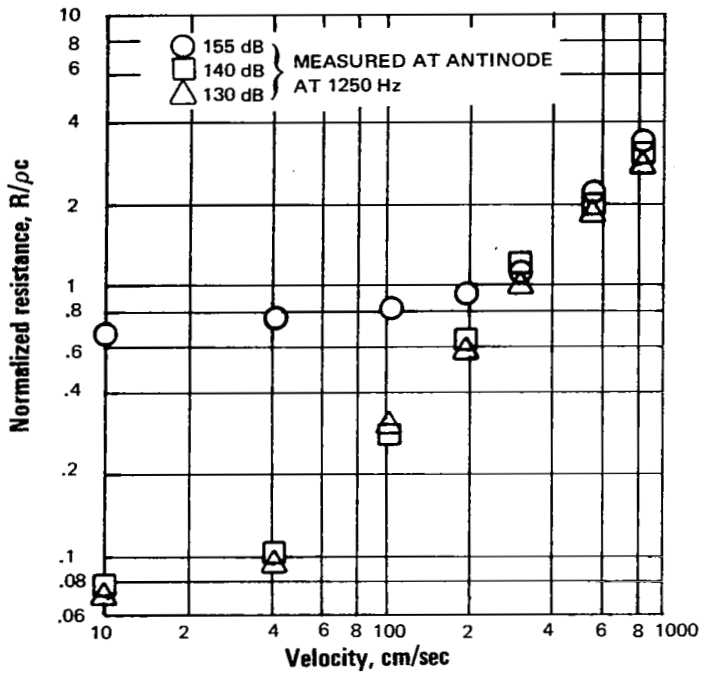

Figure 38 Effect of Through Air Velocity on the Acoustic Resistance of a 15 Percent Open-Area Perforated Plate Specimen (P-17)

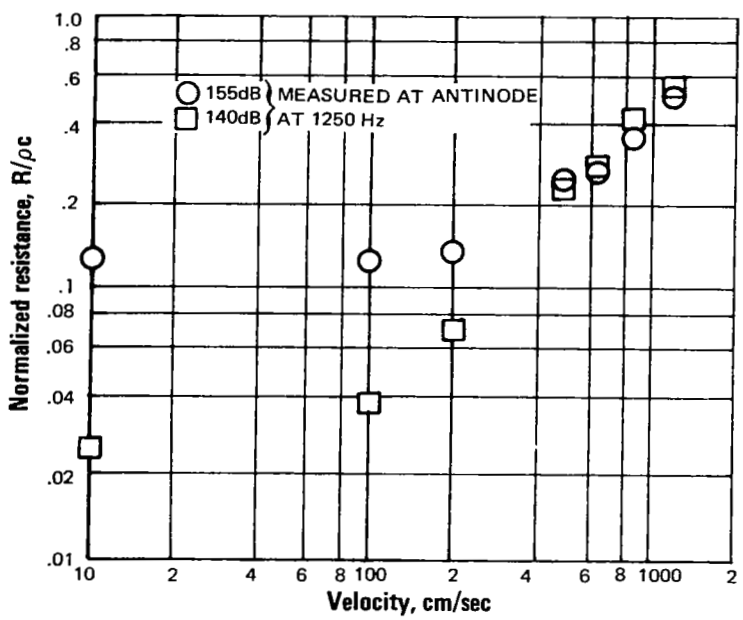

Figure 39 Effect of Through Air Velocity on the Acoustic Resistance of a 30 Percent Open-Area Perforated Plate Specimen (P-18)

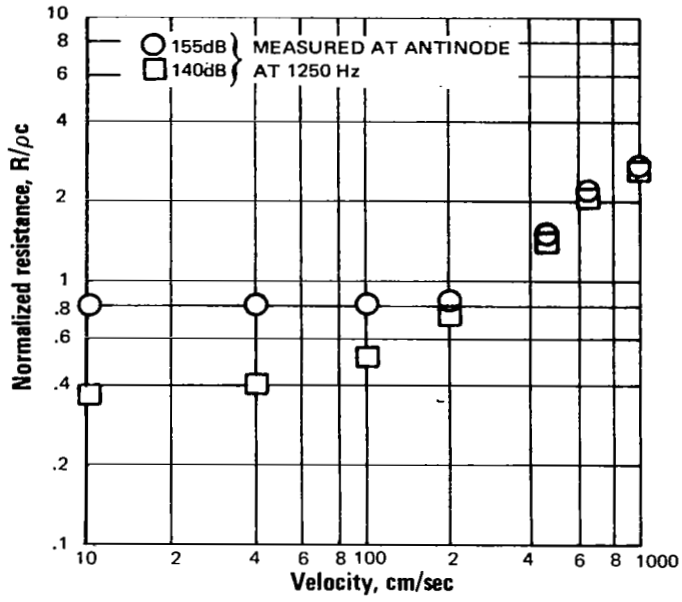

Figure 40 Effect of Through Air Velocity on the Acoustic Resistance of a 12-Rayl Fibermetal Specimen (A-10)

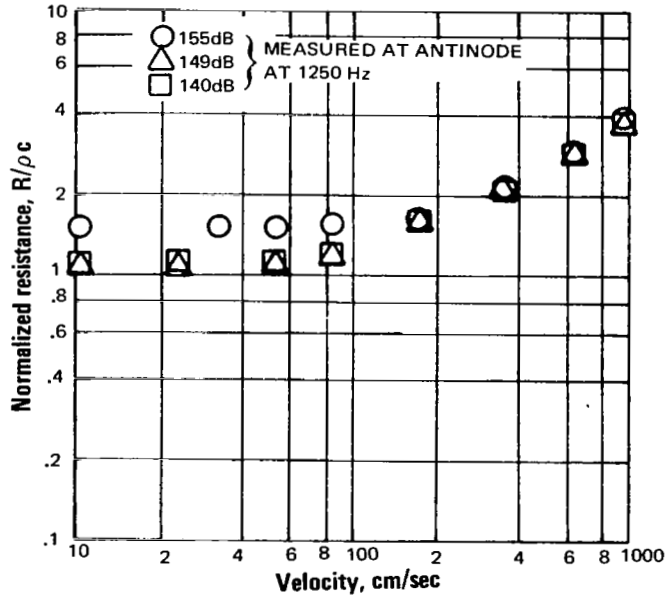

Figure 41 Effect of Through Air Velocity on the Acoustic Resistance of a 43-Rayl Fibermetal Specimen (A-26a)

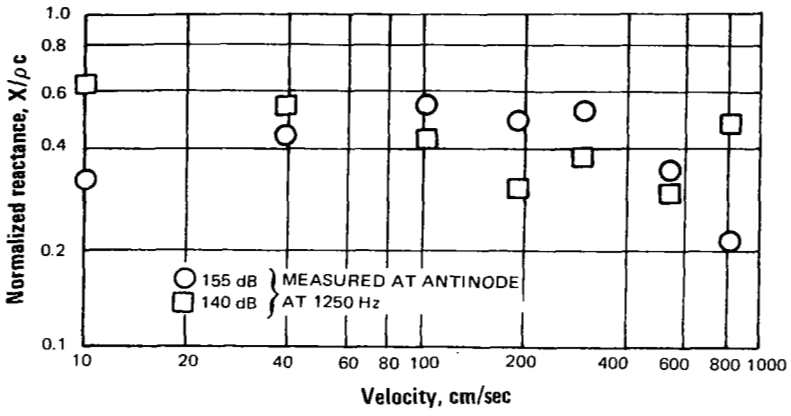

Figure 42 Effect of Through Air Velocity on the Acoustic Reactance of a 15 Percent Open-Area Perforated Plate Specimen (P-17)

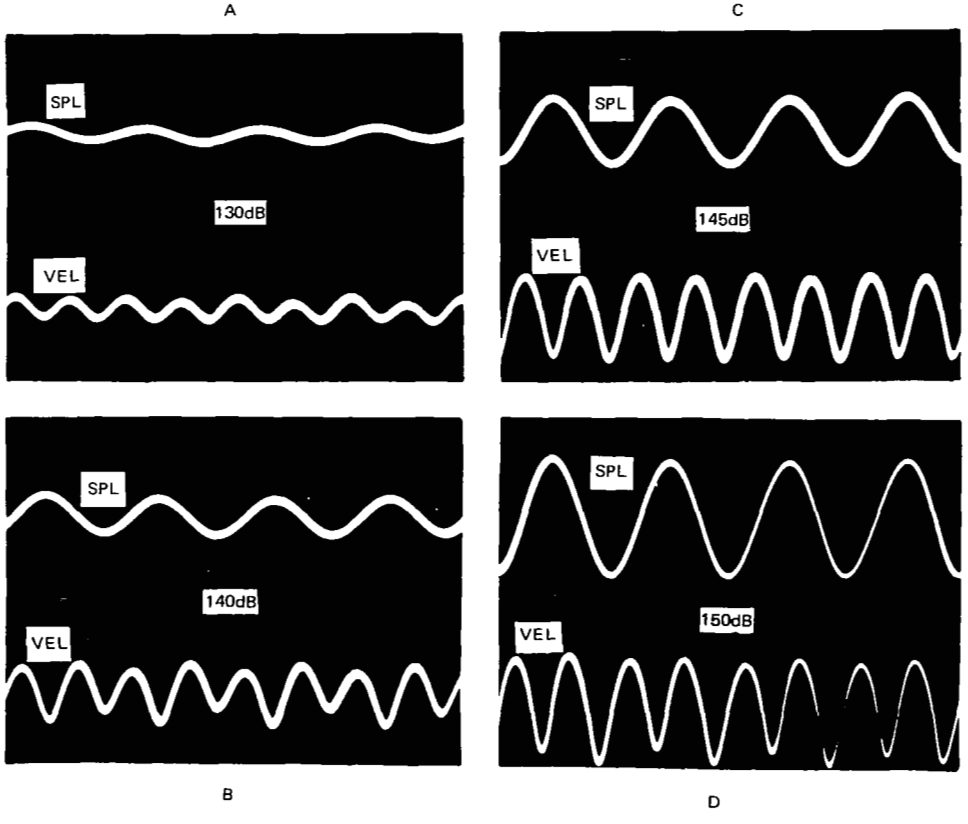

Figure 43 Oscilloscope Traces Showing Effect of Increasing Hot-Wire Rig Sound Pressure Levels

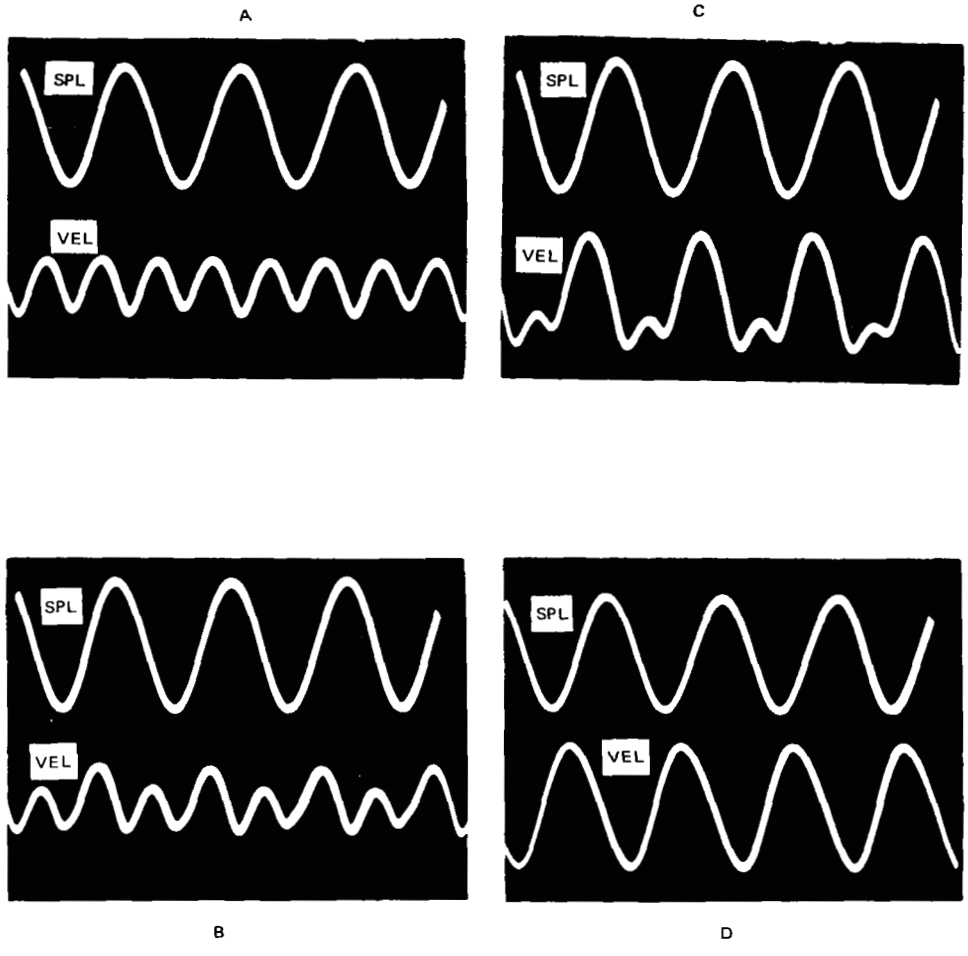

Figure 44 Hot-Wire Rig Oscilloscope Traces Showing Effect of Superimposing a Steady Airflow on the Incident Sound Pressure Waves

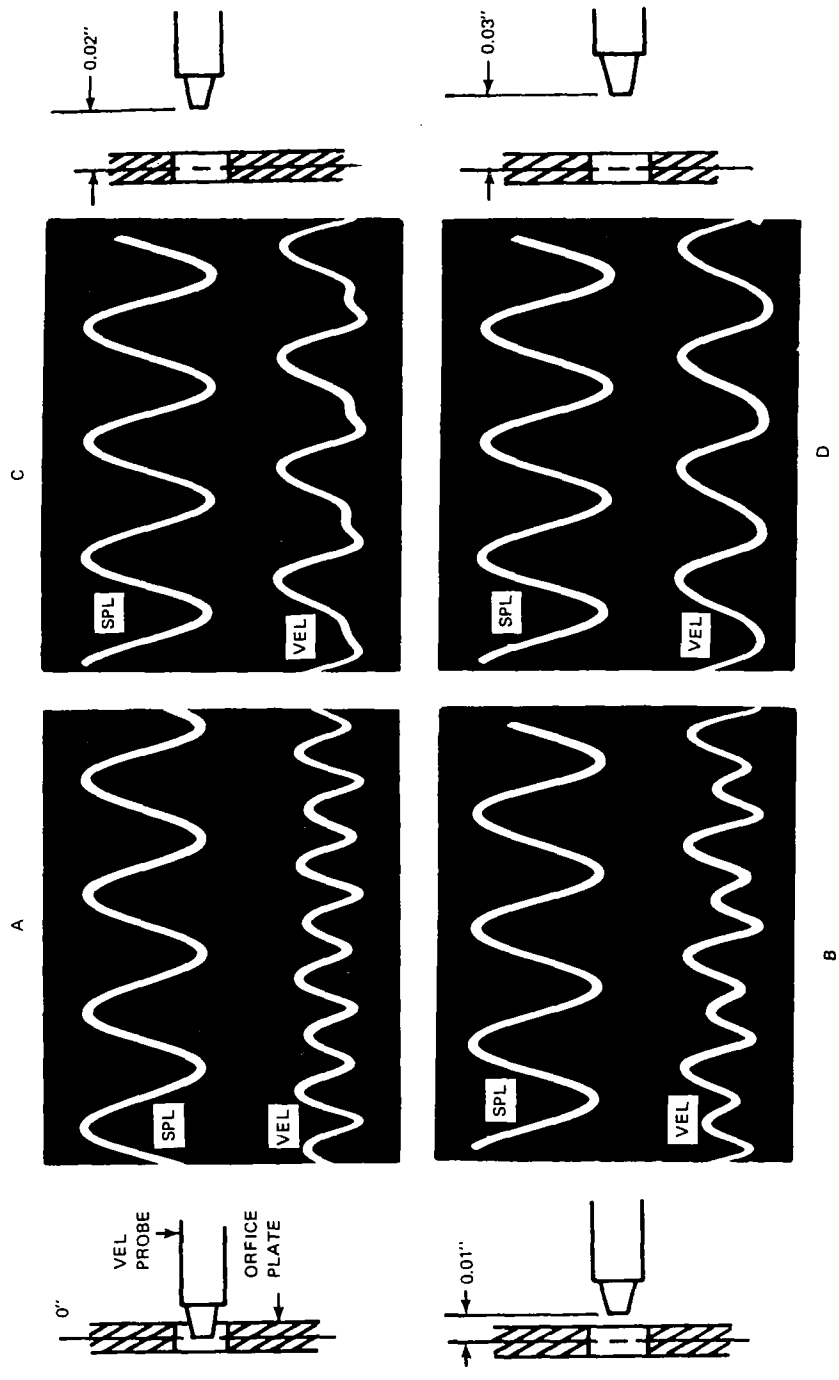

Figure 45 Hot-Wire Rig Oscilloscope Traces Showing Effect of Traversing the Probe

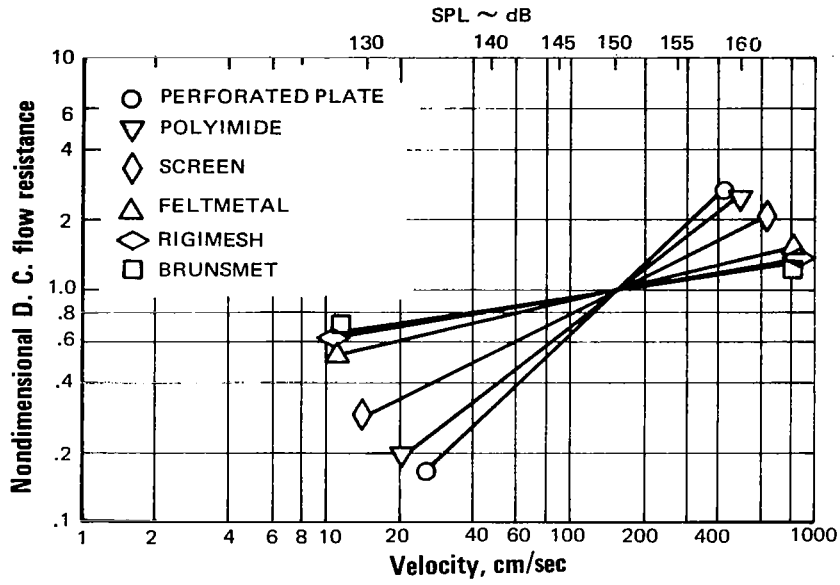

Figure 46 Average Slopes of D.C. Flow Resistance of the Various Types of Specimens

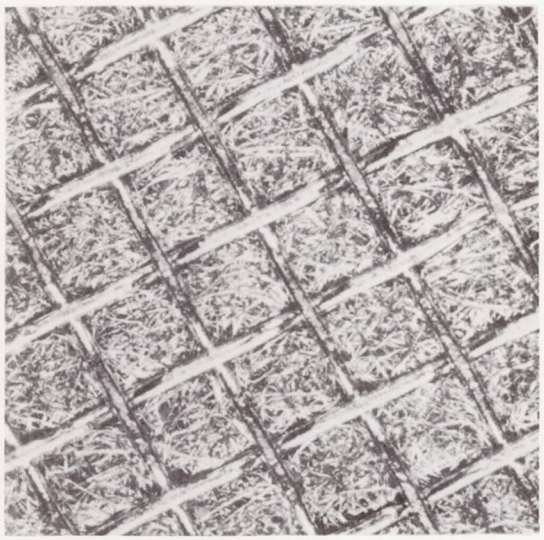

29-RAYL BRUNSMET

4-RAYL POLYIMIDE

74-RAYL RIGIMESH

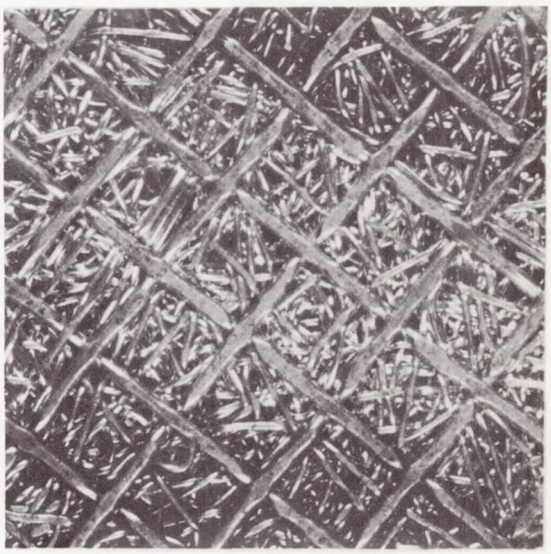

38-RAYL FELTMETAL

Figure 47 Enlarged View (10 X) of Various Resistive Specimens

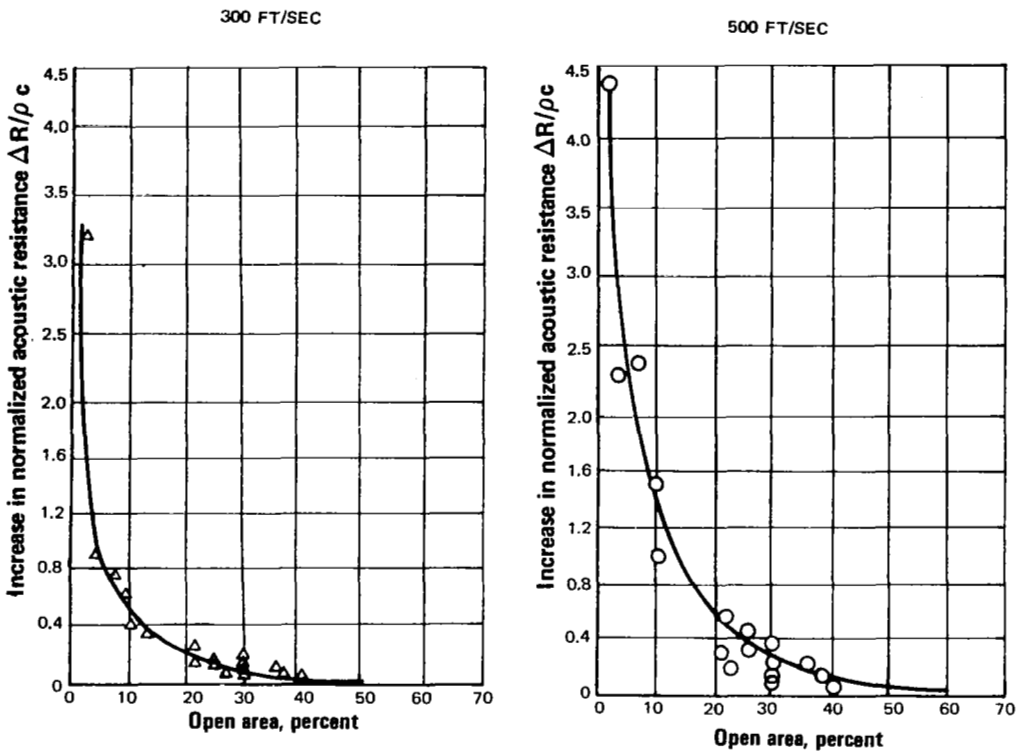

Figure 48 Difference of Normalized Acoustic Resistance Versus Percent Open-Area Perforated Plate at Airflows of 300 fps and 500 fps

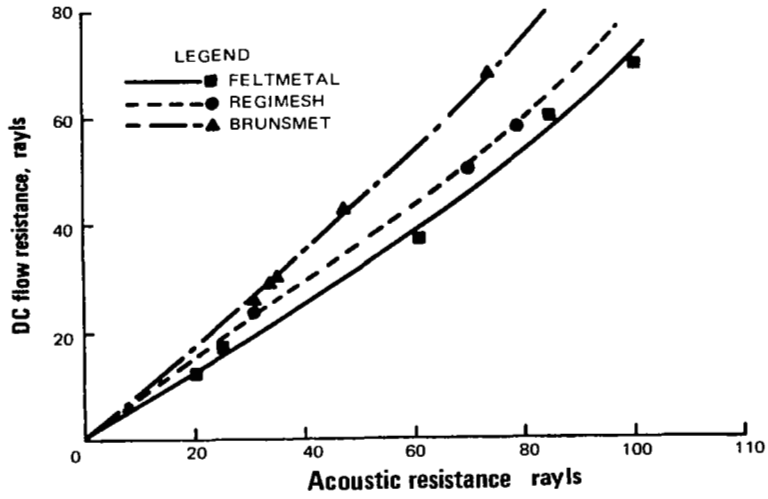

Figure 49 D.C. Flow Resistance Versus Acoustic Resistance at 300 fps for Resistive Specimens

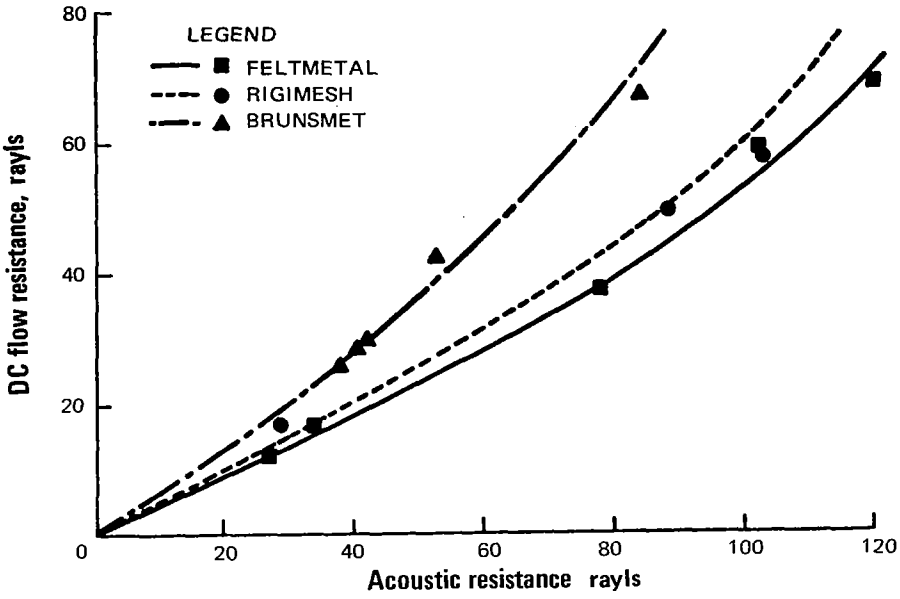

Figure 50 D. C. Flow Resistance Versus Acoustic Resistance at 500 fps for Resistive Specimens

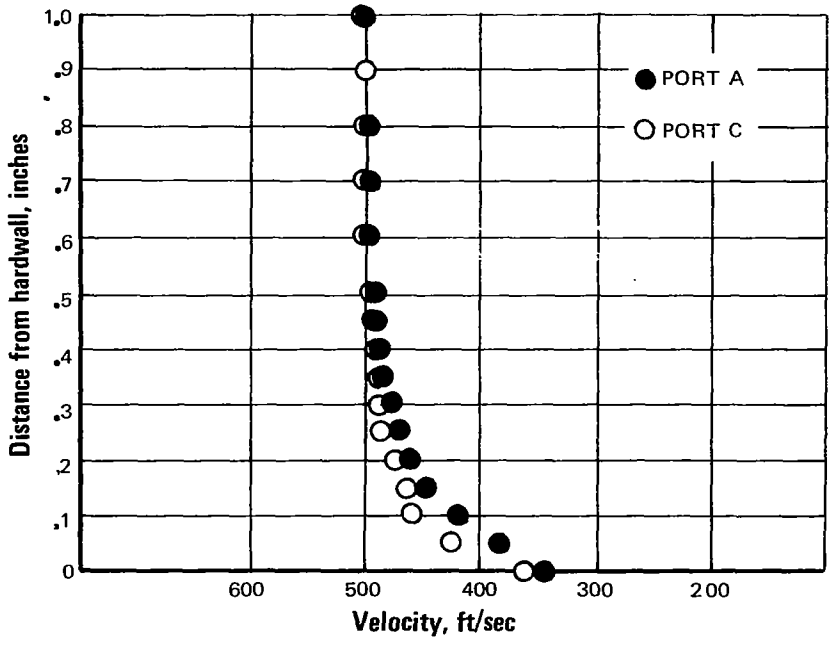

Figure 51 Boundary Layer Comparison in Port A and C at 500 fps Airflow Velocity

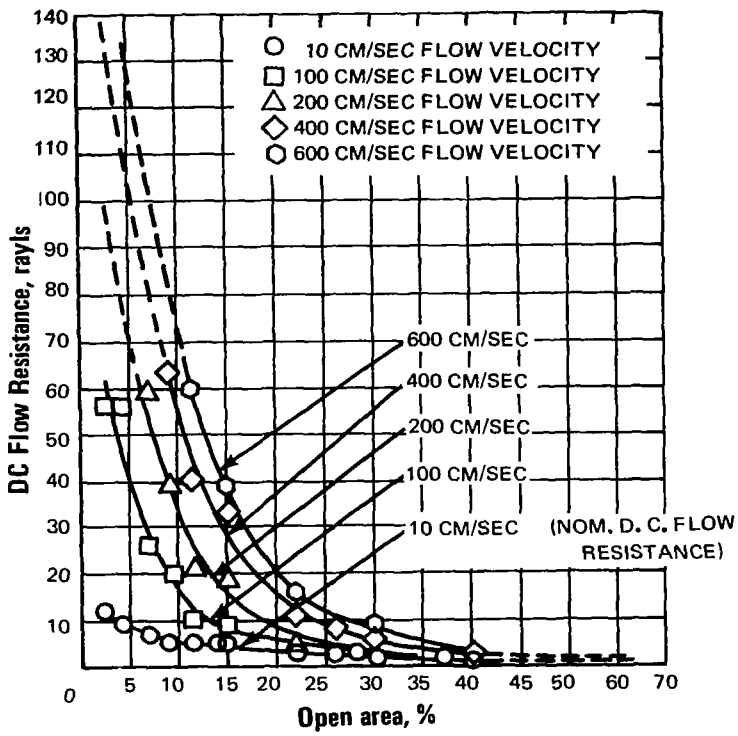

Figure 52 Effect of Through Flow Velocity on the D.C. Flow Resistance of Perforated Plate Specimens Measured in the D.C. Flow Rig

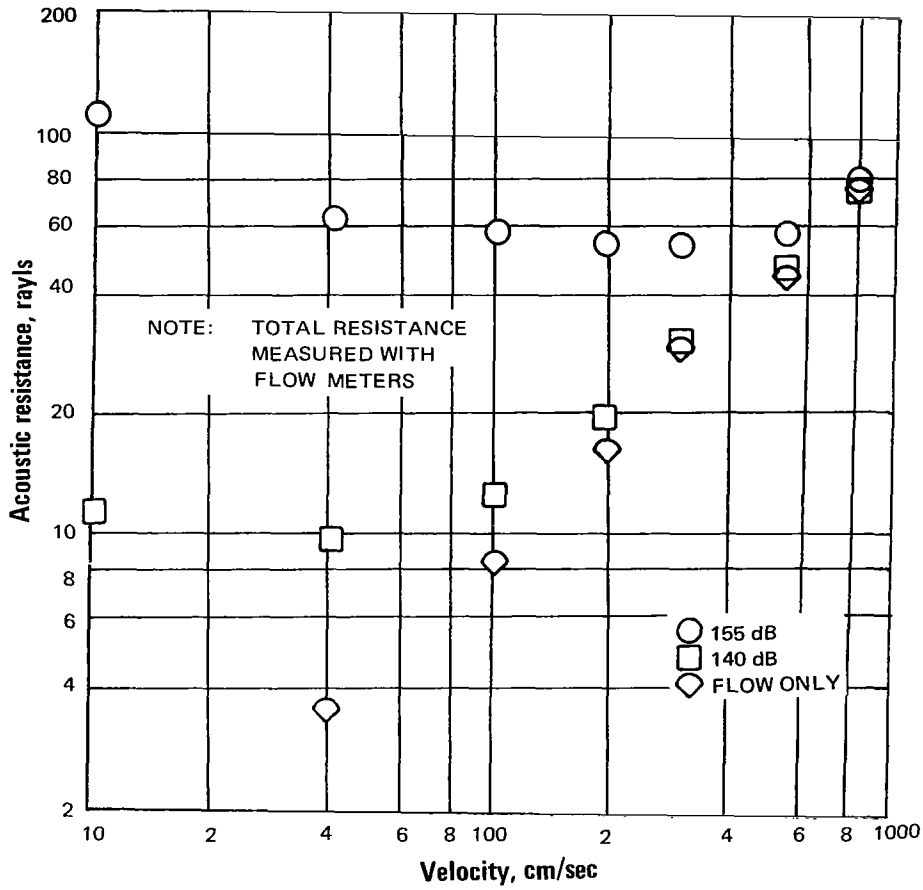

Figure 53 Effect on Resistance of Superimposing Sound Pressure Waves on Steady Air Velocity Through a 15 Percent Open-Area Perforated Plate Specimen (P-17)

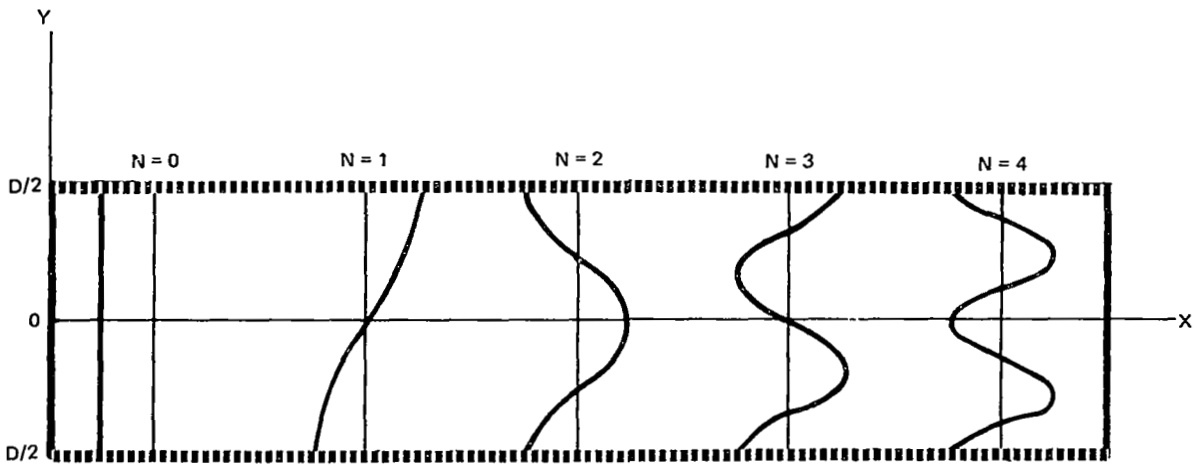

Figure 54 Transverse Cross-Section of Duct and Sound Pressure Patterns for the First Five Modes - Upper and Lower Surfaces are Treated. Sound Propagates in the z Direction, Normal to the x-y Plane. Pressure is Uniform in the x Direction.

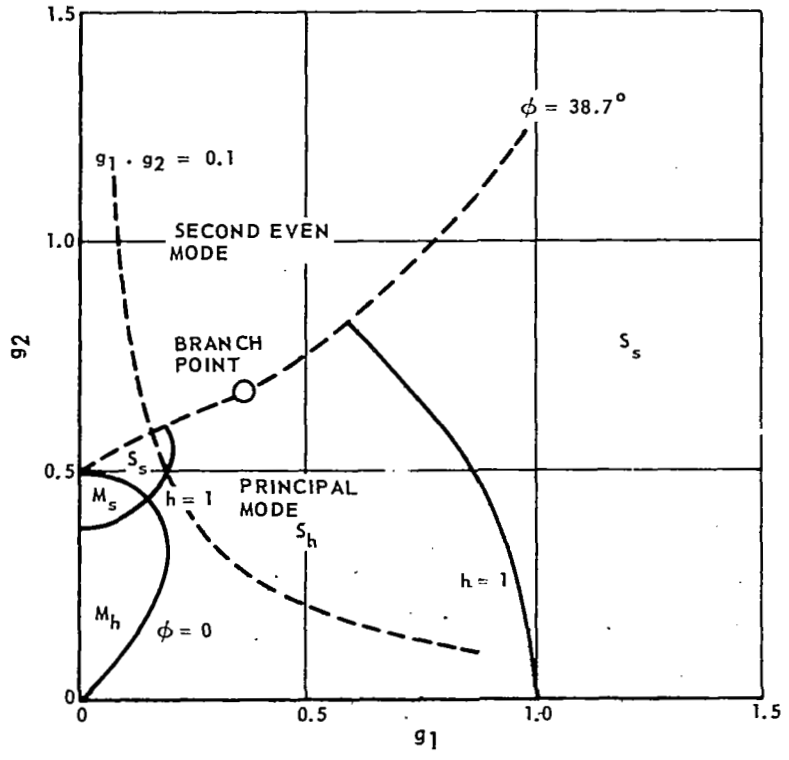

Figure 55 Wave Parameters for the Principal Mode

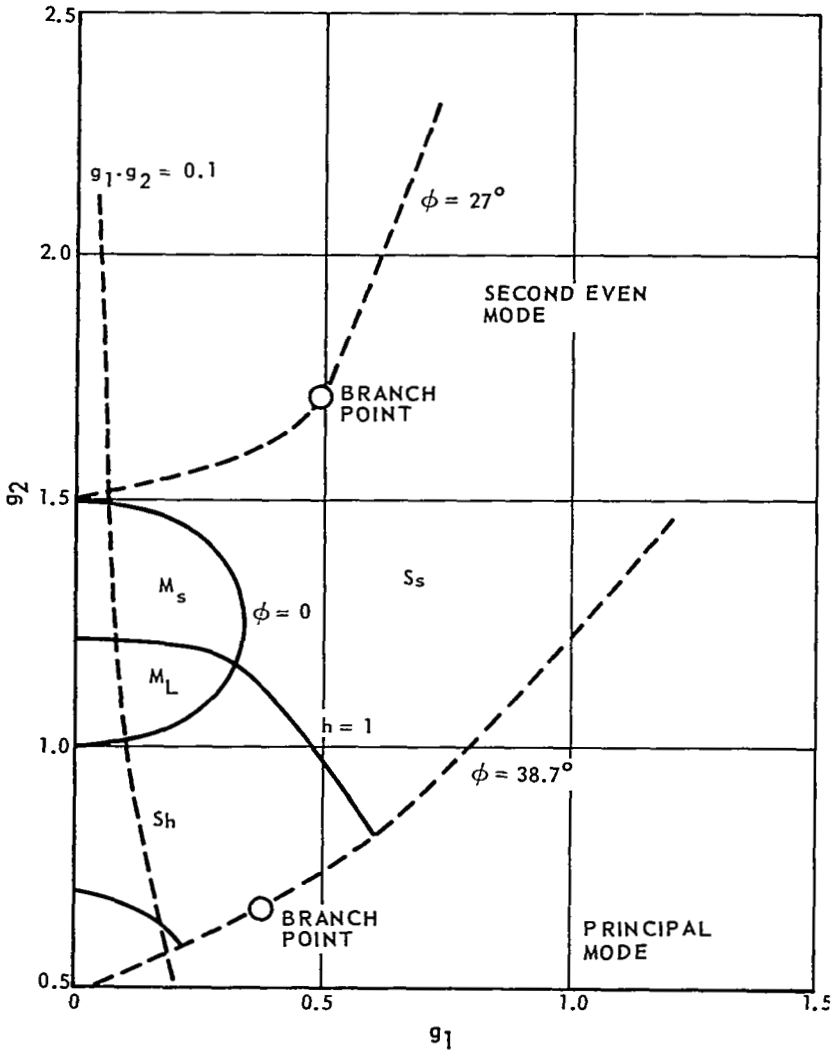

Figure 56 Wave Parameters for the Second-Even Mode

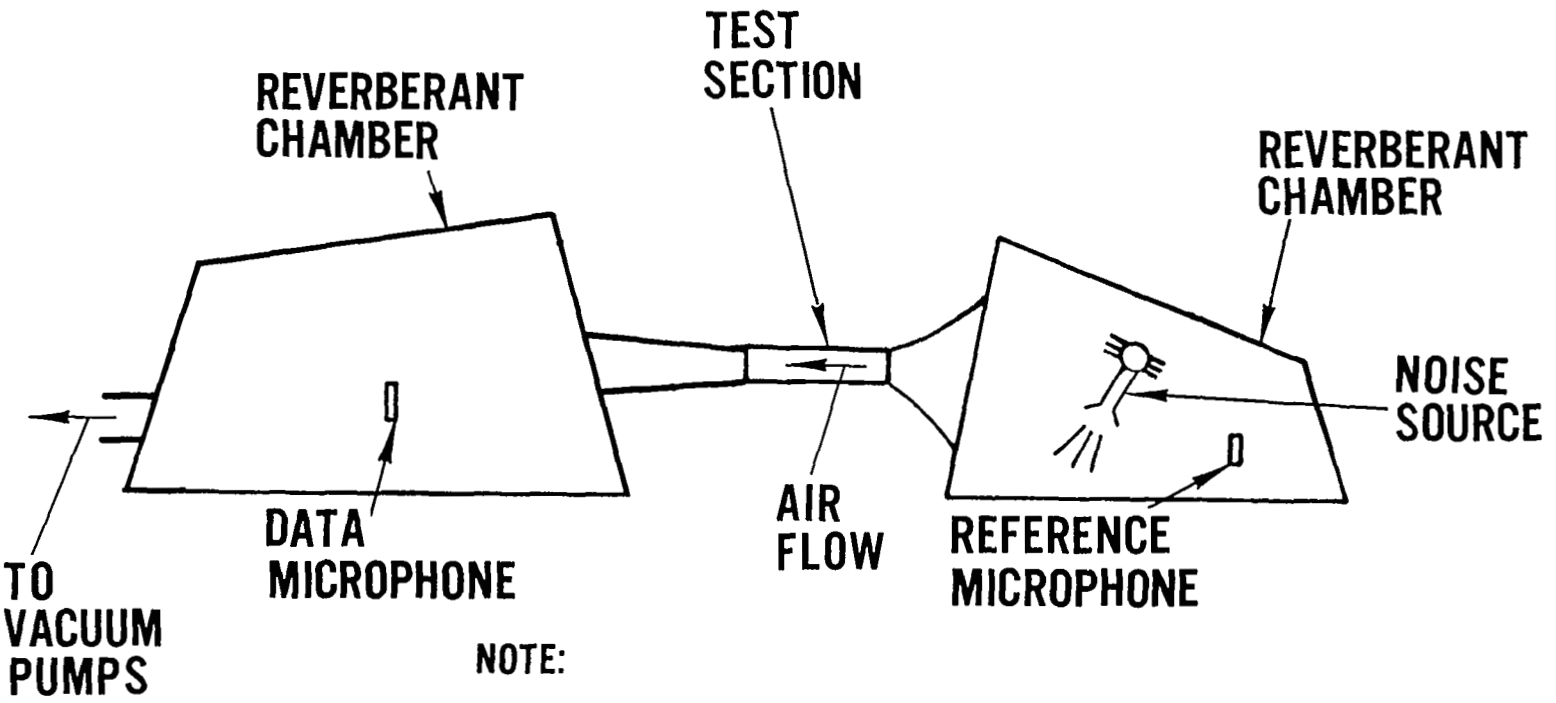

Figure 57 Reverberant Chamber Test Facility

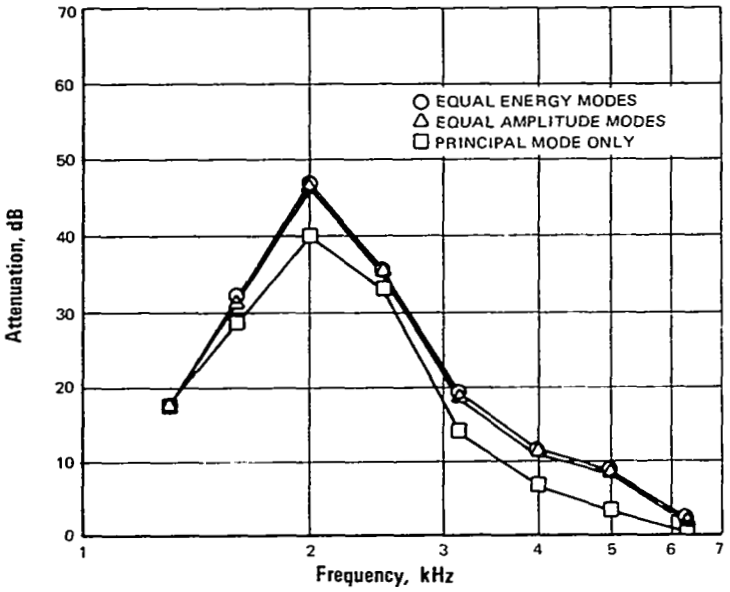

Figure 58 Attenuation Versus Frequency for Different Mode Amplitudes (d = 1, R = 1, X = 0

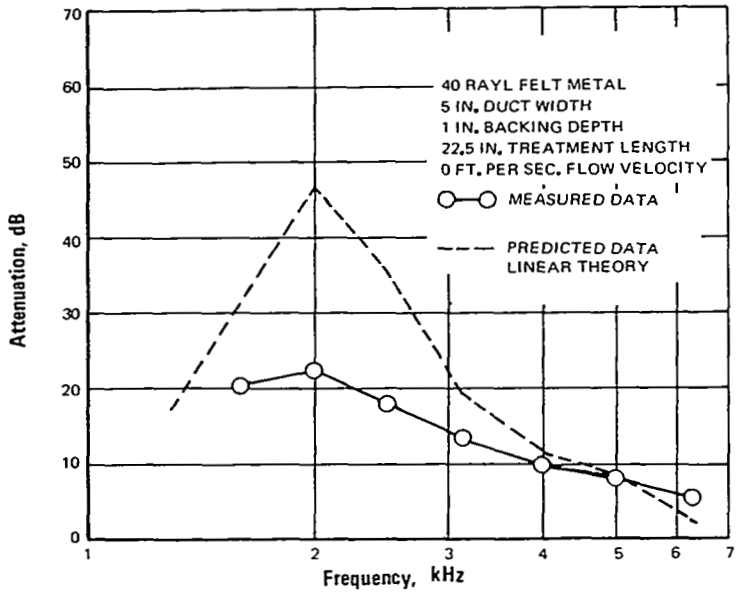

Figure 59 Attenuation Versus Frequency for Predicted and Measured Data - Values for 40-Rayl Feltmetal over Honeycomb, Backing Depth One Inch

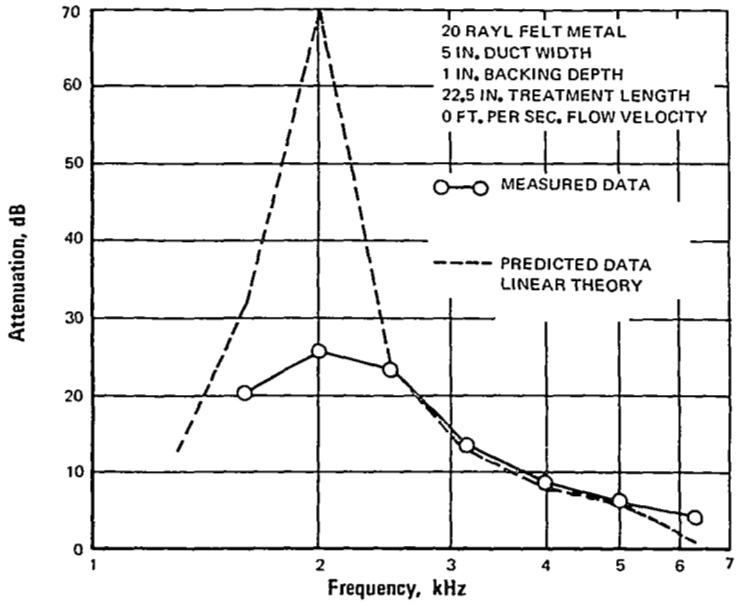

Figure 60 Attenuation Versus Frequency for Predicted and Measured Data - Values for 20-Rayl Feltmetal over Honeycomb, Backing Depth One Inch

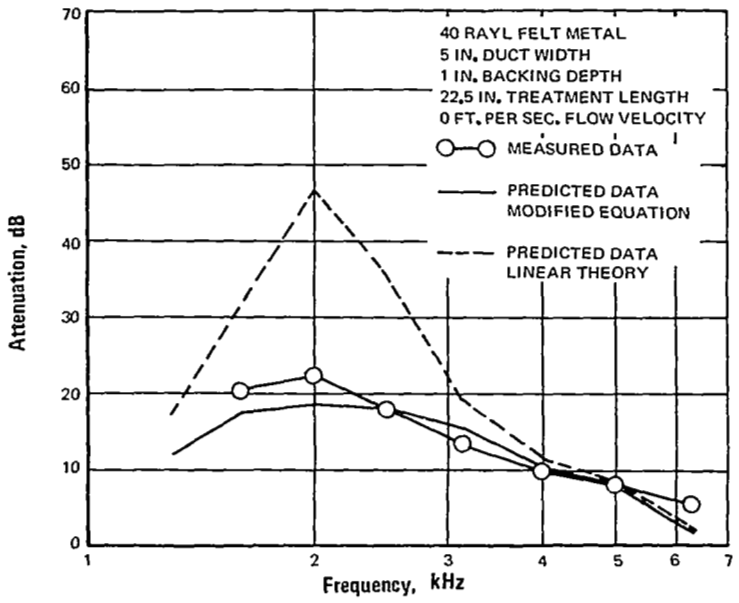

Figure 61 Attenuation Versus Frequency for Predicted, Modified Predicted, and Measured Data - Values for 40-Rayl Feltmetal over Honeycomb, Backing Depth One Inch

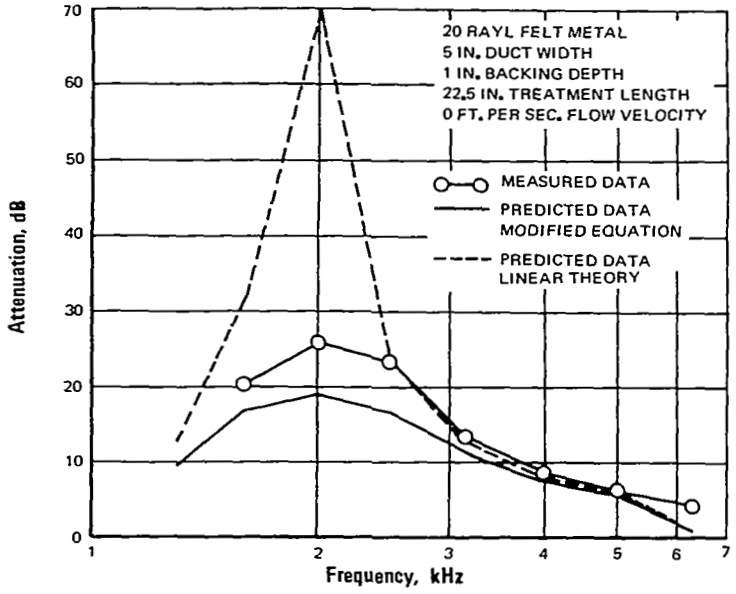

Figure 62 Attenuation Versus Frequency for Predicted, Modified Predicted, and Measured Data - Values for 20-Rayl Feltmetal over Honeycomb, Backing Depth One Inch

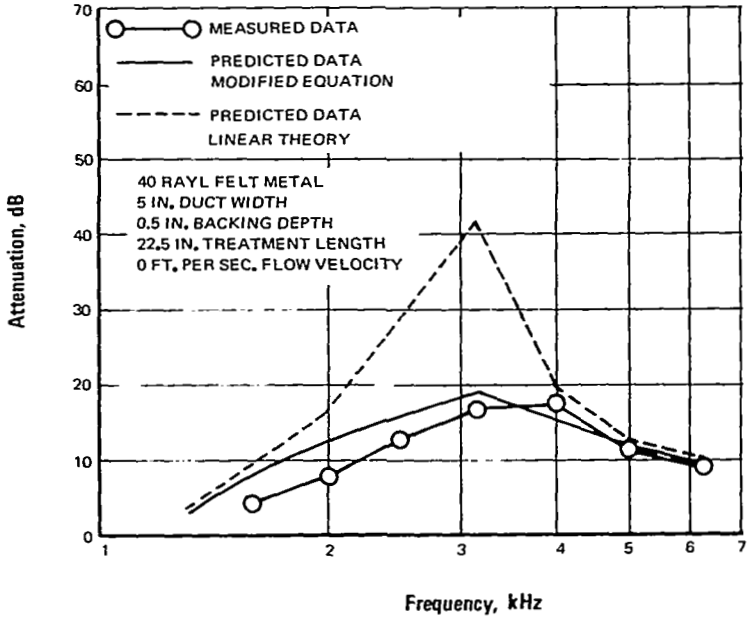

Figure 63 Attenuation Versus Frequency for Predicted, Modified Predicted, and Measured Data - Values for 40-Rayl Feltmetal over Honeycomb, Backing Depth 0.5 Inch

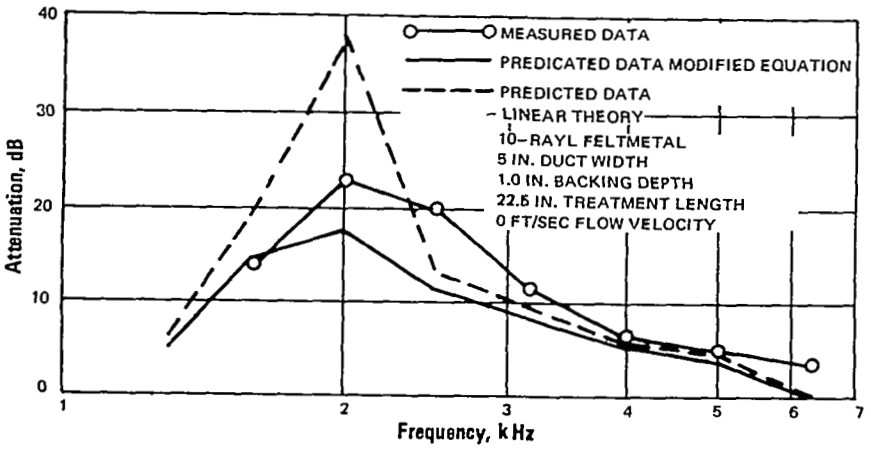

Figure 64 Attenuation Versus Frequency for Predicted, Modified Predicted, and Measured Data - Values for 10-Rayl Feltmetal over Honeycomb, Backing Depth One Inch

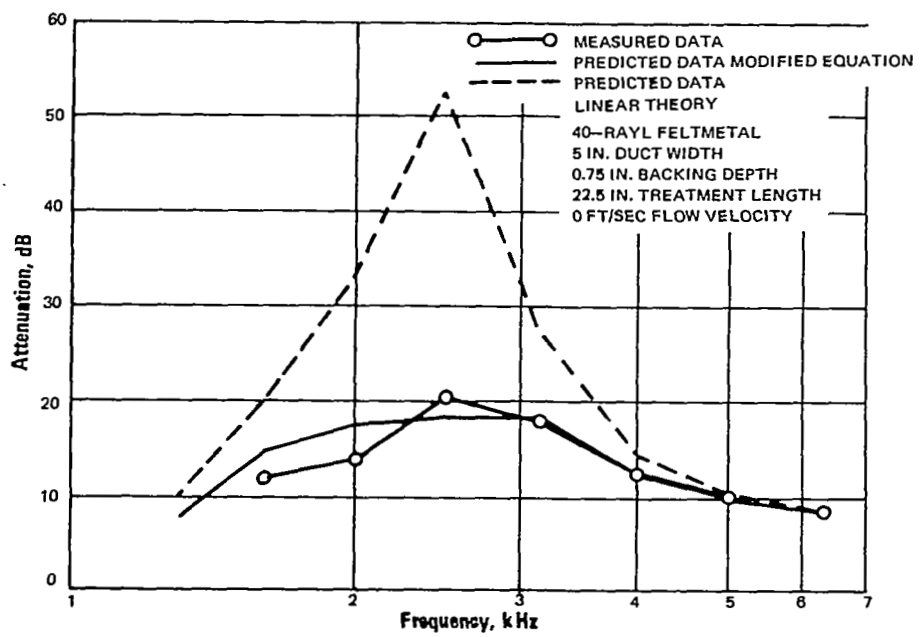

Figure 65 Attenuation Versus Frequency for Predicted Modified Predicted, and Measured Data - Values for 40-Rayl Feltmetal over Honeycomb, Backing Depth 0.75 Inch

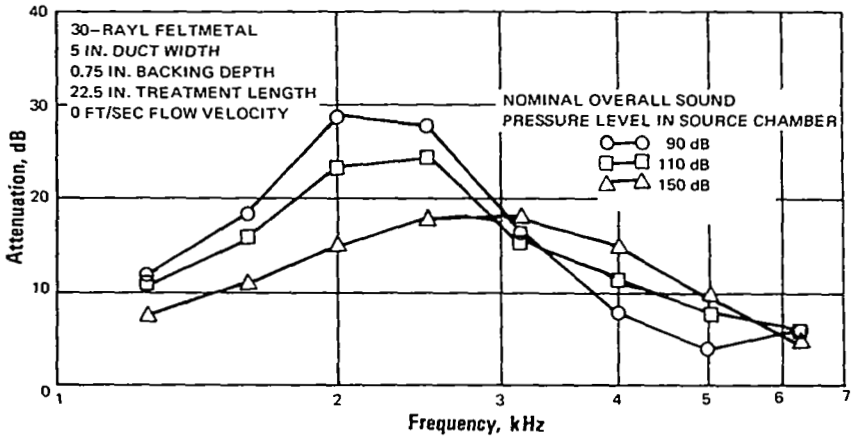

Figure 66 Attenuation Versus Frequency for Measured Data at Various Sound Pressure Levels - Values for 30-Rayl Feltmetal over Honeycomb, Backing Depth 0.75 Inch

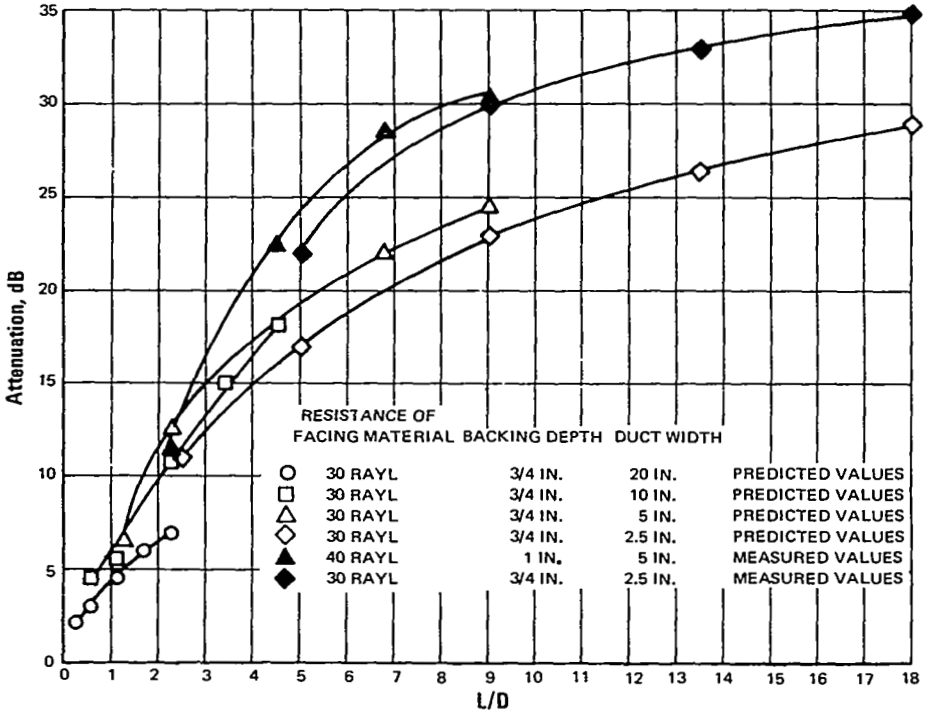

Figure 67 Peak Attenuation Versus L/D Ratio for Predicted and Measured Data for Various Materials and Backing Depths

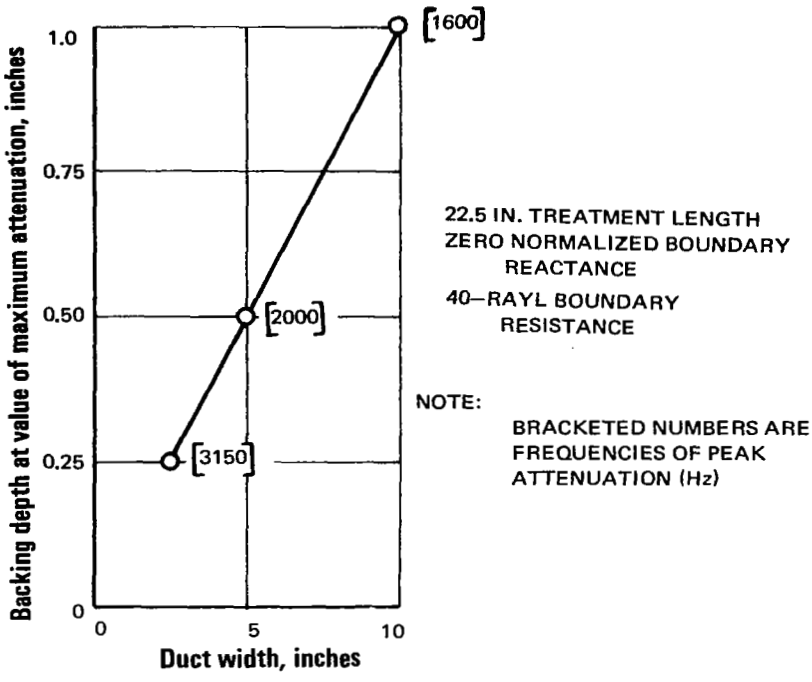

Figure 68 Predicted Backing Depth for Maximum Attenuation Versus Duct Width for 40-Rayl Feltmetal over Honeycomb

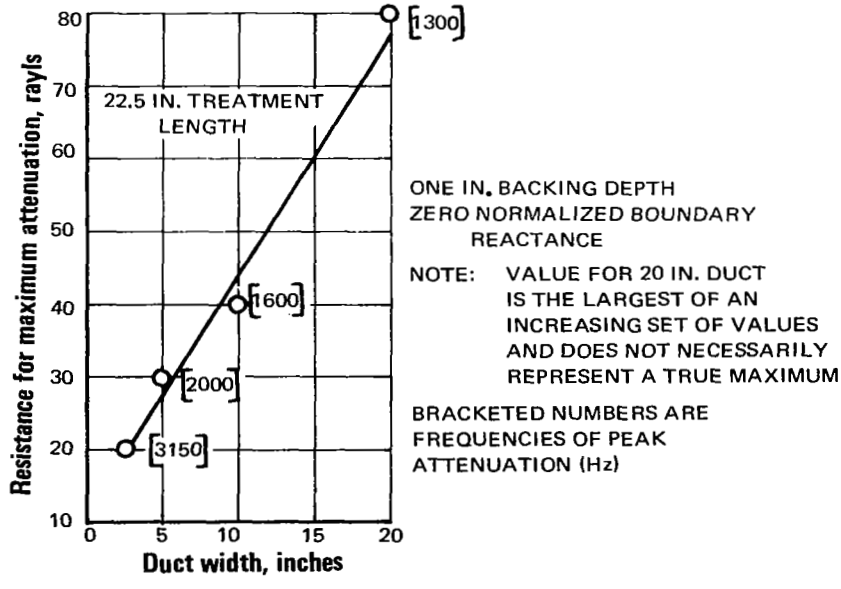

Figure 69 Predicted Resistance for Maximum Attenuation Versus Duct Width for Feltmetal over Honeycomb, Backing Depth One Inch

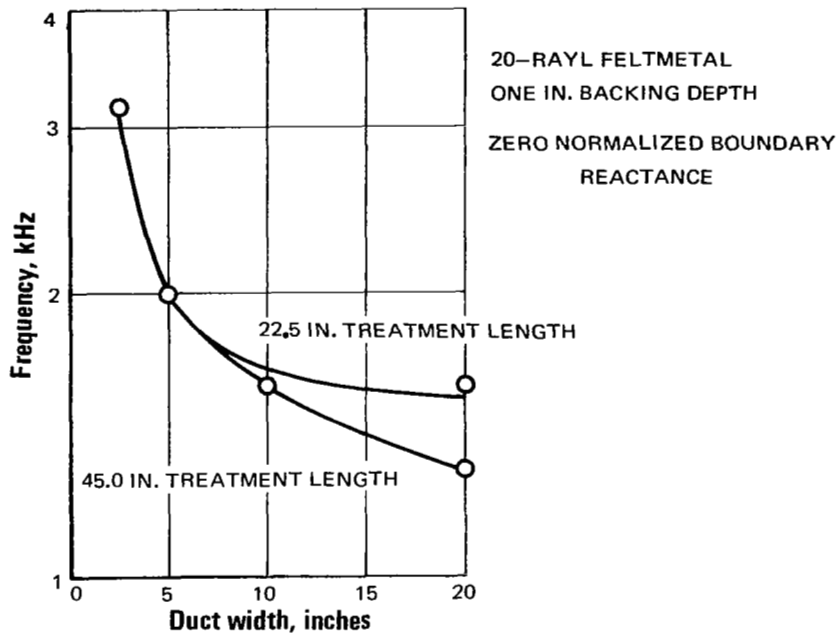

Figure 70 Predicted Frequency of Maximum Attenuation Versus Duct Width for 20-Rayl Feltmetal over Honeycomb, Backing Depth One Inch

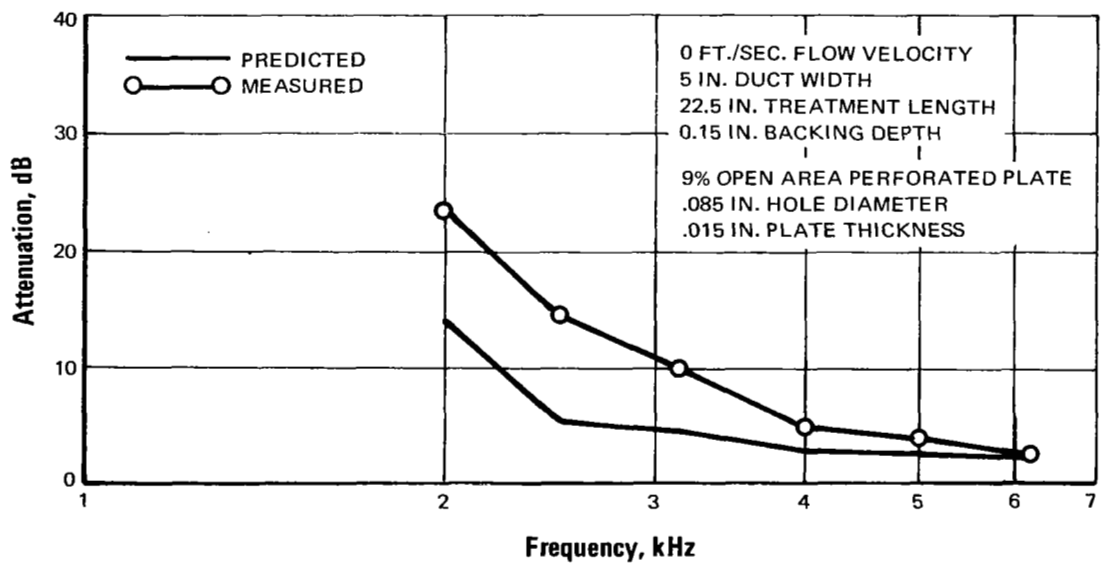

Figure 71 Attenuation Predicted and Measured Versus Frequency, 9% Open Area Perforated Plate, Flow Velocity 0 Feet Per Second

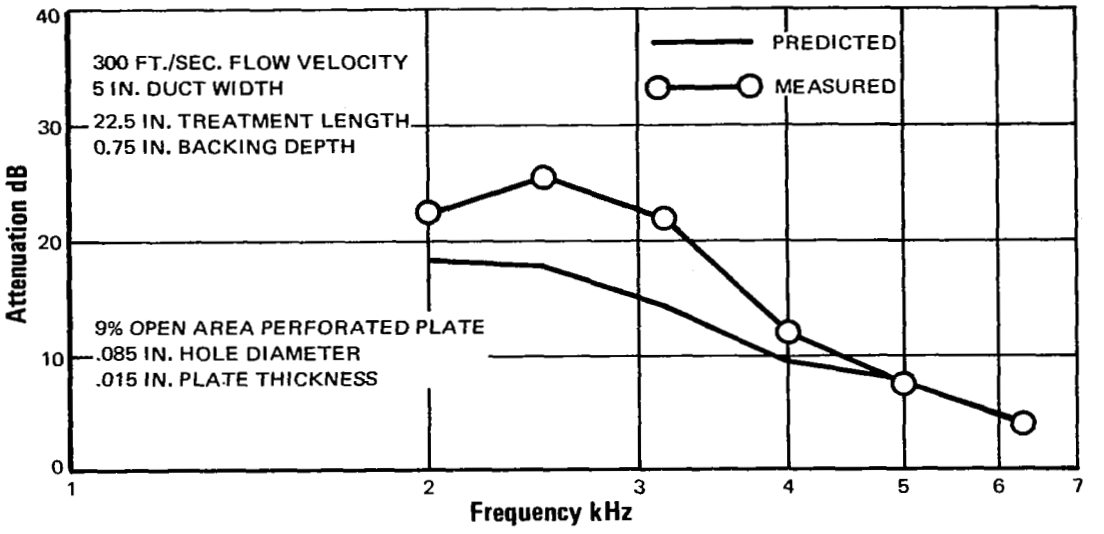

Figure 72 Attenuation Predicted and Measured Versus Frequency, 9% Open Area Perforated Plate, Flow Velocity 300 Feet Per Second

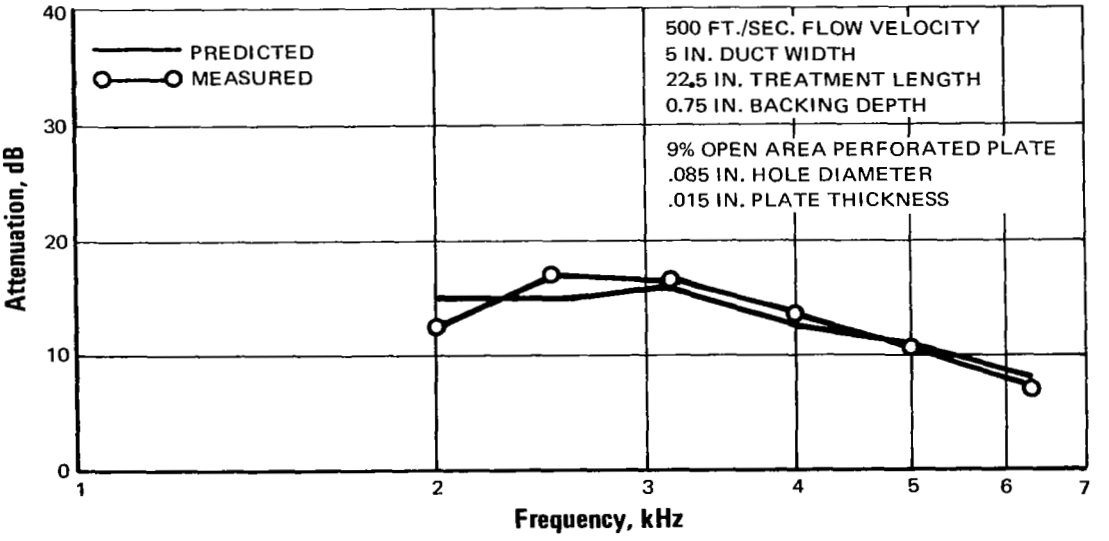

Figure 73 Attenuation Predicted and Measured Versus Frequency, 9% Open Area Perforated Plate, Flow Velocity 500 Feet Per Second

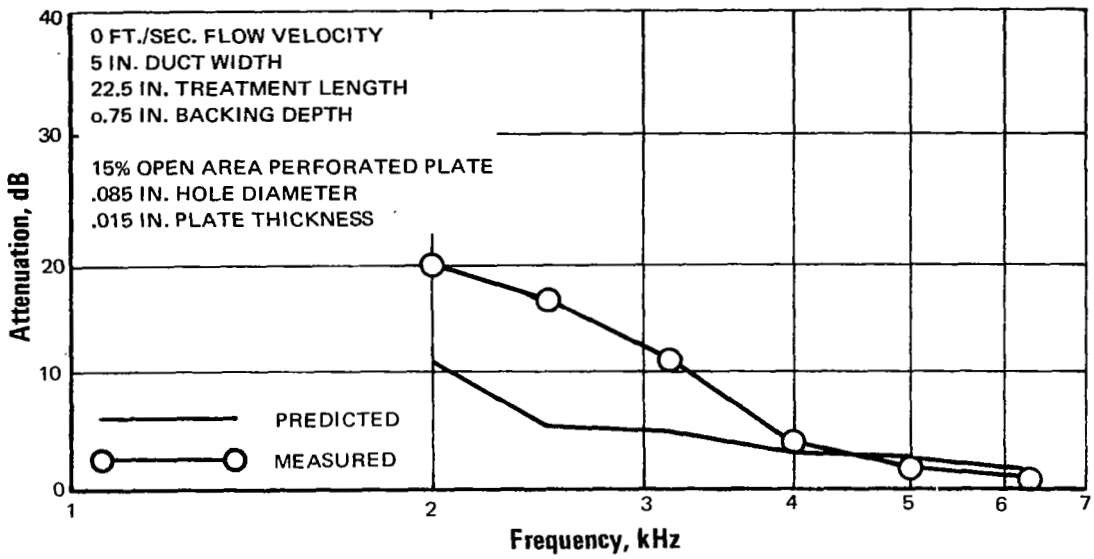

Figure 74 Attenuation Predicted and Measured Versus Frequency, 15% Open Area Perforated Plate, Flow Velocity 0 Feet Per Second

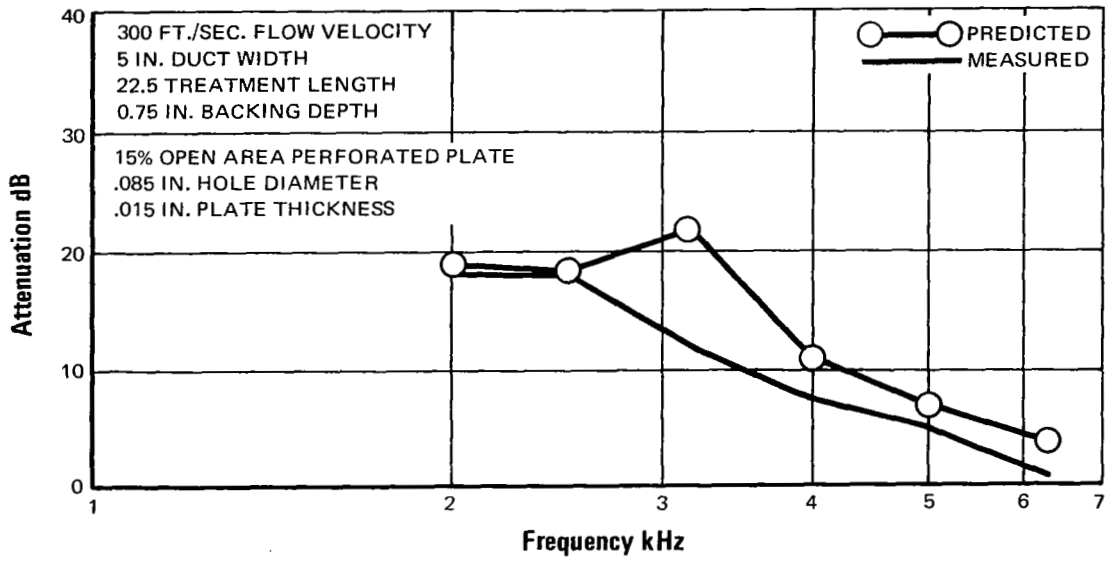

Figure 75 Attenuation Predicted and Measured Versus Frequency, 15% Open Area Perforated Plate, Flow Velocity 500 Feet Per Second

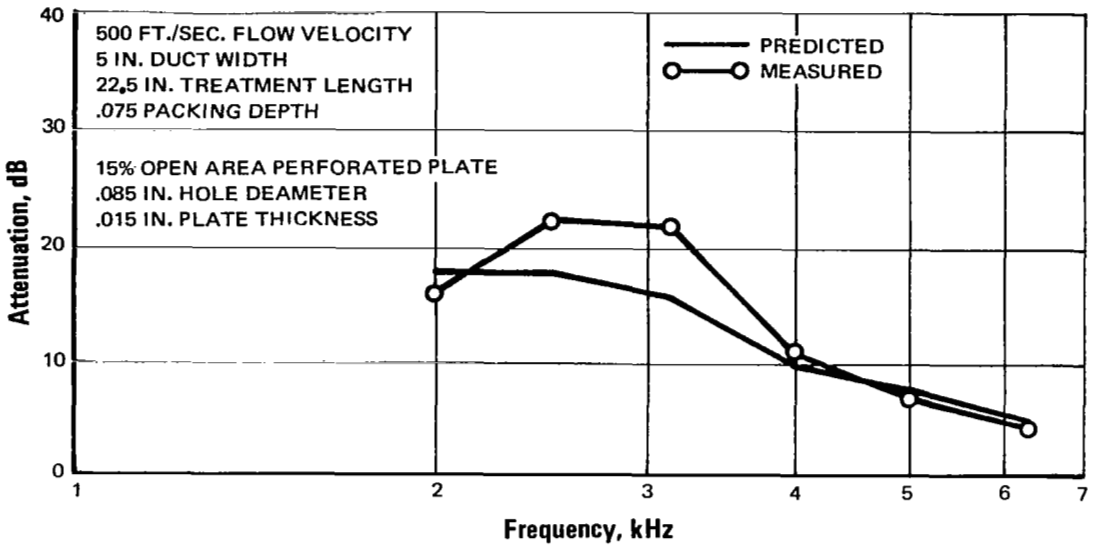

Figure 76 Attenuation Predicted and Measured Versus Frequency, 15% Open Area Perforated Plate, Flow Velocity 500 Feet Per Second

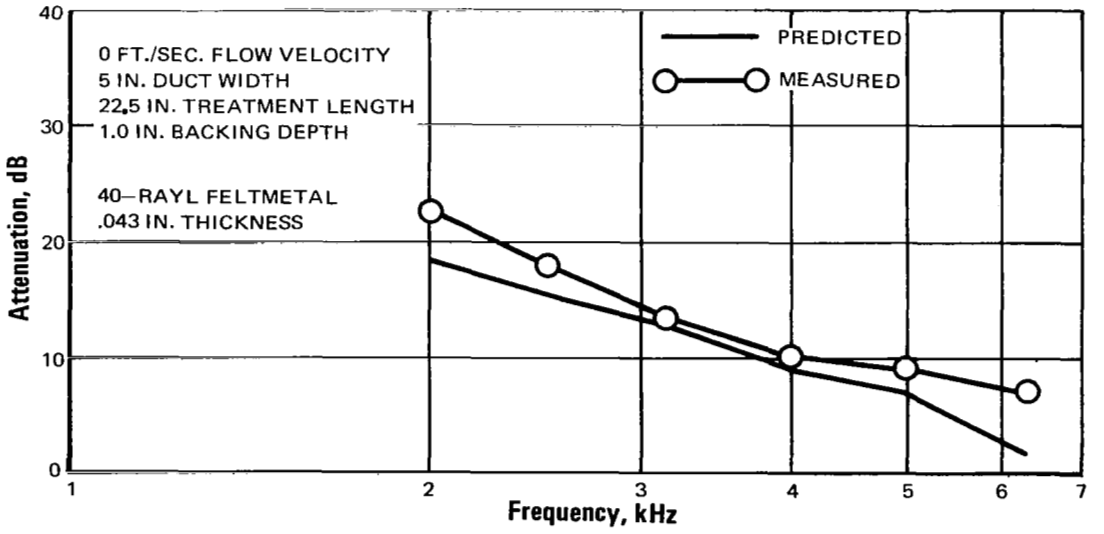

Figure 77 Attenuation Predicted and Measured Versus Frequency, 40 Rayl Feltmetal, Flow Velocity 0 Feet Per Second

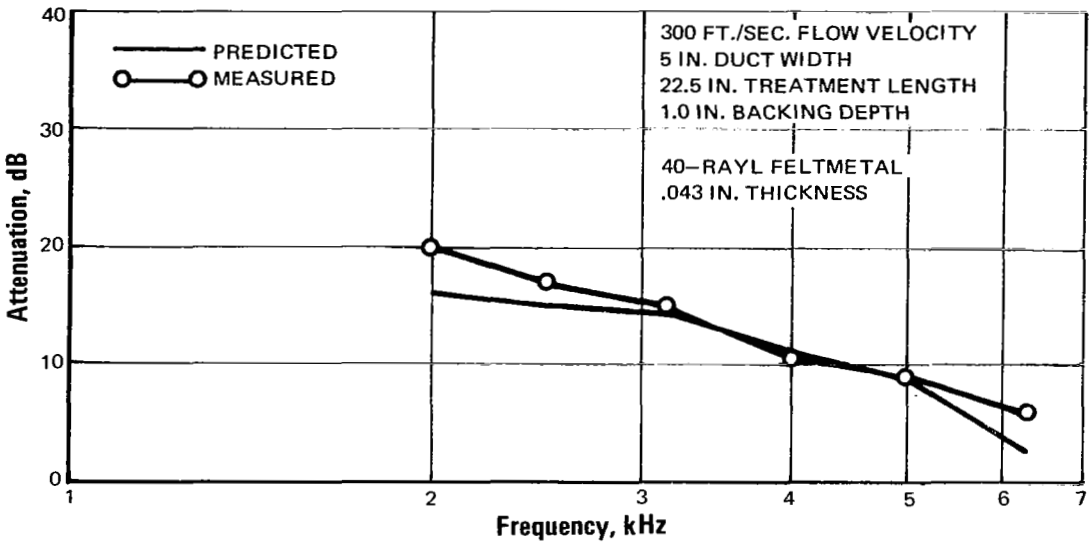

Figure 78 Attenuation Predicted and Measured Versus Frequency, 40 Rayl Feltmetal, Flow Velocity 300 Feet Per Second

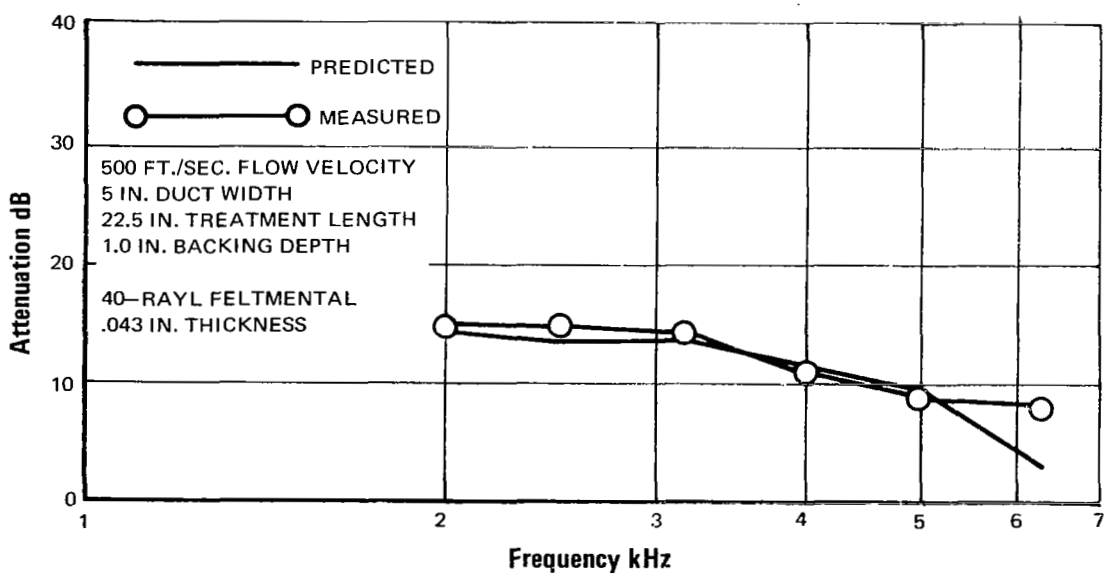

Figure 79 Attenuation Predicted and Measured Versus Frequency, 40 Rayl Feltmetal, Flow Velocity 500 Feet Per Second

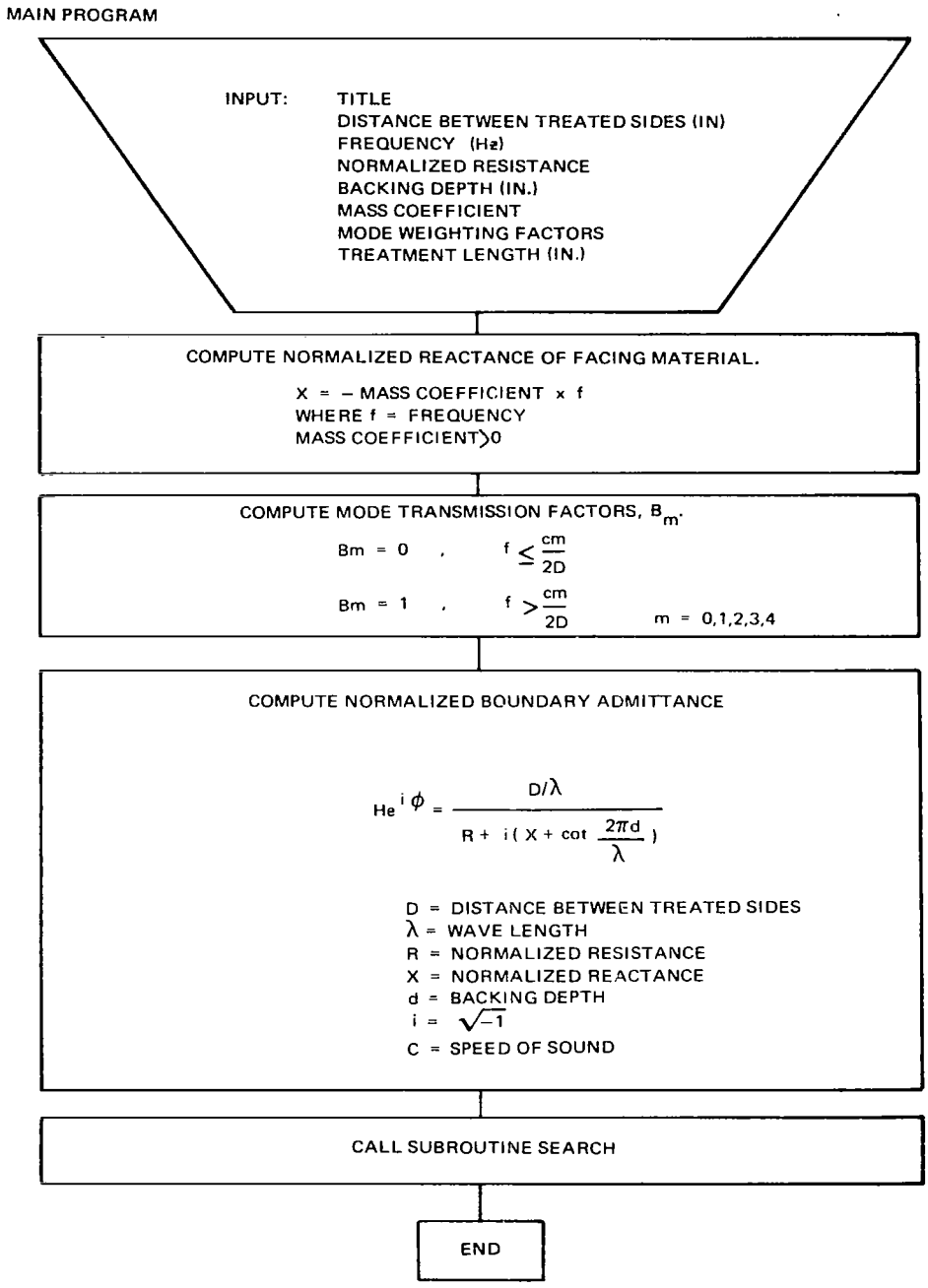

Figure 80 Computer Program Flow Chart, Main Program

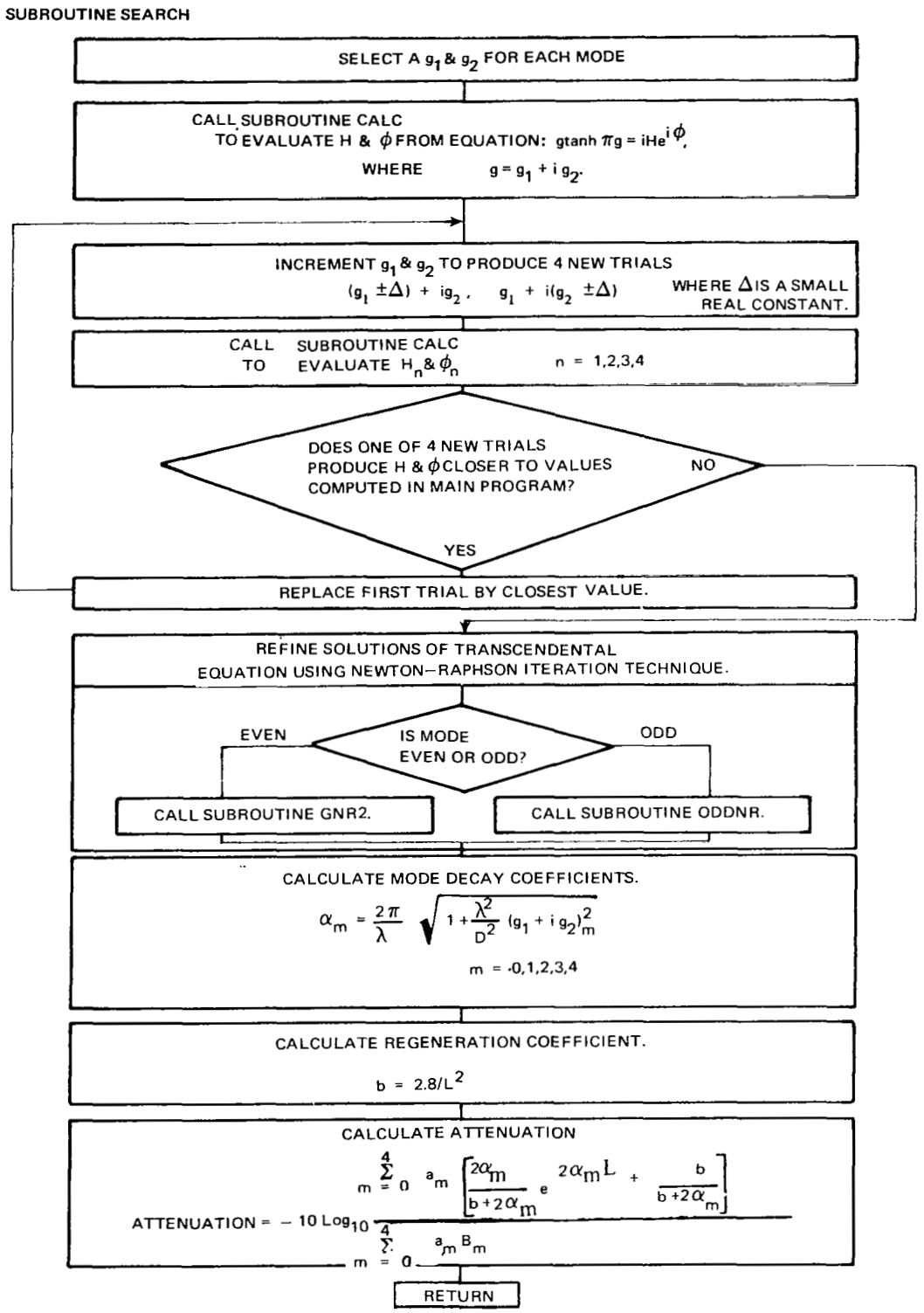

Figure 81 Computer Program Flow Chart, Subroutine Search

APPENDIX

The total acoustic energy flow in the duct is

$$W = \int \sum_{m,n} 1/2 \left(\overline{p_m u_n^*} + \overline{p_m^* u_n} \right) dS$$

Where the acoustic pressure of the mth mode is

$$p_m = p_m(x, y, z, t)$$

and the axial component of the acoustic partical velocity of the nth mode is

$$u_n = u_n(x, y, z, t)$$

The asterisk indicates complex conjugate, and $\overline{\quad}$ indicates time average. The integral is taken over the cross-section of the duct.

If the duct walls are hard or if the wall impedance is purely reactive, the integrals are zero unless m = n and the energy flow is just the sum of the contributions from the various modes. However, if the wall impedance includes a resistive term, the integrals are not zero for $m \neq n$ (ref. 1 and 2).

Defining an energy flow matrix W_{mn} such that $W = \sum_{m,n} W_{mn}$, the diagonal terms can be thought of as the power contributed by the individual modes. If only the mth mode is excited, the energy flow is simply W_{mm}. The off-diagonal terms represent energy flow due to mode coupling that occurs when more than one mode is excited.

For simplification, only the diagonal terms of W_{mn} are considered in the analysis given in the main body of the report. A limited number of calculations of attenuation in the lined duct have been made with the off-diagonal terms included, and the results were not significantly different from those obtained when only the diagonal terms were considered.

1) Morse, P.M. and Ingard, U., "Linear Acoustic Theory", section 23, Handbuch der Physic, Vol. XI, part 1, Springer-Verlag, Berlin, 1961

2) Rice, E.J., Attenuation of Sound in Soft Walled Circular Ducts, NASA TM X-52442, 1968